UNIVERSITÀ DEGLI STUDI
DI MODENA E REGGIO EMILIA

Dottorato di ricerca in Neuroscienze

Ciclo XXXVI

Unravelling the role of PCSK9 in Alzheimer's Disease pathophysiology: an *in vivo* study in 5XFAD mice

Definire il ruolo di PCSK9 nella fisiopatologia della malattia di Alzheimer: studio *in vivo* nel modello murino 5XFAD

Relatore (Tutor): Dr.ssa Antonietta Vilella

Candidato: Dr.ssa Martina Bodria

Correlatori: Prof. Michele Zoli
Prof. Daniela Giuliani

Coordinatore del Corso di Dottorato: Prof. Sandro Rubichi

TABLE OF CONTENTS

Table of abbreviations

18S	18S ribosomal RNA
24-OHC	24-hydroxycholesterol
25-OHC	25-hydroxychelesterol
27-OHC	27-hydroxycholesterol
7Hoca	7a-hydroxy-3-oxo-4-cholestenoic acid
7-KC	7-ketocholesterol
7α-OHC	7α-hydroxycholesterol
7β-OHC	7β-hydroxycholesterol
aa	Amino acid
ABC	Adenosine triphosphate-binding cassette
ABCA1	Adenosine triphosphate-binding cassette-transporter protein subfamily A member 1
ABCA7	Adenosine triphosphate-binding cassette-transporter protein subfamily A member 7
ABCG1	Adenosine triphosphate-binding cassette-transporter protein subfamily G member 1
ABCG4	Adenosine triphosphate-binding cassette-transporter protein subfamily G member 4
AD	Alzheimer's Disease
ADAM10	A disintegrin and metalloproteinase domain-containing protein 10
AICD	Amyloid precursor protein intracellular domain
ALS	Amyotrophic Lateral Sclerosis
APOE	Apolipoprotein E
APOER2	Apolipoprotein E receptor 2
APOERs	Apolipoprotein E-interacting receptors
APOEε4	Apolipoprotein E ε4 variant
APP	Amyloid precursor protein
APP/PS1	Transgenic mouse expressing human amyloid precursor protein isoform 695 with KM670/671NL mutations (Swedish) / presenilin 1 gene lacking exon 9 (line 85)
APP23	Transgenic mouse expressing human amyloid precursor protein isoform 751 with K670N, M671L mutations
APPSwe	Transgenic mouse expressing human amyloid precursor protein isoform 695

	with KM670/671NL mutations (Swedish)
Aβ	β-amyloid peptide
AβF	Aβ Fibrils
AβO	Aβ Oligomers
BACE1	β-site amyloid precursor protein cleaving enzyme 1
BBB	Blood brain barrier
BCA	Bicinconic acid assay
BHT	Butylhydroxytoluene
bp	Basepair
CA1	Cornu Ammonis 1
CA3	Cornu Ammonis 3
CAT	Catalytic domain
CC-Cg	Corpus callosum-cingulate cortex
Ccl3	Chemokine (C-C motif) ligand 3
Ccl6	Chemokine (C-C motif) ligand 6
Cd11b	Cluster of differentiation molecule 11b
CD36	Cluster of differentiation 36
Chol	Cholesterol
CHRD	Cysteine and histidine-enrich C-terminal domain
CNS	Central nervous system
CoA	Coenzyme A
CS	Conditioned stimulus
CSF	Cerebral spinal fluid
Cst7	Cystatin-F
Ctrls	Controls
Ctx	Cortex
Cx3cr1	C-X3-C motif chemokine receptor 1
CYP27A1	Cytochrome P450 oxidase family 27 subfamily A member 1
CYP46A1	Cytochrome P450 oxidase family 46 subfamily A member 1
CYP51A1	Cytochrome P450 oxidase family 51 subfamily A member 1
CypA	Cyclophilin A
D	Day
DAB	3,3'-diaminobenzidine
DEGEE	Diethylene glycol monoethyl ether

DEPC	Diethylpyrocarbonate
DG	Dentate gyrus
DHCR24	24-dehydrocholesterol reductase
DHCR7	7-dehydrocholesterol reductase
DMEM	Dulbecco's modified eagle's medium
Dpi	Day post injection
E	East
eAβ	Extracellular Aβ
EBP	3-beta-hydroxysteroid-Delta(8),Delta(7)-isomerase
EDTA	Ethylenediaminetetraacetic acid
EE	Early endosome
ELISA	Enzyme-linked immunosorbent assay
EPM	Elevated plus maze
ER	Endoplasmic reticulum
EtOH	Ethanol
FAD	Familial Alzheimer's Disease
FBS	Fetal bovine serum
FC	Fear conditioning
FDPS	(2E,6E)-farnesyl diphosphate synthase
FDT1	Farnesyl-diphosphate farnesyltransferase 1
FELASA	Federation of European laboratory animal science associations
Fw	Forward
Gapdh	Glyceraldehydes-3-phosphate dehydrogenase
GBA1	Glucosylceramidase-beta 1
GFAP	Glial fibrillary acidic protein
GWAS	Genome wide association studies
h	Hours
HD	Huntington Disease
HDL	High-density lipoproteins
HepG2	Hepatoma G2 cell line
Hil	Hilus
Hip	Hippocampus
HMG-CoA	3-hydroxyl-3-methylglutaryl-coenzyme A
HMGCR	3-hydroxy-3-methylglutaryl-coenzime A reductase

hPCSK9	Human recombinant pro protein subtilisin-kexin type 9
HR	Hinge region
HRP	Horseradish peroxidase
HSD17B7	17-beta-estradiol 17-dehydrogenase
HSD3B7	3b-hydroxy-C27-steroid dehydrogenase/isomerase
iAβ	Intracellular Aβ
IBA1	Ionized calcium-binding adapter molecule 1
Iftm3	Interferon induced transmembrane protein 3
IHC	Immunohistochemical
IL-1β	Interleukin-1 β
IL-6	Interleukin-6
ir	Immunoreactivity
JAK2	Janus-activated kinase 2
JNK	c-Jun NH2-terminal kinase
KO	Knock out
LC-MS/MS	Liquid chromatography-tandem mass spectrometry
LDL	Low-density lipoprotein
LDL-C	Low-density lipoprotein containing-cholesterol
LDLR	Low-density lipoprotein receptor
LE	Late endosome
Lmol	Stratum lacunosum-moleculare
Lpl	Lipoprotein lipase
LRP1	Low-density lipoprotein receptor-related protein 1
Lrp5	Low-density lipoprotein receptor-related protein 5
LRRK2	Leucine-rich repeat kinase 2
LSS	Lanosterol synthase
LXR	Liver X receptor
MAPK	p44/42 mitogen-activated protein kinase
MCP-1	Monocyte chemoattractant protein-1
MeOH	Methanol
min	Minutes
mo	Months old
MSMO1	Methylsterol monooxygenase 1
MVD	Mevalonate diphosphate decarboxylase

MVK	Mevalonate kinase
MWM	Morris water maze
n.d.	Non-detected
Nctx	Neocortex
NFkB	Nuclear factor kappa B
NLRC4	Nucleotide-binding domain leucine-rich repeat-containing protein family caspase activation and recruitment domain-containing protein 4
NLRP1	Nucleotide-binding domain, leucine-rich–containing family pyrin domain–containing-1
NLRP3	Nucleotide-binding domain, leucine-rich–containing family pyrin domain–containing-3
NPC	Niemann-Pick disease type C
NSDHL	Sterol-4alpha-carboxylate 3-dehydrogenase
OD	Optical density
OF	Open field
OT	Olfactory tubercle
p	Phosphor
P2ry12	Purinergic receptor P2Y
PBS	Phosphate buffered saline
PCR	Polymerase chain reaction
PCSK9	Pro protein subtilisin-kexin type 9
PCSK9i	Pro protein subtilisin-kexin type 9 inhibitor
PD	Parkinson’s Disease
PDAPP	Transgenic mouse expressing human APP isoform 770 with V717F FAD mutation
$Pde6b^{rd1}$	Phosphodiesterase-6b retinal degeneration allele
PFA	Paraformaldehyde
PMVK	Phosphomevalonate kinase
PRO	Pro-domain segment
PS1	Presenilin 1
PS2	Presenilin2
PVDF	Polyvinylidene difluoride
qPCR	Quantitative polymerase chain reaction
RE	Recycling endosome

Rer1	Retention in endoplasmic reticulum sorting receptor 1
RT	Room temperature
Rv	Reverse
RXR	Retinoid X receptor
S	South
sAPP	Soluble amyloid precursor protein
sAPPα	Soluble amyloid precursor protein α fragment
sAPPβ	Soluble amyloid precursor protein β fragment
SC5D	Sterol-C5-desaturase
sCtx	Somatosensory cortex
SD	Strandard deviation
SDS	Sodium dodecyl sulfate
sec	Seconds
SEM	Standard error of the mean
SL	Stratum lucidum
SO	Stratum oriens
SP	Signal peptide
SQ inj	Subcutaneous injection
SQLE	Squalene epoxidase
SR	Stratum radiatum
SRE	Sterol regulatory element
SREBP2	Sterol regulatory element binding protein 2
STAT3	Signal transducer and activator of transcription 3
Stmn1	Stathmin 1
SYN	Synaptophysin
TAE	Tris-acetate ethylenediaminetetraacetic acid
TBS	Tris-buffered saline
TC	Total cholesterol
TGN	Trans Golgi network
ThS	Thioflavin-S
Thy-1	Thymus cell antigen-1
TLR4	Tall-like receptor 4
TM7SF2	Delta(14)-sterol reductase
TNFα	Tumor necrosis factor α

TREM2	Triggering receptor expressed on myeloid cells 2
Tub	Tubulin
VLDLR	Very low-density lipoprotein receptor
Wt	Wild-type
αCTF	α C-terminal fragment
α-EPOX	5α,6α-epoxycholesterol
βCTF	β C-terminal fragment
β-EPOX	5β,6β-epoxycholesterol

Abstract

Alzheimer's disease (AD) is a multifactorial neurodegenerative disease and the leading cause of dementia globally. Most of the available drugs only transiently relieve symptoms, and novel therapies have failed in clinical studies, except for the expensive monoclonal antibody Aducanumab (Villain et al. 2022) not yet approved by European Medicines Agency. There is therefore a pressing need for the development of innovative therapeutic strategies.

Proprotein Convertase Subtilisin-like Kexin type 9 (PCSK9), an enzyme that degrades low-density lipoprotein receptor and regulates plasma cholesterol levels, is also expressed in central nervous system (CNS). Clinical studies have shown increased levels of PCSK9 in the cerebrospinal fluid (CSF) and the frontal cortex of AD patients (Zimetti et al. 2017, Picard et al. 2019). PCSK9 may play a role in AD pathophysiology including cholesterol dyshomeostasis (Adorni et al. 2019). For instance, recent findings demonstrated that PCSK9 alters cholesterol metabolism in astrocytes and neurons, reducing the expression of apolipoprotein E-interacting receptors (APOERs) and leading to reduced neuronal cholesterol intake. In addition, PCSK9 overexpression worsened amyloid beta (Aβ)-induced neurotoxicity (Papotti et al. 2022).

The aim of this study was to test the possible protective effects of PCSK9 on AD-related neurodegenerative processes in both *in vitro* and *in vivo* models. More specifically, we tested the pro-inflammatory effects of PCSK9 by incubating U373 human astrocytoma cells with Aβ fibrils and human recombinant PCSK9 *in vitro*. Then, we assessed the pathophysiological consequences of *PCSK9* genetic ablation in 5XFAD mice, a well-established transgenic mouse model of AD.

In vitro, our results demonstrated that PCSK9 significantly increases *interleukin-6*, *interleukin-1β* and *Tumor Necrosis Factor-α* mRNA levels and Monocyte Chemoattractant Protein-1 release in Aβ fibrils-treated U373 cells without influencing inflammasome gene expression.

In vivo, PCSK9 ablation significantly improved hippocampal-dependent spatial memory and ameliorated search strategy in 5XFAD mice at the Morris Water Maze (MWM) test; in addition, a reduction of cortico-hippocampal Aβ burden was observed, affecting neither plaque spatial/regional distribution and composition nor global BACE1 expression. Furthermore, PCSK9 loss attenuated the inflammatory state in several brain regions of 5XFAD mice decreasing microglial reactivity.

Ex vivo analysis showed an altered expression of lipid metabolism-related genes, proinflammatory cytokines and total cholesterol levels in the brain of 5XFAD mice, that was not significantly affected by the loss of PCSK9. Instead, PCSK9 deletion decreased total cholesterol levels in the serum of

both 5XFAD and control mice. Finally, knocking out *PCSK9* had no significant impact on hydroxysterol levels in any experimental group.

In a side project, several newly synthesized lipophilic small molecules (MR-compounds) were tested on human hepatoma G2 cell line (HepG2) to evaluate their cytotoxicity and PCSK9 inhibition efficacy. Among them, three compounds were selected for *in vivo* studies on C57BL/6J mice to evaluate: tolerability with SHIRPA test and biodistribution in liver.

Overall, these data support an involvement of PCSK9 in AD pathophysiology, indicating that: 1) PCSK9 enhances Aβ-induced neuroinflammatory response in U373 cells; 2) *PCSK9* deletion reduces amyloidosis and neuroinflammation improving cognitive performance in 5XFAD mice; 3) MR-compounds inhibit PCSK9 and reverse PCSK9-mediated reduction of cholesterol uptake in neuronal cells. The subacute application of selected MR compounds to C57BL/6J mice was well tolerated.

Present research point to PCSK9 as a promising pharmacological target in AD worth of further investigation and therapeutic development.

1. Introduction

1.1. Lipid and neurodegenerative disorders

Lipids represent a major class of biomolecules crucial for the function and integrity of all living cells. Lipids can be classified by their head group configuration, molecular weight, the nature and number of carbon-to-carbon bonds and whole structure into five major groups as fatty acids, glycerophospholipids, glycerolipids, sphingolipids and sterols. Besides phospholipids, cholesterol, is a fundamental constituent of animal cells and is crucial in determining membrane structure, modulating both fluidity and permeability of membrane. The brain represents the body's second most lipidated organ, and these organic compounds play a pivotal role in normal development and function of CNS, such as neurogenesis, synaptic transmission, neural communication, modulation of gene expression and energy balance. In fact, lipids are directly implicated in the formation of lipid bilayers of cell membranes, including synapses and myelin sheaths, and are involved in regulation of membrane fluidity. In addition, lipid composition forms a microenvironment in which proteins can be included/excluded, thus influencing protein functionality and cell signalling. Lipid composition and membrane fluidity influence which protein will be associated with lipids and regulate receptor partitioning, directly participating and modulating signalling processing. In this view, lipids are not only the building blocks for membranes; in fact, lipid composition, degree of unsaturation, and length of fatty acyl tails can determine fluidity of membranes, lipid rafts, membrane microdomains, and influence vesicles fusion and secretion (Mencarelli and Martinez-Martinez, 2013). Moreover, lipids are also involved in the maintenance of membrane bilayer structure relevant for optimal activity of ion channels, enzymes and receptors and its dysregulation is associated to changes in the ionic homeostasis leading to oxidative stress, mitochondrial dysfunction, and neuronal death.

During physiological aging changes in the lipid composition have been reported in different human brain regions (Rouser and Yamamoto, 1968). Also changes in lipidome profile have been described, for example an increasing susceptibility of lipid to peroxidation and a reduction of polyunsaturated fatty acids with antioxidant and anti-inflammatory activity was observed (Chen et al., 2017). Moreover, the lipid composition in lipid rafts undergoes significant modifications during aging, resulting in the alteration of several physiological functions (Díaz et al., 2018; Mesa-Herrera et al., 2019). These findings evidenced that lipid dysfunctions contribute to pathological processes involved in neurodegenerative diseases.

Genetic studies associated many genes involved in lipid metabolism to the increased risk to develop Alzheimer's Disease (AD), Parkinson's Disease (PD), and other neurodegenerative disorders. For instance, in the Niemann-Pick disease type C (NPC), an autosomal recessive disorder characterized

by prominent neurological manifestations, mutations in *NPC1* or *NPC2* genes correlate with impaired cholesterol trafficking, endosomal-lysosomal compartment cholesterol accumulation and neurodegeneration (Schulze and Sandhoff 2011; Rebiai et al., 2021).

A growing number of causative genes and risk loci for PD have also been implicated in lipid function, metabolism, and trafficking (Alecu and Bennett, 2019; Flores-Leon and Outeiro, 2023). Mutations in *leucine-rich repeat kinase 2* (*LRRK2*) are the most common risk factor for inherited PD and its polymorphisms are also associated with an increased risk of the PD sporadic form. Studies have suggested that LRRK2 may have a role in several lipid-regulated processes (Galper et al. 2022). The *glucosylceramidase-beta 1* (*GBA1*), which encodes for a lysosomal enzyme, has been classified as a critical gene in ceramide metabolism and its mutation represents penetrant genetic risk factor for PD. In addition, *GBA*-associated PD patients had significantly lower levels of total cholesterol (TC) and low-density lipoproteins (LDLs) compared to *LRRK2*-associated PD patients and healthy controls (Macías-García et al., 2021). A modification in sphingolipid levels, such as a decrease in the ganglioside GM1, has been observed in the brains of PD patients compared to healthy controls (Wu et al., 2012). Moreover, it has been suggested that GM1 is involved in the maintenance of α-synuclein helical conformation preventing its aggregation (Martinez et al., 2007). Other studies have demonstrated that anomalies in sphingolipid metabolism may also be involved in PD pathological progression. Sphingomyelinase activity has been found to increase in PD brains, leading to enhanced ceramide synthesis and neuronal apoptosis in the substantia nigra through the induction of oxidative stress in mitochondria (France-Lanord et al., 1997; Leeden et al., 2008). Additionally, *GBA* gene variants represent a risk factor also for AD and dementia with Lewy bodies (Chia et al., 2021; Bellenguez et al. 2022). In fact, the abnormal α-synuclein levels caused by lysosomal dysfunction may promote amyloid formation.

Moreover, several genome wide association studies (GWAS), exome and whole genome sequencing studies identify lipid metabolic genes associated with Amyotrophic Lateral Sclerosis (ALS) risk, such as the gene encoding a cytochrome P450 oxidase family 27 subfamily A member 1 (CYP27A1), commonly known as sterol 27-hydroxylase, involved in cholesterol metabolism (Diekstra et al. 2012). Recently, the lipid metabolism impairment was also investigated in ALS and Multiple Sclerosis (Bouscary et al., 2021; Podbielska et al., 2022). Specifically, ALS is frequently accompanied by hypercholesterolemia. In fact, high LDLs levels and a high LDLs / high-density lipoproteins ratio are associated with a higher risk of developing ALS (Mariosa et al., 2017). In addition, increased levels of phosphatidylcholine and sphingomyelin have been detected both in CSF of ALS patients and in the cortex (Ctx) of ALS mouse model expressing a G93A mutant form of human *superoxide dismutase 1* gene and correlate with the progression of the disease (Blasco et al., 2017).

Finally, lipid dyshomeostasis has been implicated also in Huntington's Disease (HD), in both humans and mouse models; in fact, huntingtin regulates the expression of transcription factor containing the sterol regulatory element (SRE) influencing the expression of cholesterol biosynthetic enzymes. Moreover, the presence of mutant huntingtin is associated with the downregulation of cholesterol related genes and decreased cholesterol levels (Valenza and Cattaneo, 2006; Di Pardo et al. 2020). However, the exact mechanisms by which reduced brain cholesterol contributes to HD pathogenesis remain to be elucidated. Recently, it has been suggested that membrane composition influences both huntingtin aggregation and lipid interactions (Stonebraker et al. 2023) and that increased sphingomyelin content favours huntingtin aggregation (Chaibva et al. 2018).

The *ε4* allele of the *apolipoprotein E* (*APOEε4*), coding for a main transporter of cholesterol between cells in the brain, is considered the strongest genetic risk factor for the development of late-onset AD and some forms of frontotemporal dementia (Wang et al., 2020). Moreover, other lipid metabolism-related risk genes have been identified through GWAS, and recently reviewed by Chew et al. (2020), involved in lipid biosynthesis, trafficking, and signal transduction.

Genetic studies have been supported by lipidomic data reinforcing the evidence that alterations in lipid metabolism represent a common feature in neurodegenerative disorders. For example, lipidomic analysis of tissue from AD patients and AD animal models has revealed alterations in the levels of several lipids, such as fatty acids, glycerophospholipids, sphingolipids and cholesterol both in plasma (Mesa-Herrera et al., 2019; Chew et al., 2020; Cunnane et al., 2012) and in the lipid rafts of the entorhinal cortex and frontal cortex at early stage of AD (Martín et al., 2010; Filippov et al., 2012).

In AD, it was also observed that an altered lipidic membrane composition, particularly in lipid rafts, promotes amyloid biogenesis. Several studies support the role of ceramide in promoting aggregation of β-amyloid peptide (Aβ) associated with lipid rafts and spread of tau and Aβ via exosomes (Han et al., 2002; Wang et al., 2008; Mielke et al., 2010, 2012; Czubowicz et al., 2019).

All these findings support the hypothesis that altered cholesterol metabolism and unbalanced lipidome could influence the onset of neurodegenerative disorders.

1.2. Alzheimer's Disease

The World Health Organization recognizes dementia as a priority in public health. Currently, about 55 million people are affected by dementia, and AD accounts for approximately 60-70% of cases in the elderly. AD represents a multifactorial neurodegenerative disorder, clinically defined by a gradual cognitive decline and a deterioration of executive capabilities (Knopman et al., 2021). Memory impairment develops gradually and represents the first symptom of the neurodegenerative process,

primarily affecting brain regions involved in memory acquisition and retention such as the hippocampus (Hip), entorhinal cortex, and the amygdala (Therriault et al., 2022). Furthermore, various cellular changes are involved in this intricate pathophysiological process, which begins at least 10-20 years prior to the manifestation of clinical symptoms. These changes include synaptic damage, mitochondrial dysfunction, microRNA dysregulation, inflammation, which collectively culminate in neurodegeneration and brain atrophy (Edwards, 2019; Oliver et al., 2019). Other manifestations of AD include loss of concentration, aphasia, apathy, and mood changes progressively accompanied by a decline in visuo-spatial functions, an inability to complete tasks, and a worsening of episodic memory. Patients require ongoing assistance, and in the final stage, complications related to advanced debilitation ultimately lead to death (Porsteinsson et al., 2021).

Aging is considered the major risk factor for the development of AD, and two primary forms are identified based on the age of onset: the early-onset AD, which occurs between the ages of 30 and 65, and the more common late-onset AD which occurs after the age of 65 (Qui et al., 2009). Approximately, 70% of the risk for developing AD can be attributed to genetics. The early-onset AD is associated with familial forms of the disease or familial AD (FAD) and is caused by genetic alterations, including autosomal dominant mutations in genes that code for amyloid precursor protein (APP), presenilin 1 (PS1), and presenilin 2 (PS2). The *APOE* gene represents the strongest genetic risk factor for late-onset AD. Specifically, the presence of APOEε4 isoform is linked to an increased risk of developing AD, particularly in female carriers (Rabinovici, 2019).

Both forms of AD are characterized by the presence of two well-known hallmarks: the extracellular accumulation of Aβ peptide and the intracellular neurofibrillary tangles. Evidence suggests that women may have a higher risk for AD compared to men, with a twofold increase in risk due to life expectancy differences and hormonal status (Pike, 2017). Additionally, women show greater regional tau protein accumulation, faster hippocampal volume changes, and greater metabolic dysfunction (Koran et al., 2017; Rahman et al., 2019; Buckley et al., 2020). Among genetic risk factors no studies identified a sex-related difference in the distributions of the most common mutations linked to early-onset AD (Altmann et al., 2014; Neu et al., 2017; Buckley et al., 2019).

In addition to non-modifiable risk factors such as age, genetics, and sex, exposure to environmental neurotoxic agents (heavy metals, pesticides, and air pollutants), unhealthy lifestyle habits (obesity, excessive alcohol consumption, and smoking), as well as the presence of cerebrovascular and cardiovascular diseases, diabetes, dyslipidemia, and hypertension, have been associated with an elevated risk of developing AD (Reitz and Mayeux, 2014). Despite understanding the clinical characteristics and risk factors of AD, the exact etiology of the disease is still unknown, and this is reflected in the absence of a specific target to revert AD pathology.

The available treatments for AD are limited and can only provide temporary relief from the symptoms (e.g., acetylcholinesterase inhibitors). The growing need for innovative strategies to prevent, reverse or slow the progression of AD has spurred the exploration of several alternatives. However, most of them have proven ineffective in clinical trials (Burns et al., 2022). Only the costly anti-Aβ human monoclonal antibody Aducanumab (Villain et al. 2022) has been approved by the Food and Drug Administration, but the safety and tolerability of the treatment are still being carefully evaluated by the European Medicines Agency. Recently, attention has shifted to other contributors to the intricate AD pathophysiology, such as changes in lipid metabolism (Yin, 2023) and neuroinflammation (Kinney et al., 2018).

1.2.1. APP processing, Aβ peptide and amyloid plaques

Aβ deposition and hyperphosphorylated tau protein in neurofibrillary tangles represent two histological markers of AD (Spires-Jones et al., 2014). APP, the Aβ precursor, is a type I transmembrane glycoprotein and three primary isoforms are encoded by a single gene located on chromosome 21: APP695, which is mainly expressed in CNS neurons, APP751, and APP770.

The physiological function of APP is not completely understood, but it has been suggested to operate as a receptor in various cellular signalling pathways and regulate synaptic development and neuronal migration (Zhang et al., 2019). The long extracellular N-terminal domain of APP comprises two segments, E1 and E2, connected by an acidic domain. Both segments contain a heparin-binding domain (within a larger growth factor-like domain only present in E1 and a copper/zinc-binding domain). The N-terminal APP domain has been demonstrated to mediate various functions, including cell-cell adhesion (Pfundstein et al., 2022). The extracellular region of N-terminal APP domain contains both the α- and β-cleavage sites, whereas the γ-cleavage site is found within the transmembrane domain. APP is synthesized in the endoplasmic reticulum and then trafficked to the Golgi complex to assume native structure and folding. Ultimately, it is transported to the plasma membrane where it is processed. Once APP reaches the cell surface, it is rapidly internalized via clathrin-mediated endocytosis and subsequently trafficked through endocytic and recycling compartments back to the cell surface or degraded in the lysosome (**Figure 1**).

Two pathways mediate APP processing, the non-amyloidogenic pathway via α-secretase, that occurs normally at cell surface, and the amyloidogenic pathway via β-secretase, that occurs mainly in the trans-Golgi network and endosomes. In the plasma membrane, APP is first cleaved by α-secretase within the Aβ region to release the soluble APP α fragment (sAPPα). The remaining membrane-bound α C-terminal fragment (αCTF or C83) is further cleaved by γ-secretase. Among the proteins with α-secretase activity, the disintegrin and metalloproteinase domain-containing protein 10 (ADAM10)

(Khezri et al., 2023), are responsible for cleaving APP in the Aβ region at the plasma membrane level, with a preference for more fluid non raft cholesterol-poor membrane regions (Yang et al., 2011), preventing the formation of neurotoxic Aβ peptide.

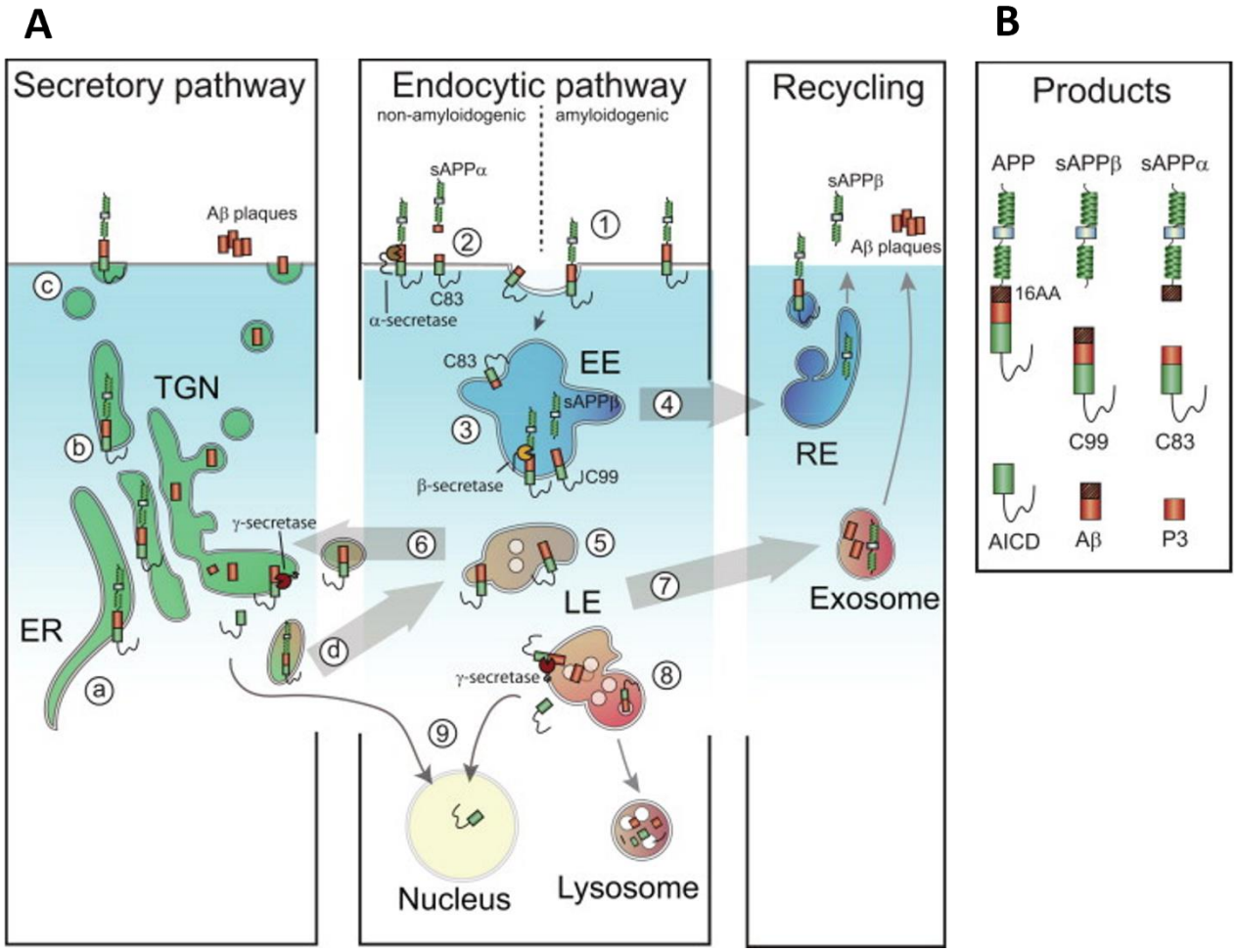

Figure 1. APP intracellular trafficking and processing. **A** APP is synthesized in the ER (a) and trafficked via the TGN (b) to plasma membrane (c). Once on the cell surface mature APP can be endocytosed (d) or processed by α-secretase (2) to release sAPPα in the extracellular environment as well as generating C83 (or αCTF) that is also endocytosed and in the TGN or in the LE cleaved by γ-secretase releasing p3 (non-amyloidogenic pathway). In the EE full-length APP and sAPP might be recycled to the plasma membrane via RE (4) or can be trafficked toward LE (5). In the LE, these fragments can subsequently be sorted toward the TGN (6), exocytosed (7), or further trafficked to the lysosome for degradation (8). In the EE, full-length APP is cleaved by the β-secretase generating sAPPβ and C99 (or βCTF) (3). The C99 fragment is cleaved by γ-secretase both in TGN and LE, releasing Aβ via the secretory pathway or via exocytosis (amyloidogenic pathway). The γ-secretase activity release AICD that can translocate to the nucleus. **B** APP proteolytic products (modified from van der Kant and Goldstein, 2015). Abbreviations: αCTF, α C-terminal fragment; βCTF, β C-terminal fragment AICD, amyloid precursor protein intracellular domain; Aβ, Amyloid peptide β; APP, amyloid precursor protein; EE, early endosome; ER, endoplasmic reticulum; LE, late endosome; RE, recycling endosomes; sAPPα, soluble APP α fragment; sAPPβ, soluble APP β fragment; TNG, trans-Golgi network.

Released sAPPα appears to play a crucial role in neuronal plasticity, survival, and neuroprotection against excitotoxicity (Zhang et al., 2011), along with αCTF. *In vivo* results demonstrated that overexpression of ADAM10 ameliorates impaired long-term potentiation and cognitive deficits in a

transgenic APP(V717I) mouse (Postina et al., 2004). Conditional knock-out (KO) of *ADAM10* dramatically reduces α-secretase cleavage products of APP in primary neurons (Jorissen et al., 2010).

The endocytic internalization of APP facilitates cleavage by the β-site APP cleaving enzyme 1 (BACE1) due to endosomes and Golgi acidic environment (Huse et al., 2002). The amyloidogenic processing of APP occurs primarily in lipid rafts, which are dynamic structures enriched in cholesterol and found preferentially in mature neurons (Malchiodi-Albedi et al. 2011). BACE1 is in part located in lipid rafts, where increased levels of cholesterol enhance its proteolytic activity (Choi et al., 2017; Barret et al., 2012; Marquer et al., 2011; Tamboli et al., 2011).

The N-terminal APP domain is targeted by BACE1 and a β-APP soluble fragment (sAPPβ) and β C-terminal fragment (βCTF or C99) are released. sAPPβ is associated with neuronal death, as well as βCTF (Nikolaev et al., 2009). αCTF and βCTF intermediates serve as substrates of γ-secretase, which is a complex comprised of PS1 and PS2, nicastrin, anterior pharynx-defective 1, and PS enhancer 2. The activity of γ-secretase results in the production of p3 (3kDa) and Aβ (4kDa), from αCTF and βCTF respectively, and APP intracellular domain (AICD). AICD contains the YENPTY motif, which mediates APP-dependent signalling by binding cytoplasmic adaptor proteins. In addition, released AICD can subsequently translocate to the nucleus, where it may regulate gene expression, including the induction of apoptotic genes. The biological properties of p3 peptide remain unclear; data from literature reported both neuroprotective effects (Han et al., 2011) and cytotoxic activity (Jang et al., 2010). As concerns Aβ, different studies reported its involvement in the regulation of synaptic activity; specifically, at picomolar concentration it acts enhancing synaptic plasticity, learning and memory by promoting long-term potentiation in the Hip (Morley et al., 2010; Puzzo et al., 2011).

The "amyloid cascade hypothesis" suggests that the accumulation of Aβ peptides, which are primary products of neurons, into extracellular plaques in the brain leads to neurotoxicity and dementia. Aβ encompasses a group of peptides ranging in size from 37 to 49 residues. The most abundant form of Aβ produced is $A\beta_{40}$, but $A\beta_{42}$ is the major component of extracellular plaques in the parenchyma of AD brains due to its hydrophobic structure and higher propensity to aggregate (Chen et al., 2017). A pathological imbalance in the overall Aβ monomers production and clearance can result in the formation of different types of aggregates, including neurotoxic Aβ oligomers (AβO), protofibrils and fibrils (AβF). The insoluble AβF form, with a parallel β-sheet structure, can assemble into aggregated plaques, while the AβO are soluble and may spread throughout the brain (**Figure 2**).

In the early phase of AD pathology, as well as in several transgenic mouse models of AD, including 5XFAD mice, an initial intracellular accumulation of Aβ (iAβ) precedes the formation of extracellular Aβ (eAβ) plaques. Early iAβ accumulation is associated with axonopathy, synaptic loss, tissue

inflammation, and neuronal death; thus, iAβ has been proposed to be one of the earliest pathophysiological events in both AD patients and rodent models (Daini et al., 2021; Welikovitch et al., 2020).

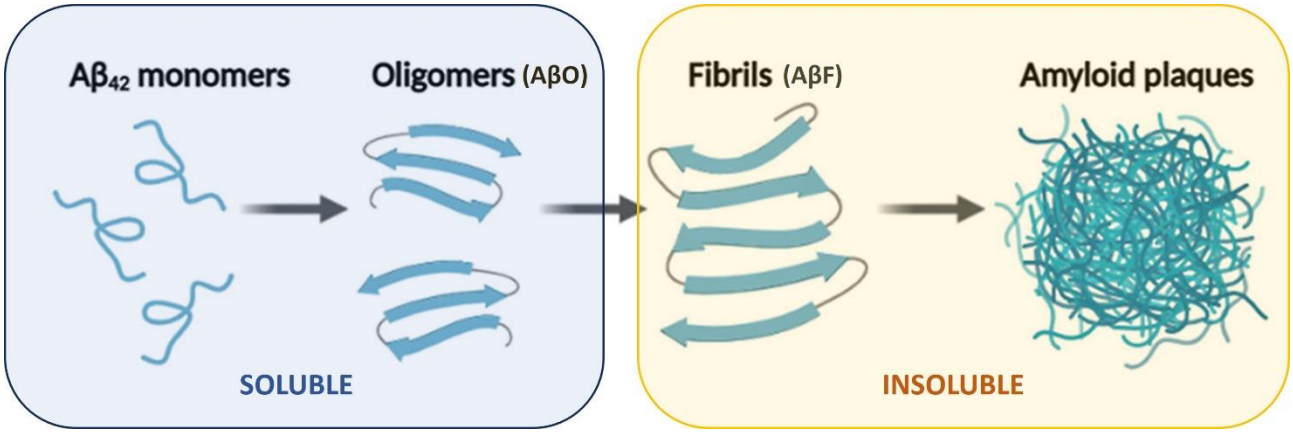

Figure 2. Amyloid aggregation state. The amyloidogenic pathway produces Aβ monomers that can be intracellularly accumulated or secreted from cell and spread throughout the brain. The instability of Aβ can result in soluble and neurotoxic AβO formation, that convert first in AβF and finally in Aβ plaques (modified from Sampaio et al. 2022). Abbreviations: AβO, Aβ oligomers; AβF, Aβ fibrils.

Aβ is an inherently unstable molecule whose conformation depends on the cellular lipidic environment and, specifically, membrane composition crucially influences the formation of β-sheet enriched protein, such as $Aβ_{42}$ (Rudajev and Novotny, 2022). Among Aβ species, AβO exhibits the greatest toxicity and can bind to many proteins in the extracellular space, including cell surface receptors, plasma membranes, and lipid rafts, and is known to cause membrane perturbation, *calcium* dyshomeostasis, reactive oxygen species production, mitochondrial and endosomal-lysosomal dysfunction, and apoptosis (Ciudad et al., 2020; Oku et al., 2017). Overall, these pathological processes disrupt cellular homeostasis thus impacting neuronal synapses and memory processes.

1.3. Cholesterol homeostasis in the central nervous system

Cholesterol is the most important lipid component of mammalian cell membranes. All nucleated cells are capable of synthesizing cholesterol in the endoplasmic reticulum. The liver is the primary site of cholesterol synthesis, although the brain also produces significant quantities (Tracey et al., 2018). The CNS is the second most lipid-rich organ and makes up about 25% of the total pool of unesterified cholesterol in the human body. In the CNS, maintaining proper cholesterol homeostasis is critical for normal cerebral functions. Cholesterol sustains membrane integrity and constitutes an essential element of synapses and myelin sheath. The most growth and differentiation of the CNS occurs in the first few weeks after birth and cholesterol is involved in various neuronal processes such as neuronal development, synaptogenesis, neurite growth, membrane trafficking, and signal transduction (Luo et al., 2020). Due to the presence of blood brain barrier (BBB), an autonomous

system for *de novo* synthesis of cholesterol in the CNS is necessary. During the embryonic development, neurons synthesize the highest levels of cholesterol through the so-called Bloch and Kandutsch–Russell pathways (Zhang and Liu, 2015; Genaro-Mattos et al., 2019). On the contrary, glial cells are characterized by very low or absent cholesterol biosynthesis rate. *De novo* cholesterol biosynthesis, also occurs in oligodendrocytes, is higher after birth and in early childhood and is required for myelin protein expression, wrapping the neuronal axon, and oligodendrocyte progenitor cells migration (Nieweg et al., 2009). Microglia do not synthesize large amounts of cholesterol since cholesterogenic enzymes in murine microglia exhibit a low transcription profile compared to other glial cells (Berghoff et al., 2021).

With age, neurons gradually lose the capacity for cholesterol synthesis, thereby necessitating the supply of cholesterol by astrocytes for the maintenance of physiological functions. In addition, it has been demonstrated that the glial cholesterol synthesis and neuronal uptake increase after neuronal cholesterol depletion in the mouse brain, supporting the dependence of adult neurons on astrocytes (Fünfschilling et al., 2007). Briefly, cholesterol is synthesized from acetyl-coenzyme A in the endoplasmic reticulum through approximately 30 consecutive reactions. The acetyl-coenzyme A is converted into 3-hydroxyl-3-methylglutaryl-coenzyme A (HMG-CoA) via a reaction catalyzed by HMG-coenzyme A-synthetase and then by HMG-coenzyme A-reductase (HMGCR) into mevalonate, a rate-limiting step in the cholesterol biosynthesis. In the adult brain, astrocytes produce cholesterol from desmosterol, a lanosterol derivate, through the Bloch pathway (Petrov et al., 2016) (**Figure 3**). The HMGCR is transcriptionally regulated by a feedback inhibition via the sterol regulatory element binding protein 2 (SREBP2).

Cholesterol is packaged into APOE particles, forming small high-density lipoprotein-like particles, and is secreted by astrocytes through the adenosine triphosphate binding cassette transporter protein subfamily A member 1 (ABCA1), subfamily G member 1 (ABCG1) and member 4 (ABCG4). Neurons can internalize the complex into clathrin-coated vesicles through APOE-binding receptors (APOERs) including LDL receptor (LDLR), low-density lipoprotein receptor-related protein 1 (LRP1), very-low-density lipoprotein receptor (VLDLR) and APOE receptor 2 (APOER2). After endocytosis, APOERs are either recycled via endosomes or directed to lysosomes for degradation (Vance and Hayashi, 2010) and cholesterol can be utilized by neurons (**Figure 4**).

Among neural cells, also microglia depend on astrocytes for cholesterol supplementation, specifically, the triggering receptor expressed on myeloid cells 2 (TREM2), toll like receptor 4 (TLR4) and the LDLRs are the mediators of APOE-particles internalization into these cells (Loving and Bruce, 2020). Given the role in the neuronal cholesterol supply, in astrocytes the production of cholesterol is closely regulated and the maintenance of the appropriate cholesterol levels in the

endoplasmic reticulum is critical for its metabolism. When cholesterol levels decrease in the endoplasmic reticulum, SREBP2 can move to the nucleus and triggers cholesterol production and upregulation of related genes.

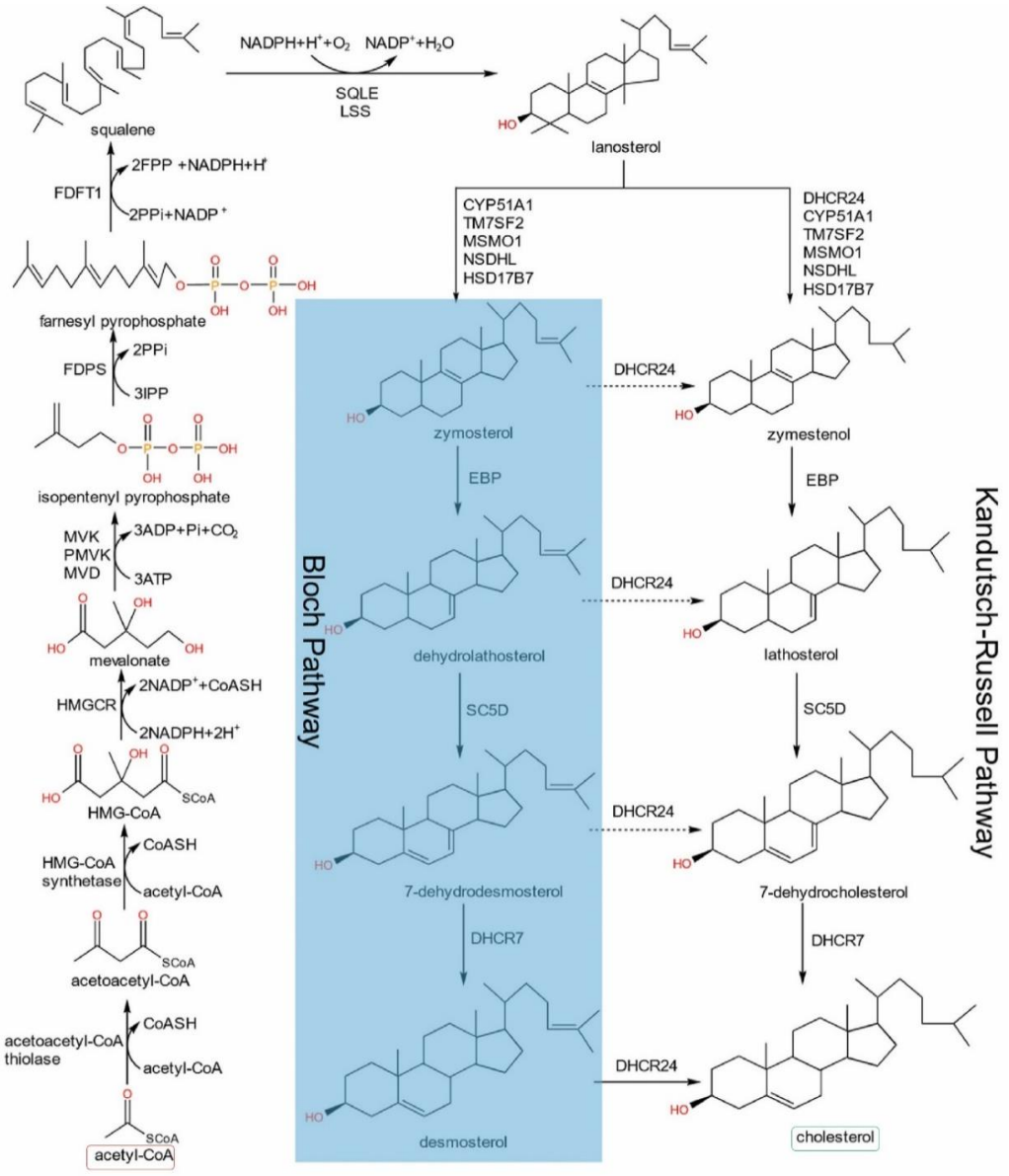

Figure 3. Schematic representation of cholesterol synthesis pathways. The cholesterol biosynthesis begins with the formation of mevalonate from acetyl-CoA catalyzed by HMG-CoA synthase and HMG-CoA reductase, mevalonate is then converted to lanosterol by a series of enzymatic reactions, followed by complex oxidation, reduction, and demethylation processes. The synthesis from lanosterol to cholesterol contains two alternative pathways. In the Kandutsch-Russell pathway, the lanosterol is first converted in 24,25-dihydrolanosterol by DHCR24 and then other intermediates before cholesterol synthesis. While in the Bloch pathway, the lanosterol is converted into desmosterol and then subjected to DHCR24 activity for cholesterol production (modified from Gao et al., 2023). Abbreviations: acetyl-CoA, acetyl coenzyme A; CYP51A1, cytochrome P450 family 51 subfamily A member 1; DHCR7, 7-dehydrocholesterol reductase; DHCR24, 24-dehydrocholesterol reductase; EBP, 3-beta-hydroxysteroid-Delta(8),Delta(7)-isomerase; FDPS, (2E,6E)-farnesyl diphosphate synthase; FDT1, farnesyl-diphosphate farnesyltransferase 1; HMG-CoA; 3-hydroxyl-3-methylglutaryl-coenzyme A; HMGCR, HMG-coenzyme A-reductase; HSD17B7, 17-beta-estradiol 17-dehydrogenase; LSS, lanosterol synthase; MSMO1, methylsterol monooxygenase 1; MVD, mevalonate diphosphate decarboxylase; MVK, mevalonate kinase; NSDHL, sterol-4alpha-carboxylate 3-dehydrogenase; PMVK, phosphomevalonate kinase; SC5D, sterol-C5-desaturase; SQLE, squalene epoxidase; TM7SF2, delta(14)-sterol reductase.

On the other hand, high levels of cholesterol inhibit SREBP2, and the excess of cholesterol can be esterified by acetyl-coenzyme A cholesterol acyltransferase-1 to form esterified cholesterol stored in lipid droplets or converted to 24S-hydroxycholesterol (24-OHC) by cholesterol 24-hydroxylase (or cytochrome P450 family 46 subfamily A member 1, CYP46A1), which is only expressed by neurons in healthy conditions.

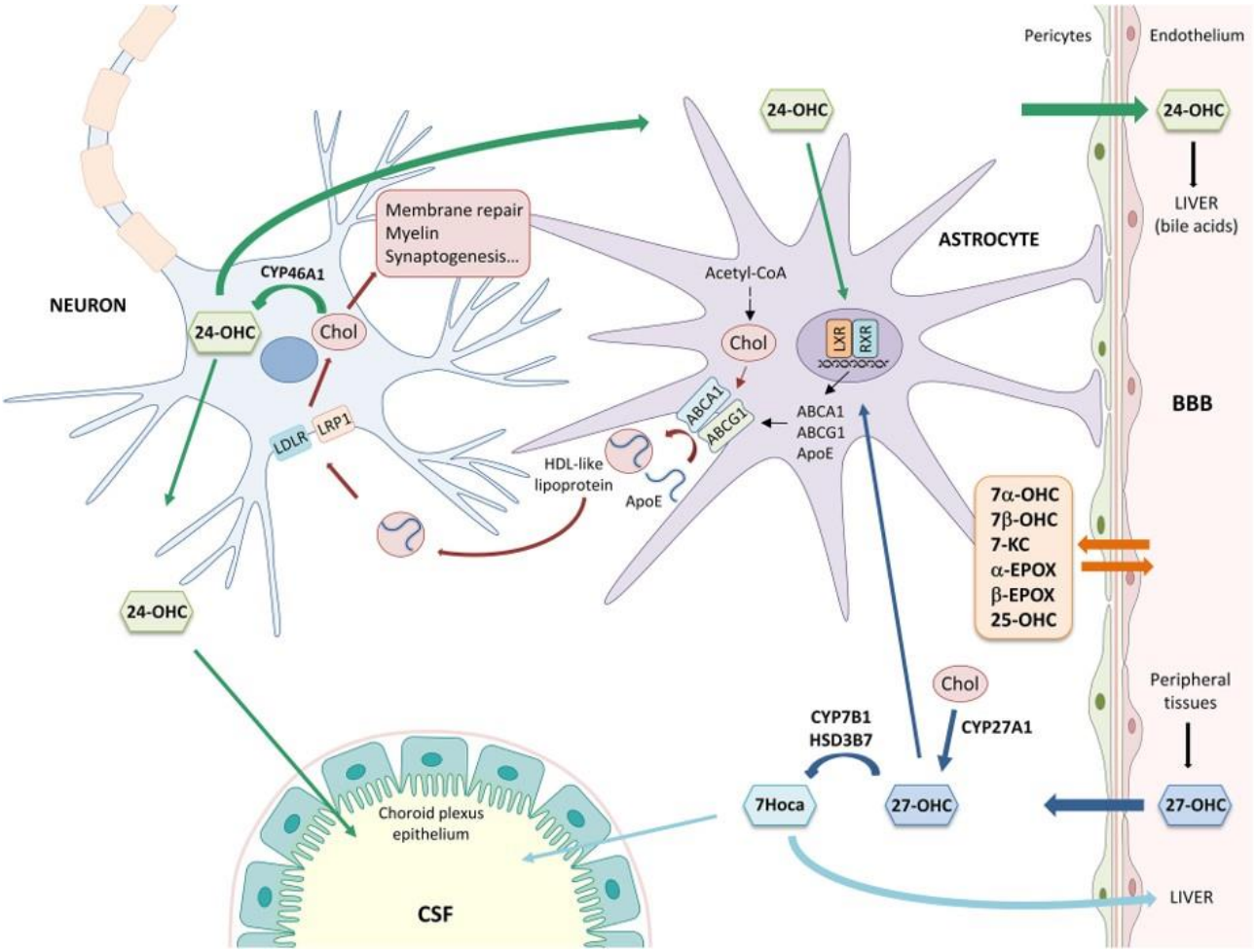

Figure 4. The main mechanisms involved in cholesterol homeostasis in the brain. Abbreviations: α-EPOX, 5α,6α-epoxycholesterol; β-EPOX, 5β,6β-epoxycholesterol; 24-OHC, 24-hydroxycholesterol; 25-OHC, 25-hydroxycholesterol; 27-OHC, 27-hydroxycholesterol; 7α-OHC, 7α-hydroxycholesterol; 7β-OHC, 7β-hydroxycholesterol; 7Hoca, 7a-hydroxy-3-oxo-4-cholestenoic acid; 7-KC, 7-ketocholesterol; ABC, adenosine triphosphate-binding cassette; acetyl-CoA, acetyl coenzyme A; ApoE, apolipoprotein E; BBB, blood-brain barrier; Chol, cholesterol; CSF, cerebrospinal fluid; HDL, high density lipoprotein; HSD3B7, 3b-hydroxy-C27-steroid dehydrogenase/isomerase; LDLR, low density lipoprotein receptor; LRP1, LDL receptor-like protein 1; LXR, liver X receptor; and RXR, retinoid X receptor (Gamba et al., 2019).

The 24-OHC crosses the BBB through diffusion in the CSF and its concentration in the blood reflects brain cholesterol turnover. Instead, the 27-hydroxycholesterol (27-OHC) mainly derived from cholesterol oxidation in peripheral tissue by CYP27A1, is usually found in the CNS due to its ability to diffuse through the BBB, but at lower concentration than in the plasma. The 27-OHC is rapidly converted into the steroid acid by neuronal oxysterol 7α-hydroxylase and reintroduced into

circulation. Moreover, the 25-hydroxycholesterol (25-OHC) is produced by a specific enzyme of the endoplasmic reticulum, the cholesterol-25-hydroxylase. Low levels in physiological conditions are produced by macrophages, especially microglial cells, and are increased during inflammatory response (Odnoshivkina et al., 2022). Finally, all these brain oxysterols are metabolized by hepatocytes (Luo et al., 2020; Olsen et al., 2012).

1.4. Altered cholesterol metabolism and AD pathogenesis

The first evidence about a link between altered cholesterol metabolism and AD comes from a study by Sparks and colleagues in 1990 reporting the presence of high amount of Aβ plaques in the brains of non-demented individuals affected by coronary artery disease, a condition associated with hypercholesterolemia (Sparks et al., 1990). Other clinical studies confirmed that individuals with familial hypercholesterolemia, exposed to high cholesterol levels from early life, were more likely to have abnormal cognitive function that met the criteria for mild cognitive impairment (Zambòn et al., 2010). It has been hypothesized that serum hypercholesterolemia may be an early risk factor for the AD development.

Subsequently, *in vivo* studies demonstrated that chronic administration of 2% cholesterol diet to rabbits progressively increased iAβ deposition in the Hip and Ctx (Sparks et al., 1994). In addition, a parallel increase in cerebral cholesterol levels and Aβ deposits, as well as a positive correlation between plasma and CNS cholesterol and total Aβ levels have been demonstrated in PSAPP mice, a transgenic mouse model of AD, subjected to a hypercholesterolemic diet (Refolo et al., 2000). Furthermore, high levels of circulating cholesterol in rabbits induced an increased endothelial inflammation and BBB damage (Sparks et al., 2000). Similarly, another study reported that the brains of C57BL/6J mice after 16 months of high-fat diet treatment are characterized by an increase in hippocampal fibrillar aggregates and Aβ-diffuse plaques, that correlate with neuroinflammatory status and autophagy impairment (Busquets et al., 2017). In fact, it has been reported in literature that high-fat diet administration in rodent models reproduce some features of sporadic AD (de Bem et al., 2021), including amyloidogenesis, neuroinflammation and cognitive impairments, such as a decrease in spatial and working memory (Ajayi et al. 2021; Wu et al., 2018).

Mouse models fed with either short- or long-term cholesterol-rich diets experienced a worsening of AD pathology. After being on a high-fat diet for 10 weeks, male 13-month-old (mo) 5XFAD mice display decreased learning abilities in the MWM test, elevated Aβ deposits in the walls of cerebral blood vessels, increased levels of oxidative stress in the Hip, and decreased levels of Occludin, a protein responsible for BBB function. However, these mice have not shown any differences in $A\beta_{40}$ and $A\beta_{42}$ deposits in the Ctx and Hip compared to the control groups (Lin et al., 2016). Moreover,

according to Fitz et al. (2010), a 16 weeks high-fat diet in a 9 mo mouse model of AD expressing human APP isoform 751 containing the K670N, M671L FAD mutations (APP23) results in an exacerbation of cognitive deficits and an increase in Aβ deposits in the cerebral parenchyma.

A recent study investigated the lipidomic profile of different brain areas in 5 mo AD model APP (expressing human APP isoform 695 with KM670/671NL FAD mutations, APPSwe)/*PS1* gene lacking exon 9 (APP/PS1) mice and showed an increase of ceramide levels in the Hip, cerebellum, and amygdala of these mice (Ferré-González et al., 2024). Alteration of ceramide metabolism was previously associated with Aβ aggregation, tau hyperphosphorylation, neuroinflammation and cell death. On the contrary, sterol lipid showed similar levels in all brain areas between AD mice and controls.

Additionally, another recent study reported an increase in lipid droplets content in the subicular microglial cells around Aβ burden of 5XFAD mice compared to controls, leading to an impaired Aβ clearance ability (Prakash et al., 2023).

In humans, studies over the years have often shown conflicting results regarding the relationship between circulating cholesterol levels, brain cholesterol metabolism and AD. The causal role of high cholesterol levels in AD or mild cognitive impairment has not been confirmed (McFarlane and Kedziora-Kornatowska, 2020). In fact, a meta-analysis study in AD patients failed to find a significant association between TC blood levels and any biomarkers of AD pathologies, such as $A\beta_{42}$ and phospho (p)-tau, neurodegeneration, or clinical impairment diagnosis (Nilsson et al., 2021). On the contrary, alternative systematic reviews have identified a robust connection between plasma lipids and AD. Specifically, an increase in circulating LDL and TC serum levels were found in AD patients (Agarwal and Khan, 2020; Xin et al., 2021).

In recent years, an increasing number of loci and genes involved in lipid metabolism have been identified through Mendelian inheritance, GWASs, and transcriptomic studies. For example, variants associated to gain or loss of function mutations are reported for the following genes: *APOE* and *clusterin*, which are involved in extracellular cholesterol transport; *bridging integrator-1*, *sortilin-related receptor 1* and *phosphatidylinositol binding clathrin assembly protein* regulating cholesterol-rich protein internalization; *ABCA1*, *ABCG1* and *ABCA7* involved in active extracellular transport; moreover *TREM2*, and *SREBP2* (de Rojas et al., 2021; De Roeck et al., 2019; Hollingworth et al., 2011; Jones et al., 2010). Of note, these loci and gene variants are associated to various neurodegenerative disorders, including AD, PD, HD, and ALS.

The most striking example is the evidence that *APOEε4* gene is one of the most powerful predictive factors for late-onset AD onset (Liu et al., 2013). The APOE protein serves as the primary lipid carrier

in the CNS, expressed mainly by astrocytes. It plays a physiological role in synapse formation and tissue repair (Bu et al., 2009). Additionally, APOE is involved in different processes related to Aβ pathology, and the lipidic composition of these particles affect Aβ seeding and clearance (Koutsodendris et al., 2022; Raulin et al., 2022; Jiang et al. 2008). *In vivo* studies demonstrated the effect of *APOE* silencing on AD pathology. For example, *APOE* KO mice, originally developed to study atherosclerosis, have also represented a tool to study the pathophysiology of neurodegenerative disorders. Previous studies have found that *APOE* KO mice subjected to a high-fat diet, display impaired spatial and working memory, increased hippocampal neuronal death, neuroinflammation in the Hip, and disruption of BBB integrity. However, there was no evidence of Aβ plaque deposition in these mice (Evola et al., 2020; Rahman et al., 2005; Crisby et al., 2004; Methia et al., 2001; Shnerb Ganor et al., 2018). Additionally, *APOE* KO in PDAPP mouse (expressing a human APP isoform 770 containing the V717F FAD mutation), showed a significant reduction in fibril formation and Aβ deposition, accompanied with a decreased astrogliosis and microgliosis (Bales et al., 1999), without improving cognitive function (Dodart et al. 2000). Contrarily, the peripheral administration of an anti-APOE antibody reduces Aβ deposition and improves cognitive deficits in APP/PS1 mice (Liao et al., 2014).

Clinical studies demonstrated an increased risk to develop AD in *APOEε4* carriers. In fact, healthy carriers of *APOEε4* allele have lower levels of $A\beta_{42}$ in the CSF, the most neurotoxic form of Aβ, accompanied with a higher level of fibrillar aggregate forms in the brain (Prince et al. 2004). *In vivo* imaging results also demonstrated that APOEε4 isoform is associated with an enhanced rate of Aβ aggregation and spread in the Ctx of AD patients (Toledo et al., 2019). Furthermore, total APOE levels were found decreased in *APOEε4* carriers compared to non-carriers (Mahley, 2016). The molecular mechanism through which APOEε4 influences Aβ production has been clarified *in vitro*. For example, APOEε4 stimulates the endocytic recycling of APP (Ye et al., 2005), increases the expression of BACE1 (Dafnis et al., 2018) and promotes *de novo* transcription of *APP* (Huang et al., 2017; Koutsodendris et al 2022, Yamazaki et al 2019). The APOEε4-containing particles have less cholesterol than those containing APOEε3 (Zhao et al., 2017). APOEε4 besides the lower lipidation rate (Kanekiyo et al., 2014) is also associated with a reduced receptor binding ability, leading to a compromised cholesterol trafficking capacity (Hatters et al., 2006). Furthermore, it has been reported that in PDAPP mice expressing the human APOE isoforms ε2, ε3 or ε4, those expressing the APOEε4 isoform showed a reduction in Aβ clearance and higher amyloid deposition (Castellano et al., 2011). Finally, abnormal accumulation of cholesterol and APOE has been detected in cores of mature plaques of postmortem AD brain and in the brain of 24 mo APPSwe mice (Mori et al., 2001). Higher

levels of esterified cholesterol stored in lipid droplets were observed in both human and AD mouse model brains (Farmer et al., 2020; Hamilton et al., 2015).

Multiple studies indicate that alterations in brain cholesterol levels significantly impact the pathophysiology of AD. For example, the membrane cholesterol content contributes to Aβ production, aggregation, and toxicity. While the non-amyloidogenic α-secretase pathway was observed predominantly in non-rafts domains (Allinson et al., 2003; Yuan et al., 2017), the APP amyloidogenic processing occurs in lipid rafts and is significantly regulated by the membrane lipid environment. In fact, higher cholesterol levels in membrane bilayer promote β- and γ-secretases stabilization, reducing their degradation and promoting their enzymatic activity leading to the formation of Aβ monomers (Rudajev and Novotny, 2022; Crivelli et al. 2020; Qui et al., 2009).

The protein aggregation process involves several steps, including the primary nucleation of monomers into misfolded oligomers that convert into more ordered species which can then grow into Aβ fibrils, and the secondary nucleation of monomers in a fibril-catalyzed manner (Knowles et al., 2014; Michaels et al., 2020). In the lipid membrane the pro-aggregation activity of phosphatidylcholine and phosphatidylethanolamine, is balanced by the anti-aggregation activity of phosphatidylglycerol and phosphatidylserine (Sanguanini et al., 2020). In an altered lipid environment with higher levels of cholesterol and gangliosides, and in the presence of enhanced levels of Aβ, the primary nucleation of Aβ monomers was promoted. Lipid membranes, in turn, can be affected by Aβ aggregation. Oligomers and protofibrils showed cytotoxic activity enhancing membrane permeability to *calcium* ions. In a molecular dynamic model, Aβ have been shown to oligomerize into *calcium*-permeable pores (Rudajev and Novotny, 2022; Fantini et al., 2014). Additionally, the ability of toxic Aβ to penetrate the membrane was associated with oxidative stress, lipid peroxidation, mitochondrial damage, and apoptosis (Campioni et al., 2010; Zampagni et al., 2011).

If on the one hand, hypercholesterolemia significantly impacts AD pathology, several data report that also hypocholesterolemia produces similar effects. In fact, depletion of cholesterol in neurons leads to hyperphosphorylation of tau protein, alterations in Aβ metabolism, and induction of oxidative stress at the neuronal level, ultimately leading to neurodegeneration (Koudinov et al., 2009; Koudinov et al., 2005).

As a result of cholesterol dyshomeostasis, also oxysterols concentration is affected in AD. The functional role of 24-OHC in AD brain is inconsistent. Higher levels of 24-OHC were detected in the CSF of individuals with AD when compared to healthy controls (Panza et al., 2006; Leoni et al., 2003). Additionally, a reduction in 24-OHC was observed in the Ctx of postmortem human AD brains

in late-stage of the disease compared to early-stage AD patients and control (Hascalovici et al., 2009; Kao et al., 2020; Varma et al., 2021); similarly, these observations were also confirmed in aged APPSwe mice (Haverin et al., 2004). This decrease in 24-OHC levels may potentially be due to progressive neuronal loss.

Certain studies suggest that 24-OHC can exert a protective role against tau hyperphosphorylation and Aβ production. Testa and colleagues demonstrated that 24-OHC up-regulates the synthesis of the neuroprotective enzyme Sirtuin-1 in neuroblastoma SK-N-BE cells (Testa et al., 2018), and promotes tau degradation by inducing its Sirtuin-1-dependent deacetylation (Min et al., 2010), also supported by *in vivo* evidence (Testa et al., 2018). Moreover, 24-OHC favors APP processing via the non-amyloidogenic pathway in SH-SY5Y neuroblastoma cells by increasing α-secretase activity (Famer et al., 2007; Prasanthi et al., 2009). In APP23 and APP/PS1 mice, in which the expression of 24-OHC was increased by means of genetic manipulation, it has been reported a reduction in Aβ plaques deposition followed by an improvement in spatial memory performance (Hudry et al., 2010).

Other investigations demonstrated 24-OHC potential role in promoting inflammatory and amyloidogenic outcomes. *In vitro* studies reported that 24-OHC significantly enhances both expression and synthesis of APP and BACE1 in human primary neuronal cells (Alexandrov et al., 2005) and elicits a pro-inflammatory response in mouse primary astrocytes (Staurenghi et al., 2021).

In contrast, increased levels of 27-OHC maybe due to dysfunction of BBB and blood-CSF barrier (Leoni et al., 2006) promote neuroinflammation, elevated Aβ levels, oxidative stress, and cellular death *in vitro* (Gamba et al., 2021). A study conducted *in vivo* demonstrated that subcutaneous injection of 27-OHC promoted systemic inflammation and aggravated amyloidosis as well as cognitive deficit in APP/PS1 mice (Wang et al., 2020). Additionally, an increased expression of APP and BACE1, and a decrease in LRP1 and ADAM10 has been reported in the same mice (Zhang et al., 2019).

1.5. Proprotein Convertase Subtilisin/Kexin Type 9 (PCSK9) and cholesterol metabolism

Among the proteins involved in cholesterol metabolism, PCSK9 is a non-basic amino acid-specific convertase belonging to the proteinase K subfamily of subtilases. Native PCSK9 is a glycoprotein synthesized as a zymogen containing a signal peptide, a pro domain, a catalytic domain and a Cysteine and Histidine-rich C-terminal domain. In the endoplasmic reticulum, PCSK9 is rapidly self-cleaved by the catalytic domain at the FAQ152/SIPK site to release a mature heterodimer consisting of pro-domain segment masking the catalytic activity of PCSK9. This process and the presence of the C-terminal domain are required for PCSK9 secretion (Deng et al., 2020) (**Figure 5**).

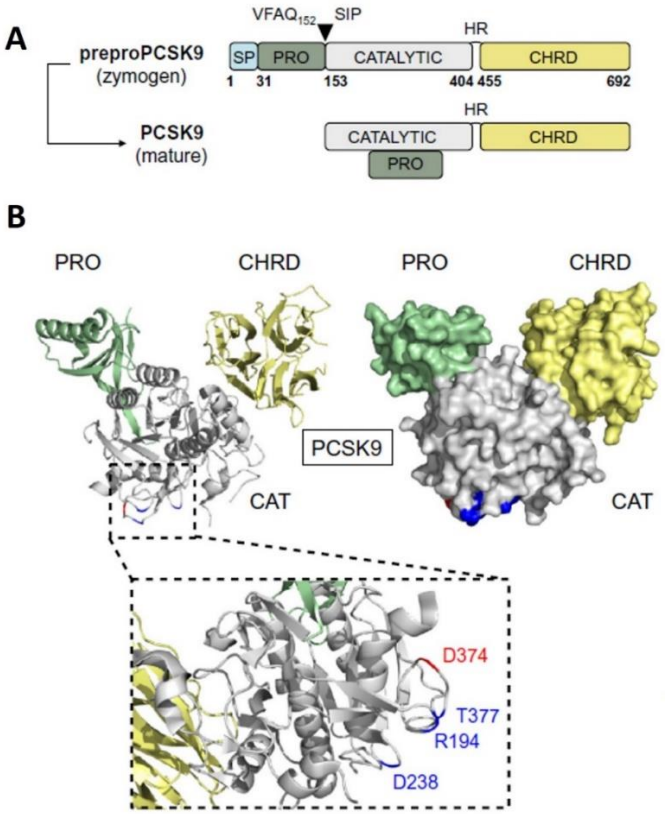

Figure 5. PCSK9 structure. A The human PCSK9 gene is located on chromosome 1p32.3 and is translated into a ~82-kDa zymogen in the ER. After removal of the SP (aa 1–30, light blue), human proPCSK9 is autocatalytically cleaved at position Q152 within the ER, resulting in mature PCSK9 comprising the PRO (aa 31–152, green), CAT (aa 153–404, gray), HR (aa 405–454), and CHRD (aa 455–692, yellow). PCSK9 is secreted as a heterodimer protein with its ~17 kDa pro-domain still bound to its catalytic domain to inhibit its catalytic activity. **B** Crystal structure of PCSK9 was visualized using MacPymol (Protein Data Bank ID code 2P4E). PCSK9 residues (R194, D238, T377, and D374) interacting with LDLR are emphasized (inset). PCSK9 residue D374, highlighted in red, is the site of D374Y gain of function mutation causing severe hypercholesterolemia (modified from Poirier and Mayer, 2013). Abbreviations: aa, amino acid; CAT, catalytic domain; CHRD, cysteine and histidine-enrich C-terminal domain; ER, endoplasmic reticulum; HR, hinge region; LDLR, low-density lipoprotein receptor; PRO, pro-domain segment; SP, signal peptide.

The most prominent role of PCSK9 is represented by the interaction with the LDLR in the liver. Therefore, PCSK9 has a significant role in peripheral cholesterol homeostasis by binding to LDLR, promoting its degradation and in turn, preventing recycling of most receptors involved in cholesterol uptake (Rashid et al., 2005). This ultimately reduces the LDL clearance, leading to increased LDL containing cholesterol (LDL-C) concentrations in the plasma. Once secreted by hepatic cells, PCSK9 directly interacts via the C-terminal domain with the epidermal growth factor repeat A domain of the LDLR at the cell surface, favouring the internalization of LDLR/PCSK9 complex into hepatocytes by clathrin-dependent endocytosis (Zhang et al., 2007). The presence of PCSK9 on LDLR disrupts its normal recycling and LDLR is directed to the lysosome compartment for degradation (Macchi et al., 2020). Thus, by interfering with LDLR recycling and promoting its degradation, PCSK9 acts as a regulator of the plasma LDL-C content (Tveten et al., 2012) (**Figure 6**). Notably, elevated plasma concentration of LDL-C is a contributing factor to various cardiovascular diseases (Mortensen and

Nordestgaard, 2020). Of note, mutations in the human *PCSK9* gene, located on chromosome 1p32.3, are associated with decreased or increased LDLR-degradating activity.

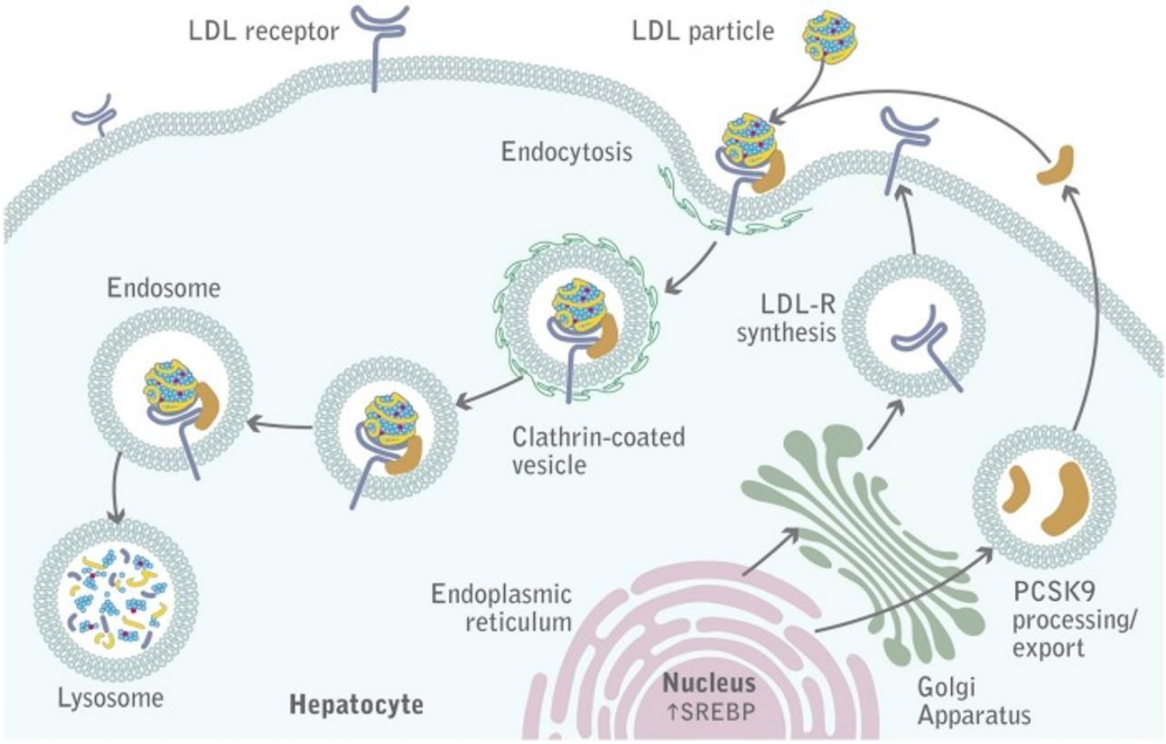

Figure 6. PCSK9-mediated degradation of LDLR. PCSK9 is mainly secreted by hepatocytes into the blood stream and exists in the plasma in an active and inactive form. The active form consists of a full-length heterodimer (~62 kDa) that is predominantly associated with the LDL particle, which protects PCSK9 from being cleaved by furin into its inactive form. The inactive heterodimer (~55 kDa), representing 15–40% of total circulating PCSK9, circulates freely and has at least a twofold lower affinity to LDLR and a limited ability to degrade it. A complex of LDL particle, LDLR, and PCSK9 is internalized into clathrin-coated pits and subsequently undergoes lysosomal degradation (modified from Lambert et al., 2012). Abbreviations: LDL, low-density lipoprotein; LDL-R, low-density lipoprotein receptor; PCSK9, pro-protein convertase subtilisina kekxin type 9; SREBP2, sterol-regulatory element-binding protein 2.

The gain of function mutations in PCSK9 cause hypercholesterolemia by reducing LDLR availability on the cell surface, thus increasing circulating LDL-C in the plasma of many human populations. On the other hand, loss of function variants results in the development of hypocholesterolemia, with low LDL-C levels and a decrease in the cardiovascular events (Horton et al., 2009; Costet et al., 2008). Although gain of function mutation is rare and occur in <0.1% of the general population, loss of function variants in *PCSK9* are present in 1% to 3% of adults. Blacks more commonly manifest Y142X and C679X nonsense *PCSK9* loss of function variants, which are associated with larger reductions in LDL-C than the missense R46L variant that is more common in whites. For example, there is some evidence that the *PCSK9* loss of function variants are associated with a lower prevalence of peripheral arterial disease and a reduced risk of coronary heart disease (Choen et al., 2006).

PCSK9 role in the brain

Almost all plasma circulating PCSK9 is derived from the liver, but is also expressed in other tissues including kidney, intestine, pancreas, and CNS. The exact role of PCSK9 in the brain, the most cholesterol-rich organ in the body, is only partially clarified.

PCSK9, firstly identified in primary cerebellar neurons as a mRNA upregulated during apoptosis, was originally called as neural apoptosis-regulated convertase-1 (Seidah et al., 2003). In fact, several studies suggested that PCSK9 promotes cell death through the extrinsic and intrinsic apoptotic pathways and likely acts through the c-Jun NH2-terminal kinase (JNK) pathway *in vitro* (Bingham et al., 2006). Interestingly, APOER2 has been shown to promote neuronal survival by inactivating the JNK pathway; a pro-apoptotic activity of PCSK9 may, at least in part, be exerted through controlling APOER2 levels (Wu et al., 2014).

PCSK9 is highly expressed in developing telencephalic neurons as well as in other cells with proliferative ability including hepatocytes and kidney mesenchymal cells. As concerns CNS development, PCSK9 is detectable at the start of neurogenesis (three-somite stage, 10.33 hours (h) post fertilization) in zebrafish and during telencephalon and cerebellum neurogenesis in mice (embryonic day 12.5 and from embryonic day 17 to post-natal day 15, respectively). However, in the adult brain, neuronal PCSK9 expression is restricted to specific areas, characterized by continued neurogenesis like cortical, intracranial, and cerebellar granule neurons in zebrafish and the rostral extension of the olfactory peduncle in rodents (Seidah et al., 2003).

PCSK9 promotes neurogenesis by driving neuronal differentiation, as its overexpression in mouse embryonic neural progenitor cells resulted in an increase in the number of postmitotic neurons and a *PCSK9* mRNA knocking down induces defective neurogenesis resulting in impaired neuronal development and premature embryonic death in zebrafish (Poirier et al., 2006). In contrast, the loss of PCSK9 in mice does not affect survival or the proper development of CNS structures (Rashid et al., 2005), and cognitive functions, such as motor learning and spatial memory abilities, are preserved (Pärn et al, 2023).

Given its expression in the adult brain, it was suggested that PCSK9 may regulate cholesterol metabolism in the CNS, containing almost 25% of the body's total cholesterol, with distinct cholesterol synthesis and regulation from peripheral tissues. Neither cholesterol nor PCSK9 are able to cross the BBB under normal conditions. One mechanism regulating the uptake of cholesterol in neuronal cells involves the degradation of APOERs by endogenous proteases such as PCSK9. These receptors bind APOE, the principal cholesterol carrier in the brain, and transport APOE-bound

cholesterol out of the pericellular fluid and into neurons, thus lowering cholesterol levels. The exact mechanism through which PCSK9 in the brain targets LDLR, VLDLR, and APOER2 for degradation is still unknown. In various cell lines, Poirier and colleagues demonstrated that PCSK9 enhances the degradation of VLDLR and APOER2, either through its co-expression or cell-surface internalization, in a catalytic-activity independent manner (Poirier et al., 2008). Conflicting data exist regarding the effect of PSKC9 on LRP1. Benjannet's research in 2004 found evidence of a degradation effect only on LDLR (Benjannet et al., 2004), while Canuel's later study demonstrated degradative activity *in vitro* on LRP1 and at the same time the lower affinity for PCSK9 that could explain other experimental results (Canuel et al., 2013).

In vivo studies conducted on *PCSK9* KO or human PCSK9-overexpressing mice demonstrated alterations in hepatic levels of LDLR without affecting brain LDLR, as well as VLDLR, and APOER2 levels (Liu et al., 2010). However, other studies demonstrated that LDLR expression is modulated by PCSK9 during brain development and after transient ischemic stroke (Rousselet et al., 2011). It is possible that modification of PCSK9 activity may result in reduced cholesterol uptake by neurons, thereby playing a role in the development of AD pathology (Koudinov and Koudinova, 2005).

These discrepancies, which may be due to cell- and tissue-specific functions of PCSK9 or its lower concentrations in the brain, underscore the need for further studies to unravel the role of PCSK9 in brain cholesterol homeostasis.

PCSK9 role in neuroinflammation

In the field of cardiovascular health, PCSK9 is known to be involved in the inflammatory pathway of atherosclerosis (Momtazi-Borojeni et al., 2019). Previous studies have reported the pro-inflammatory effect of PCSK9 in macrophages, which involves the TLR4/Nuclear factor kappa B (NFkB) pathway (Jaén et al., 2022; Badimon et al., 2021; Ricci et al., 2018; Tang et al., 2017).

Recently, a potential role of PCSK9 in neuroinflammation has been proposed. Apaijai and colleagues observed that the activation of glial cells was accompanied by an increase in levels of p-NFkB/NFkB in a rat model of cardiac ischemic reperfusion injury. Peripheral inhibition of PCSK9 was able to rescue the number and phenotype of the microglial and astrocytic cells (Apaijai et al., 2019), indicating that modulating systemic inflammation by lowering serum PCSK9 was able to produce central effects.

In addition, also APOE removal influences the inflammatory responses mediated by microglia and astrocytes in the brains of *APOE* KO neonatal mice (Liu et al., 2015). It is possible that PCSK9,

through its well-known degradative action on APOER, may be involved in neuroinflammatory processes by regulating LDLR and APOE levels. In an *in vitro* study conducted on lipopolysaccharide treated murine BV2 microglial cells and human THP-1 monocytes, it was found that APOE and APOE mimics reduced the activation of neuroinflammatory processes, including p44/42 mitogen-activated protein kinase (MAPK) and janus-activated kinase 2 (JAK2)/activator of transcription 3 (STAT3) pathways. Additionally, by interacting with LDLRs, APOE and APOE mimics reduced the lipopolysaccharide-induced secretion of tumor necrosis factor α (TNFα) and interleukin-6 (IL-6). This anti-inflammatory effect was prevented in the presence of PCSK9 (Wang et al., 2019).

However, due to the limited data available, further studies are necessary to investigate the involvement of PCSK9 in the systemic and local control of inflammation and immunity in the brain.

1.5.1. PCSK9 and AD pathogenesis

There is mounting evidence indicating that altered brain cholesterol metabolism and trafficking play a regulatory role in brain physiology leading to neurodegeneration (see above). Given the role of PCSK9 in apoptosis, lipoprotein receptor metabolism, and inflammation, PCSK9 might represent a pathogenic factor for AD development (Turri et al., 2022; Zuin et al., 2021; Marchi et al., 2019). Aging and cell death contribute to AD development; *in vitro* studies suggested a pro-apoptotic effect of PCSK9 by degrading APOER2, which confers neuronal survival (Kysenius et al., 2012). In addition, polymorphisms in the *APOER2* gene are associated with AD risk and adult *APOER2* KO mice had an accelerated loss of corticospinal neurons during normal aging (Ma et al., 2002). Moreover, in a mouse model lacking APOE and fed with a high-fat diet, an increase in *PCSK9* mRNA was observed accompanied by neuronal apoptosis in the Hip of mice (Zhao et al., 2017); on the contrary, *PCSK9* silencing mitigates neuronal apoptosis induced by cerebral ischemia, consequently reducing brain damage in mice (Wang et al., 2018).

PCSK9 may also exert a protective role by reducing Aβ production (Wu et al., 2014) and processing, but the exact mechanism is still unknown. Several lines of evidence have suggested that BACE1, the protease that produces toxic Aβ that accumulates in neuritic plaques of AD brains, might represent a target for PCSK9 activity. In fact, overexpressing PCSK9 in human neuroglioma H4 cells reduced levels of mature and immature forms of BACE1, while downregulating *PCSK9* with short interfering RNA increased expression of BACE1 in Chinese hamster ovary cells. Neocortex homogenate of transgenic mice lacking PCSK9 exhibit increased BACE1, C99 and total Aβ compared to controls (Jonas et al., 2008). On the other hand, pre-treatment with small molecule inhibiting PCSK9 resulted in attenuated dendritic spine loss, reduced cerebral Aβ deposits and neuroinflammation in a rat model of ischemia/reperfusion injury (Apaijai et al., 2019), suggesting a negative impact of PCSK9.

However, further studies did not indicate a direct regulation of BACE1 levels or APP processing by PCSK9 in the brains of mice (Liu et al., 2010; Fu et al., 2017).

The possible mechanisms underlying the involvement of PCSK9 in AD may be related to its ability to degrade the neuronal APOERs, as occurs with LDLR in the liver (Canuel et al., 2013; Kysenius et al., 2012; Poirier et al., 2008), thereby interfering with cholesterol uptake by neurons, the only process that ensures the supply of cholesterol to adult neurons for the maintenance of physiological functions (Mahley, 2016). Consistently, studies demonstrated that 3 mo *LDLR* KO mice exhibited impaired learning and memory. These mice also showed reduced hippocampal neurogenesis, neuronal and synaptic dysfunction, and increased hippocampal astrogliosis (de Oliveira et al., 2020a; Mulder et al., 2007; Mulder et al., 2004). However, these changes were not associated with the overproduction of endogenous Aβ.

While a direct mechanistic link between PCSK9 levels and protein aggregation in AD is still unknown, a growing number of studies supports the association between PCSK9 and AD (Adorni et al., 2019). A significant positive correlation between PCSK9 levels and p-181-tau and total tau levels in the CSF of subjects at risk has been demonstrated. Additionally, the presence of *PCSK9* risk allele rs4927193, associated with late-onset AD, affected both CSF biomarkers in a gender-specific manner (Picard et al., 2019).

In addition, increased PCSK9 levels have been reported in the serum and the CSF of mild cognitive impairment and AD patients compared to healthy controls, and correlated with Aβ accumulation (Kang et al., 2016; Courtemanche et al., 2018; Zimetti et al., 2017). Additionally, in AD groups, increased levels of PCSK9 were positively correlated with APOEε4 levels; individuals carrying *APOEε4* displayed the highest levels of PCSK9 in their CSF (Zimetti et al., 2017). Consistently, an increased expression of PCSK9 was observed in the frontal cortex of AD patients, which is a brain region affected by the pathology (Picard et al., 2019).

Recently, another study supporting the hypothesis of PCSK9 involvement in AD demonstrated an interfering activity of PCSK9 on astrocytic cholesterol metabolism *in vitro*. Specifically, recombinant PCSK9 induced a reduction in intracellular cholesterol content in U373 astrocytoma cells, which was worsened by co-incubation with $A\beta_{42}$ fibrils. At molecular level, this reduction was accompanied with a decrease in LDLR and APOER2 expression, resulting in a reduced cholesterol uptake. Notably, Aβ fibrils reduced the ABCA1-mediated cholesterol efflux, highlighting a direct relationship between amyloidogenesis in AD and cholesterol metabolism. Moreover, regardless Aβ, PCSK9 overexpression in human neuroblastoma SH-SY5Y cell line lead to lower cholesterol uptake by

decreasing LDLR and APOER2 expression, reducing intracellular cholesterol content (Papotti et al., 2022).

Another mechanism may involve LRP1, an APOER, expressed in several brain cell types including neurons and astrocytes. LRP1 is responsible for the transport and metabolism of cholesterol and clearance of several ligands into the circulation at the BBB, including toxic proteins (Sagare et al., 2012). Human studies revealed that AD patients have reduced Aβ clearance through the BBB, a process mediated by LRP1 on the surface of astrocytes under normal conditions. The expression of LRP1 decreases with aging in brain and that is even more severe in AD patients (Kang et al., 2000; Silverberg et al., 2010). In addition, postmortem studies demonstrated that LRP1 levels are decreased in neurons and increased in astrocytes surrounding Aβ plaques in human AD and PDAPP mouse brains (Arélin et al., 2002; Donahue et al., 2006) thus suggesting a direct relation between cell specific LRP1 expression and Aβ complex. In addition, in a human astrocytoma cell line, Aβ clearance assay showed that APOE can compete with Aβ for binding to LRP1, and the loss of LRP1 on the surface impairs the Aβ clearance (Verghese et al., 2013).

To unveil this link, several studies conducted in *in vitro* BBB model demonstrated a reduced Aβ transcytosis through the BBB due to PCSK9 degradation of LRP1 (Mazura et al., 2022); this process potentially results in increased plaque deposition in the brain. Of note, *in vivo* evidence confirmed that the inhibition of PCSK9 modulates LRP1 endothelial expression and promotes Aβ clearance across the BBB. In addition, the specific deletion of LRP1 in brain endothelial cells resulted in an increase of soluble brain Aβ, leading to worsened spatial learning and memory deficits in 5XFAD mouse model of AD (Storck et al., 2016).

Neuroinflammation, defined as activation of glial cells, such as microglia and astrocytes, has been only recently identified as a substantial contributor to AD pathogenesis, given the elevated levels of various inflammatory factors such as cytokines and chemokines surrounding senile plaques and affected neurons in the brains, observed in AD patients (Heneka et al., 2015). It was hypothesized that Aβ activates microglia through interaction with TLR4 leading to the activation of a pro-inflammatory response via NFκB pathways, causing neurotoxicity and neurodegeneration (Balducci et al., 2017; Walter et al., 2007). PCSK9 appears to induce a pro-inflammatory state in brain cells. Specifically, PCSK9 enhances the cluster of differentiation 36 (CD36) receptor expression in macrophages and microglial-like cells and their activation in the presence of Aβ and triggers the release of pro-inflammatory cytokines (Badimon et al., 2021; Jaen et al., 2022; Ricci et al., 2018; Tang et al., 2017). Moreover, it was found that PCSK9 may contribute to exacerbate neuro-inflammation through enhancing TLR4, promoting NFkB activation (Tang et al., 2012; Stewart et al., 2010).

1.6. Targeting cholesterol levels as a new therapeutic strategy for AD

Several recent reports have established a correlation between PCSK9 and the pathogenesis of AD, providing evidence that lipid dysmetabolism raises the risk of developing AD (O' Connel et al., 2020; Adorni et al., 2019; Ce et al., 2018). As a result, restoring normal levels of cholesterol and other lipids has emerged as a promising therapeutic approach to decrease the development of amyloidogenic aggregates and halt AD progression.

Since the identification of PCSK9, findings from *in vivo* studies have illustrated the pivotal role of SREBP2 in the regulation of cholesterol metabolism. Activation of SREBP2 occurs in response to low intracellular cholesterol levels, triggering *LDLR* gene expression. This, in turn, amplifies LDLR concentration, facilitating the increased clearance of LDL from circulation. Simultaneously, SREBP2 stimulates the expression of PCSK9, which accelerates the degradation of LDLR. Consequently, the coordinated interplay of SREBP2-mediated transcription of both LDLR and PCSK9 governs circulating LDL levels (Horton et al., 2003; Horton et al., 2002). These revelations have spurred the exploration and development of therapeutic agents aimed at reducing LDL levels by targeting PCSK9 activity.

PCSK9 inhibitors (PCSK9is) primarily serve as alternative treatment option for patients who are intolerant to HMGCR inhibitors, such as statins, experiencing statin-induced side effects, or have developed statin resistance (Dubuc et al., 2004). These drugs are used to treat hyperlipidemia, atherosclerosis, and related ischemic cardiovascular diseases, with remarkable efficacy (Liu et al., 2022). Particularly, monoclonal antibodies Evolocumab and Alirocumab, are commonly used to inhibit peripheral PCSK9 and increase the density of LDLRs on cell surfaces to treat hypercholesterolemia by lowering plasma cholesterol levels (Chaudhary et al., 2017).

Some clinical trials have highlighted a potential association between treatment with PCSK9 monoclonal antibodies and cognitive changes, given the reports of such adverse events with statins and intense LDL-C reduction (Robinson et al, 2015; Sabatine et al, 2015). However, FOURIER phase 3 clinical trials with larger sample sizes and longer follow-up periods indicated no significant neurocognitive adverse events linked to the combination of the PCSK9i Evolocumab and statin therapy (Gencer et al., 2020; Giugliano et al., 2017a; Sabatine et al., 2017). This finding was further confirmed by a recent meta-analysis (Bajaj et al., 2018; Harvey et al., 2018).

However, the impact of PCSK9i monotherapy on neurocognitive function remains poorly investigated.

Schlunk and colleagues observed the development of atherosclerosis in an established mouse model of familial dysbetalipoproteinemia (APOE*3Leiden.Cholesteryl Ester Transfer Protein or CETP model), after 6 weeks of a western type diet containing 1.25% Cho. Additionally, they found that treatment with the fully human anti-PCSK9 antibody CmAb1, equivalent to Evolocumab, had no impact on the learning, spatial or recognition memory abilities, or anxiety behavior of treated mice compared to control (Schlunk et al., 2021).

Another group conducted a study to determine the effect of administering different doses of Alirocumab subcutaneously to male rats with high-fat cholesterol diet-induced-AD-like conditions, to assess cognitive abilities. They found that the inhibition of PCSK9 mitigates cognitive deficits in a dose-dependent manner, which correlates with a decrease in hippocampal BACE1 and $A\beta_{42}$. Additionally, the improvement was accompanied by restoring cholesterol homeostasis, achieved by increasing LRP1-expression levels, and by reducing the neuroinflammatory state in the Hip of the treated groups (Abuelezz et al., 2021). However, the study was limited to males and did not examine the effects of histological abnormalities, such as plaque deposition, which are typically observed in areas affected by AD.

Although these antibodies have proven effective in decreasing circulating cholesterol levels, their use in treating neurodegenerative diseases like AD reveals various limitations, including monoclonal antibodies inability to penetrate the BBB. The BBB limits the access of PCSK9 (Rousselet et al., 2011) and particularly, of monoclonal antibodies like Alirocumab or Evolocumab, to the CNS (Mazura et al., 2022). Mazura's research shows that 6 mo female 5XFAD mice without LRP1 do not raise Aβ elimination from the brain post-treatment with monoclonal antibodies, which emphasizes the significance of LRP1 presence in mediating peripheral drug action (Mazura et al., 2022). However, this study does not explore the effect of PCSK9 inhibition on another typical marker of pathology, such as neuroinflammation.

When the BBB is functioning properly, tight junctions prevent the transcellular diffusion of antibodies across the capillary. Therefore, the penetration of antibodies into the brain is generally estimated to be approximately 0.1% in humans and animals alike (Tabrizi et al., 2010). However, in certain pathological conditions like diabetes or AD, the BBB may be compromised (Sousa et al., 2023; Rom et al., 2019).

Additionally, there are several drawbacks associated with these treatments, including their high costs, subcutaneous administration that can lead to poor adherence to indications, and potential immunogenicity with prolonged use. Furthermore, Inclisiran, which is the most recently approved short interfering RNA targeting liver PCSK9 synthesis, also has several downsides (Nishikido et al.,

2019). Consequently, there is a significant interest in searching affordable, orally bioavailable small molecules PCSK9is that can regulate directly or indirectly PCSK9 level (Kuzmich et al., 2022).

Over the past few years, numerous small molecules effective as direct inhibitors of PCSK9 have been developed (Evison et al., 2020; Petrilli et al., 2020). Various analogues with the ability to inhibit transcription of *PCSK9* were developed from natural compounds such as barberine, which is a well-known PCSK9i (Wu et al., 2019; Fan et al., 2021).

Although several small-molecule inhibitors have been patented and reported in the literature in recent years, no candidates suitable for clinical phase trials have been identified to date.

2. Aim of the work

Increasing evidence suggests that dysfunction in lipid metabolism and mutations in genes involved in lipid metabolism are main risk factors of many neurodegenerative disorders. Including AD. Recent findings indicate an involvement of PCSK9 in AD pathogenesis, due to its extrahepatic functions. In fact, PCSK9 is involved in neurodevelopment and apoptosis, and in adult healthy brain the expression of PCSK9 is restricted to certain areas.

The mechanisms underlying PCSK9 involvement in AD may relate to the ability to degrade the neuronal APOERs, as occurs for the LDLR in the liver resulting in neuronal cholesterol depletion (Papotti et al., 2022).

The causal role of PCSK9 in AD remains largely unknown and even genetic studies have not provided robust and conclusive evidence of an association between *PCSK9* variants and disease risk in humans.

This project aims to help fill knowledge gaps through two main objectives:

AIM1) elucidate the pathophysiological role of PCSK9 in AD in both *in vitro* and *in vivo* models; to this purpose, the possible deleterious effect of PCSK9 on neuroinflammation has been firstly investigated *in vitro* on Aβ fibrils-treated U373-MG human astrocytoma cell line. Subsequently, the impact of *PCSK9* genetic ablation in 5XFAD mice, a severe AD mouse model, has been assessed across multiple biochemical, histological, and behavioral parameters.

AIM2) identify a new class of PCSK9i with the ability to cross the BBB and modulate cholesterol metabolism; particularly, several newly synthesized small molecules (MR-compounds) derived from 2-pyridone have been preliminary tested *in vitro* on human HepG2. After identifying the safest and most effective molecules for inhibiting PCSK9, the *in vivo* tolerability has been assessed in C57BL/6J mice.

3. Materials and methods

Aim I

3.1. *In vitro* inflammation studies

The U373-MG human astrocytoma cell line, generously provided by Professor Bussolati from the Department of Medicine and Surgery at the University of Parma (Italy), was used to study inflammation *in vitro*. The authenticity of the cell line was confirmed through the Cell Line Authentication service by Eurofins Genomic in Ebersberg, Germany, prior to use. Cells were cultured in Dulbecco's modified Eagle's medium (DMEM) high glucose, supplemented by 10% fetal bovine serum (FBS), 1% penicillin/streptomycin solution (10.000 U/mL and 10 mg/mL, respectively), 1% 200 mM L-glutamine and 1% non-essential amino acids 100X solution. All cell culture reagents were acquired from EuroClone (Milan, Italy). Aβ and recombinant human PCSK9 (hPCSK9) were purchased from Bachem (cat. n. 4014447.1000) and Cayman Laboratories (cat. n. 20631), respectively. To assess the impact of PCSK9 on inflammation, cells were exposed to recombinant hPCSK9 (5 μg/ml) for 24 h, followed by a 24 h incubation with Aβ fibrils (1 μM) prepared from monomers as previously described (Papotti et al., 2022). After the incubation period, total mRNA was isolated with the iScriptTM RNA extraction kit from Bio-Rad and 1 μl of the total extract was employed for one-step quantitative polymerase chain reaction (qPCR) (one-step qPCR SYBR mix from A&A Biotechnology) using specific primer combinations as listed in **Table 1**. In each experiment, 18S ribosomal RNA (18S) served as the loading control. Following the treatment, to measure the secretion of monocyte chemoattractant protein-1 (MCP-1), the culture medium was collected, and enzyme-linked immunosorbent assay (ELISA) was conducted using the human MCP-1 ELISA kit from R&D Systems (cat. n. DCP00). The dose of recombinant hPCSK9 used for in vitro studies was based on literature (Adorni et al., 2017; Papotti et al., 2022) and manufacturer's recommendation, demonstrating its efficacy in reducing LDL uptake through LDLR degradation.

Data are presented as mean ± standard deviation (SD), and statistical comparisons were performed using one-way ANOVA followed by the Tukey's multiple comparison test. A value of $p < 0.05$ was considered statistically significant.

Table 1: List of primers used for Real-Time PCR analyses.

Function	Transcript	NCBI Ref Seq	Primer	sequence (5'- 3')
Housekeeping genes	*Gapdh*	NM_008084.3	Fw	CAAGGTCATCCATGACAACTTTG
			Rv	GGGCCATCCACAGTCTTCTG
	CypA	NM_008907.2	Fw	AGCATACAGGTCCTGGCATC
			Rv	TTCACCTTCCCAAAGACCAC
	Rer1	NM_026395.2	Fw	CCACCTAAACCTTTTCATTGCG
			Rv	TTTGTAGCTGCGTGCCAAAAT
Lipid-related genes	*ApoE*	NM_001305843.1	Fw	TGTGGGCCGTGCTGTTGGTC
			Rv	GCCTGCTCCCAGGGTTGGTTG
	Lpl	NM_008509.2	Fw	GGATGGACGGTAACGGGAAT
			Rv	GGCCACATCATTTCCCACCA
	Lrp1	NM_008512.2	Fw	AAGGATGACTGTGGAGAC
			Rv	ACTACAGCCACCATTATTC
	Lrp5	NM_008513.3	Fw	CAGTGTGCCCCTCTATGACC
			Rv	CGAATGACGTAGGGCCTGTA
	Cd36	NM_001159558.1	Fw	GGAGCAACTGGTGGATGGTT
			Rv	TACGTGGCCCGGTTCTACTAA
	Pcsk9	NM_153565.2	Fw	AACCTGGAGCGAATTATCCCA
			Rv	TTGAAGTCGGTGATGGTGACC
	Hmgcr	NM_001360165.1	Fw	CACGACCTAATGAAGAATG
			Rv	ATTGACCAACTGGATGAT
Microglial factors	*Stmn1*	NM_019641.4	Fw	AGGTGCTCCAGAAAGCCATC
			Rv	TCCACGTGCTTGTCCTTCTC
	P2ry12	NM_001357010.1	Fw	CATTGCTGTACACCGTCCTG
			Rv	AACTTGGCACACCAAGGTTC
	Ifitm3	NM_025378.2	Fw	CCGTGAAGTCTAGGGATCGGA
			Rv	GTGTGAAGGTTTTGAGCGTT
	Cd11B	NM_001082960.1	Fw	TACCGTCTACTACCCATCTGGC
			Rv	TTGGTGAGCGGGTTCTGG
	Cx3cr1	NM_009987.4	Fw	ACGGAGACAGTGGCGTTCAG
			Rv	CGGCCAGGCACTTCCTATAC
	Cst7	NM_009977.3	Fw	CAGGAAGACCATGCATCACCA
			Rv	ATAGAGTCCGCTTCAAGGCAG
Inflammatory mediators	*Il1B*	NM_008361.4	Fw	ATCTTTGAAGAAGAGCCCATCC
			Rv	TGTAGTGCAGTTGTCTAATGGG
	Il6	NM_031168.2	Fw	CCTCTCTGCAAGAGACTTCCATCCA
			Rv	GGCCGTGGTTGTCACCAGCA
	TnfA	NM_013693.3	Fw	TCTTCTGTCTACTGAACTTCGG
			Rv	AAGATGATCTGAGTGTGAGGG

	Ccl3	NM_011337.2	Fw	CATATGGAGCTGACACCCCG
			Rv	TCTTCCGGCTGTAGGAGAAGC
	Ccl6	NM_009139.3	Fw	CTGGCCTCATACAAGAAATGGA
			Rv	TTGGAGGGTTATAGCGACGAT
Human primers for *in vitro* analysis				
Housekeeping gene	*18S*	X03205.1	Fw	CGGCTACCACATCCACGGAA
			Rv	CCTGAATTGTTATTTTTCGTCACTACC
Immune cell factors	*Pyrin*	NM_000243	Fw	GTACTTCTCAGAAACCCTGCG
			Rv	AGATGAGGTTGGGGTAAGCG
	NLRP1	NM_033004	Fw	TTCTACGTTGGCCACTTGGG
			Rv	GTGAAGGTACGGCTATGCGG
	NLRP3	NM_001243133	Fw	AAGTGGGGTTCAGATAATGCACG
			Rv	CACTGGAATCTGCTTCTCACG
	NLRC4	NM_001199138	Fw	CCTACAGAATCAACGGCTGC
			Rv	TCAGGCCTTCAGCTAGTTTTATAGC
Inflammatory mediators	*TNFA*	NM_000594	Fw	ACTTTGGAGTGATCGGCC
			Rv	GCTTGAGGGTTTGCTACAAC
	IL6	NM_000600	Fw	GGTACATCCTCGACGGCATCT
			Rv	GTGCCTCTTTGCTGCTTTCAC
	IL1B	NM_000576	Fw	ATGCACCTGTACGATCACTG
			Rv	ACAAAGGACATGGAGAACACC

For each transcript analyzed in *ex-vivo* or *in vitro* experiments, forward (Fw) and reverse (Rv) primer sequences are indicated alongside with general functional classification and NCBI reference.

3.2. Transgenic mouse line generation and genotyping

A new transgenic mouse line was generated using a two-step approach. Progenitors with no *phosphodiesterase-6b retinal degeneration* (*Pde6b*^{rd1}) allele were acquired from Jackson Laboratories, Bar Harbor. First-generation littermates were obtained by crossing hemizygous 5XFAD mice (B6SJL-Tg (APPSwFlLon, PSEN1*M146L*L286V) 6799Vas/Mmjax, mentioned as 5XFAD^{Het}) and *PCSK9*$^{-/-}$ (B6;129S6-Pcsk9tm1Jdh/J, mentioned as PCSK9^{KO}) breeders. The 5XFAD mouse co-expresses two transgenes with a total of five FAD mutations: the human *APP* with three mutations (Swedish: K670N, M671L; Florida: I716V; London: V717I) and the human *PS1* with two mutations (M146L and L286V), both under the transcriptional control of the neuron-specific Thymus cell antigen-1 (Thy-1) promoter. 5XFAD^{Het}PCSK9^{Het} mice were selected from the progeny and crossed with PCSK9^{KO} mice to obtain 5XFAD^{Het}PCSK9^{KO} mice and their related controls (Wild type (Wt)-PCSK9^{Het} and Wt-PCSK9^{KO}, hereinafter referred to as Ctrls). Mice were housed in a controlled environment with stable temperature (22 °C ± 2), humidity (55% ± 10) and 12/12 h light/dark cycle;

food and water were available *ad libitum*. All animal procedures were approved by the Committee on Animal Health and Care of the University of Modena and Reggio Emilia (protocol number: n° 511/2019-PR) and conducted in accordance with National Institutes of Health guidelines. Mouse genotyping was performed on DNA samples extracted from ear tissue biopsies as described below.

The ear tissue (4 mm diameter, obtained using an ear punch) was incubated with 19 µL of lysis buffer (50 mM Tris-HCl, pH 8.0; 1 mM ethylenediaminetetraacetic acid (EDTA), pH 8; 20 mM NaCl; 1% Sodium Dodecyl Sulfate (SDS); milliQ H_20 + diethylpyrocarbonate (DEPC)) and 1 µL of Proteinase-K solution (20 mg/mL; Sigma) at 56°C for 120 minutes (min). After digestion, 180 µl of milliQ water was added, and the reaction was halted by incubating at 100°C for 10 min.

The progeny required to obtain the four experimental groups (Wt-PCSK9^{Het}; Wt-PCSK9^{KO}; 5XFAD^{Het}PCSK9^{Het}; 5XFAD^{Het}PCSK9^{KO}) was selected through polymerase chain reaction (PCR) using G2 GoTaq polymerase (Promega) and specific primers purchased from Sigma-Aldrich, following the protocols provided by Jackson Laboratories.

5XFAD cycling parameters: 94°C 3 min - (94°C 30 sec - 60°C 1 min - 72°C 1 min) x 30 cycles - 72°C 2 min and 4°C hold. Three different primers were used: mutant (product code: 27367): CGGGCCTCTTCGCTATTAC; common (product code: 37598): ACCCCCATGTCAGAGTTCCT; wt (product code: 37599): TATACAACCTTGGGGGATGG.

PCSK9 cycling parameters: 94°C 3 min - (94°C 30 sec - 60°C 1 min - 72°C 1 min) x 28 cycles - 72°C 2 min and 4°C hold. Three different primers were used:

- mutant (product code: oIMR5170): GATTGGGAAGACAATAGCAGGCATGC;
- common (product code: oIMR5171): ATTGTTGGAGGGAGAAGTACAGGGGT;
- wt (product code: oIMR5172): GGGCGAGCATCAGCTCTTCATAATCT.

Finally, gel electrophoresis was performed using 1.5% agarose (Thermo Scientific) in TAE (tris-acetate EDTA) buffer (0,04 M Tris-HCl; 0,02 M CH_3COOH; 0.01 M Na_2EDTA, pH 8.0) stained with 0.1% ethidium bromide. For 5XFAD: a 129 basepair (bp) band identifies the mutant allele while a 216 bp product the wt one. For PCSK9: ~320 bp mutant, 653 bp and ~320 bp heterozygote, 653 bp wt.

3.3. Behavioral tests

To assess the impact of PCSK9 loss *in vivo*, 10 mo male and female mice from the four experimental groups underwent a battery of behavioral tests. All animal behavior evaluations were conducted in a sound-proof room and recorded using the ANY-maze video tracking system (Stoelting) for automated analysis. To minimize bias, all tests were carried out by an operator unaware of the treatment. All

experimental mice were transferred to the behavior testing room 30 min prior to the trial to minimize stress. The behavioral apparatus was thoroughly cleaned with a 70% Ethanol (EtOH) solution after each animal's session to prevent any olfactory cue.

Elevated plus maze test

The elevated plus maze test is commonly used to measure anxiety in rodents (Locchi et al., 2008) and is based on the conflict between their aversion to open space and their natural inclination to explore new environments (Walf et al., 2007). Mice were tested in a plus-shaped apparatus with two opposing opened (40 x 9 cm) and two opposing closed (40 x 9 x 15 cm) arms separated by a central area (9 x 9 cm). The apparatus was elevated 70 cm above the floor level. The animal was placed in the central part with its head facing one closed arm and let free to explore the apparatus for 5 min. If the animal fell from the apparatus, the test was stopped, and the mice excluded from the analysis. Total distance travelled during test session, the number of entries (line-crossing) and time spent in the open and closed arms, were measured. The percentage of time spent in open arms was considered an anxiety index.

Morris water maze test

The MWM test was used to evaluate spatial learning and memory in mice (Runfola et al. 2021). Animals were placed in a circular black pool with a diameter of 120 cm filled with 22± 1°C water mixed with a white non-toxic paint, with nose facing the wall. Mice were allowed to swim for 90 seconds (sec) or until they found the location of a hidden circular platform with 11 cm diameter; during this learning phase mice were trained with 4 trials per day (starting from a different quadrant with different visual cues at each trial) for 7 days with a 30 min inter-trial interval. For each trial, the time to reach the platform, located in the South (S) quadrant of the pool was recorded (learning curve Day1-Day7, D1-D7). On the 8^{th} day the platform was moved to the East (E) quadrant and two cues were removed; mice underwent a second learning phase consisting in 4 trials per day with a 60 min inter-trial interval between D8-D13. To assess memory retention, the platform was removed on D14 and the animals were allowed to swim for 60 sec (probe test), and the latency to reach the platform area, total entries in the platform area and the % of time spent in target quadrant (E) were evaluated. The analysis of target search strategy was carried out according to current literature (Vorhees and Williams, 2006). Briefly, spatial accurate strategy and non-spatial strategy were distinguished considering individual swim paths during probe test and manually scored by two operators unaware of the treatment.

Fear conditioning test

To assess associative fear learning and memory, contextual and cued fear conditioning (FC) test was performed as described previously (Bianchi et al. 2010). For the purpose, the Ugo Basile any-maze controlled Fear conditioning System (Gemonio, VA, Italy), consisting of a plexiglass cage (21 × 24 × 30 cm) with an electrified grid floor (conditioning chamber), inside a soundproof cubicle with a light and a speaker, was used. Mice were exposed to a white noise throughout the task. The FC protocol took place in two consecutive days. On the first day (training phase), mice were placed in the conditioning chamber for a 2-min-acclimation period without any cue. Afterwards, animals were exposed to two 15 sec acoustic stimuli (80 dB, 2000 Hz-conditioned stimulus, CS) paired, during the last 2 sec, with an electric foot-shock (1.5 mA). This procedure was repeated, and mice were removed from the chamber 30 sec later. Before the start of each session, the grid floor of the apparatus was cleaned with 70% EtOH. On the second day, mice were returned to the same chambers in which training occurred (contextual session) for 5 min. Approximately 3 h later, mice were placed in a modified chamber (altered session) and after 5 min recording the CS was presented for 3 min (cued session) without shock. The new environment consisted of a grey smooth floor and walls with alternating black and white stripes. For each trial, every 10 sec, the blind operator manually recorded the presence or the absence of freezing behavior. Freezing was defined as the absence of body activities except for respiratory-related movements lasting longer than 1 sec.

3.3.1. Statistical analysis

All data, shown as mean ± standard error of the mean (SEM), were analysed with one-way ANOVA, two-way repeated measure ANOVA or chi square test, as appropriate, using the statistical package SPSS (version 26). Due to the unequal distribution of male and female mice in the experimental groups, and the documented impact of sex on behaviour and other AD related parameters (Forner et al., 2021; Oblak et al., 2021), the possible effect of sex on experimental parameters was preliminarily tested and, when a statistically significant difference was observed, sex was used as a covariate in the subsequent statistical analysis. $p < 0.05$ was considered as the level for a significant difference and $0.10 > p > 0.05$ as trend for a significant difference.

3.4. Immunohistochemical analysis

At 10 mo of age mice were anesthetized with isoflurane and sacrificed for histological analysis according to established protocols (Daini et al., 2021; Rigillo et al., 2018). Briefly, after intracardial infusion of 50 ml of 0.9% NaCl (saline solution), a 7 min-long perfusion was performed with cold 4% paraformaldehyde (PFA) (speed: 10 mL/min), brain was dissected out and postfixed in the same solution for 24 h, rinsed in a cryoprotective solution of 20% sucrose-phosphate buffered saline (PBS)-

(Sigma) for approximately 48 h and then in a 30% sucrose-PBS for 72 h. Brains were frozen using dry ice and stored at -80°C. Coronal 20 µm thick section series were cut at a cryostat (Leica CM1520), washed in cold PBS and stored at -20°C in a 50% glycerol-PBS solution until use. Brain sections were processed according to established protocols to investigate specific AD-linked alterations at synaptic and cellular level using specific antibodies (Abs, **Table 2**) through immunohistochemical (IHC) analysis. A pre-treatment with formic acid was performed for anti-Aβ Abs. Vectastain ABC-Horseradish Peroxidase (HRP) (cat. n. PK-4002; cat. n. PK-4001) kits were used for peroxidase 3,3'-diaminobenzidine (DAB) stainings; slices were placed on gelatinized glass slides, dehydrated, and mounted with Eukitt® mounting medium. Thioflavin-S (ThS, Sigma, cat. n. 1892) and Congo Red (Sigma, cat. n. 6277) stainings were performed according to established protocols (Daini et al., 2021).

Table 2: List of primary and secondary antibodies used for different applications.

Primary antibodies	**Host**	**Dilution**	**Source**	**Cat. N°**
anti-human Aβ/APP 6E10 (epitope human Aβ1-16)	mouse	1:500	Signet	n. 9300-10
anti-human Aβ 11A1 (epitope synthetic peptide of E22P-Aβ 10-35 part)	mouse	1:500	Tecan	n. 10379
anti-ionized calcium-binding adapter molecule 1 (IBA1)	rabbit	1:1000	Wako	n. 019-19741
anti-glial fibrillary acidic protein (GFAP)	rabbit	1:2000	Dako	n. Z0334
anti-synaptophysin (SYN)	mouse	1:1000	SYSY	n. 101111
anti-beta-site APP-cleaving enzyme 1 (BACE1)	rabbit	1:1000	Cell Signaling	n. 5606
anti-β tubulin (Tub)	rabbit	1:2000	Cell Signaling	n. 2146S
Secondary antibodies				
anti-rabbit IgG HRP	goat	1:200	Cell Signaling	7074S
anti-mouse IgG HRP	goat	1:200	Abcam	AB97245

3.4.1. Image and statistical analyses

All experimental procedures were performed blind on coded slides, by a minimum of two experimenters, to avoid biases. Immunolabeled brain slices were observed and captured using a Nikon Eclipse CiL microscope (with 10x and 40x Nikon plan fluor objectives) with a Nikon DS-Fi3 camera, maintaining consistent light conditions. Shading correction was applied prior to image acquisition to address microscope field illumination irregularities.

Assessing Aβ pathology, ThS- or Aβ-immunoreactive plaque analysis was performed on 10x images. Amyloidosis was evaluated within the neocortex (Nctx), and Hip (Bregma between -1.46 and -1.58 mm) and olfactory tubercle (OT) (Bregma between 0.7 and 0.2 mm from (Paxinos and Franklin, 2019)) through Nikon NIS-Elements D software (5.21.00v) or ImageJ Fiji software (1.53tv). Thanks

to specific tools, following manual selection, the acquisition of morphometric parameters of the plaques, including both the overall number and individual areas, was performed. Amyloid plaques in the considered regions of 5XFAD mice brain were classified according to their size into four ranges ($\leq$ 200, 200 – 500, 500 - 1000, and >1000 μm^2).

For SYN and BACE1 immunoreactivity (ir) analysis, three slices per mouse of somatosensory cortex (sCtx) (exclusively for BACE1) and cornu Ammonis 3 (CA3) field of Hip (Bregma between -1.46 and -1.58 mm from Paxinos and Franklin, 2019) were captured using a 10x objective. Subsequently, counterstaining with Nissl stain (only for SYN) was performed to enhance the delineation of Hip subregion boundaries. First, images underwent manual editing to eliminate edge artifacts, folds, and blood vessels. Then, thresholding was applied following a previously described method (Zoli et al., 1990b). The semi-quantitative densitometric and morphometric analyses, involving measurements of area, length, and thickness, were performed on CA3 region following established protocols (Zoli et al., 1990a; Zoli et al., 1992) using routines from Nikon NIS-Elements D and ImageJ Fiji softwares. For densitometric analysis, acquired images were converted to 32-bit grayscale and specific optical density (OD) values were obtained by subtracting the OD of the sampled region from the OD of non-specific staining (i.e., pyramidal layer for CA3 analysis). Moreover, BACE1-labelled brain slices were co-labelled with Congo Red stain and the number of double positive Congo Red^+-$BACE1^+$ plaques in sCtx were manually counted.

For glial fibrillary acidic protein (GFAP) and ionized calcium-binding adapter molecule 1 (IBA1) analysis, at least three slices/mouse from corpus callosum-cingulate cortex (CC-Cg) (Bregma between -0.5 and -0.9) (only for GFAP), Ctx (only for IBA1) and Hip (Bregma between -1.46 and -1.58 mm from Paxinos and Franklin, 2019) were acquired with 10x objective. Images were converted to 32-bit grayscale and binarized using the following thresholds: for GFAP staining -35, -20, -40, -5 grayscale units from the peak mean grey value for hippocampal CA1 field, CA3 field, dentate gyrus (DG) hilus and CC-Cg; for IBA1 staining -10 grayscale units for Ctx and DG hilus. The percentage of area occupied by positive cells, i.e., the area covered by pixels with gray value above the threshold, was analyzed using the "analyse particle" function of ImageJ. For microglia analysis, the count of $IBA1^+$ cells was performed manually within the area of interest using a 10x objective.

Values are shown as mean ± SEM or 95% confidence interval as appropriate. Group differences among different brain regions were analysed by means of two-way repeated measure ANOVA or two-way ANOVA. When a main effect of AD genotype was demonstrated, the main effect of PCSK9 expression in AD mice was tested by means of one- or two-way ANOVA as appropriate. Proportions were analysed by means of the Chi square test. Statistical analyses were performed through SPSS

software, with $p < 0.05$ as the level for a significant difference and $0.10 > p > 0.05$ as trend for a significant difference.

3.5. Total cholesterol quantification in mouse brain and serum

A separate group of mice was quickly sacrificed by decapitation under isoflurane anaesthesia and peripheral blood was collected into BD VACUTAINER plastic blood collection tube with serum clot activator and after 1 h incubation at room temperature (RT), serum was isolated by centrifugation at 2500 revolutions per minute for 10 min; then the fluorometric Amplex® Red Cholesterol assay (Thermo Fisher Scientific, MA, USA) was used to quantify TC following the manufacturer`s instructions. Moreover, the right cerebral hemisphere of each mouse was weighted and mechanically homogenized. The homogenates underwent lipid extraction with the Folch's Solution (Chloroform: Methanol (MeOH) [2:1] v/v) for 24h. The lipophilic phase was then evaporated under nitrogen stream and re-suspended in reaction buffer (0.5 M K_3PO_4, 0.25 M NaCl, 25 mM cholic acid and 0.5% Triton X-100). The fluorometric Amplex® Red Cholesterol assay was used to quantify cholesterol content in lipids extracted from brain following the manufacturer's instructions.

All data are shown as mean ± SEM. Statistical comparisons between the four genotypes were performed using the two-way ANOVA considering $p \leq 0.05$ as statistically significant and $0.10 > p > 0.05$ as a trend for a significant difference. Statistical comparisons between wild type B6SJL and 5XFAD mice were performed by one-way ANOVA, considering $p < 0.05$ as statistically significant.

3.6. Hydroxysterols quantification in mouse brain and serum

The three main hydroxysterols (24-OHC, 27-OHC and 25-OHC) quantification in mouse brain and sera was performed by liquid chromatography-tandem mass spectrometry (LC-MS/MS) (Borah et al., 2020; Del Puppo et al., 1998). Specifically, the lipophilic phase extracted through the Folch's solution from the left cerebral hemisphere, as well as from 0.2 ml of serum, were supplemented with Butylhydroxytoluene (BHT, 0.1 µg/µl) and underwent alkaline hydrolysis in 1 ml of 1 M NaOH in 90% EtOH for 2 h at 60°C. One ml of saline was then added and sterols were extracted with 2 ml of Petroleum Ether 40°-60°C. Dried lipid extracts were then resuspended in 2 ml of deionized H_2O supplemented with 5% v/v of MeOH and oxysterols were separated by Solid Phase Extraction Cartridges C18 (Waters, MA, USA), as previously described.

LC-MS/MS analysis was then carried out by adding to each dried sample 100 µl of MeOH enriched with 1 µg/µl of 24-, 25- and 27-deuterated OHC (Avanti Polar Lipids, AL, USA), used as internal standards. Samples were subsequently eluted through a C18 Synergi Hydro-RP column (150 mm x 3mm, 80A, 4 µm particles; Phenomenex, CA, USA), equipped with a C18 pre-filtering column. The

mobile phase was made of MeOH: acetonitrile: H_2O [14:1:0.6], added with 0.1% v/v formic acid. The elution was isocratic at a flow rate of 200 µl/min for 50 min, the injection volume was 20 µl and each sample was injected in duplicate. The analysis was carried out using an Agilent HP 1200 chromatographic system (Agilent Technologies, CA, USA), with a 100-vial capacity sample tray and coupled with a QTRAP 4000 triple quadrupole mass spectrophotometer (ABSCIEX, CA, USA), equipped with a pneumatically assisted ESI interface. Nitrogen (99.99% of purity) was used as a sheath gas and the auxiliary gas was delivered at flow rates of 45 and 5 arbitrary units, respectively. Optimized conditions of the interface were set as follows: ESI voltage 5.5 kV; declustering potential 35V; entrance potential 10V; collision exit potential 10V and capillary temperature 350°C. Experiments were performed under positive ion-selected reaction monitoring conditions, using nitrogen as a collision gas (pressure of 2.1 x 10-3 mbar). The analytical method performed was initially set up by using 24-, 25- and 27-OHC spiked with 1 µg/µl of the respective deuterated internal standard.

All data are shown as mean ± SEM and statistical comparisons were performed with one or two-way ANOVA as appropriate.

3.7. Total RNA extraction, reverse transcription, and real time polymerase chain reaction

A separate group of mice was sacrificed after deep anaesthesia, through intracardiac 50 ml injection of PBS, the brain was isolated, and the dissected Ctx was lysed by mechanical disruption in 1 ml of Trizol reagent (Qiagen), homogenized following the procedure provided by the manufacturer (RNeasy Plus Mini Kit, Qiagen) and processed for qPCR as described (Villacampa et al., 2015). Isolated mRNA was quantified with Thermo Scientific NanoDrop™ 1000 Spectrophotometer and reverse transcribed to cDNA using random hexamers and M-MLV Reverse Transcriptase (Promega Corporation) following the instructions provided by the manufacturer. Samples were heated at 70 °C for 5 min to eliminate any secondary structures, then incubated at 23 °C for 10 min, 1 h at 37 °C, and 5 min at 95 °C before being chilled at 4 °C using a thermocycler T Gradient (SimpliAmp, Applied Biosystem). The amount of cDNA was quantified with iTaq Universal SYBR Green Supermix (Bio-Rad) using a Bio-Rad RT-PCR iCycler. Each PCR reaction was performed in triplicate using 300 nM of each primer (**Table 1**), 10 µL of iTaq Universal SYBR Green Supermix (Bio-Rad), cDNA and nuclease-free water with the following cycling parameters: 2 min at 95 °C and 40 cycles of 5 min at 95 °C and 30 sec at 60 °C, followed by 5 sec at 95 °C and 65° to 95 °C melting curve analysis.

For gene expression analysis, mRNA levels of each experimental gene target were normalized to the average of three housekeeping genes. *Glyceraldehydes-3-phosphate dehydrogenase* (*Gapdh*), *retention in endoplasmic reticulum sorting receptor 1* (*Rer1*) and *cyclophilin A* (*CypA*) reference

genes were used as endogenous controls. For quantitative evaluation of changes, the comparative ΔΔCt method was performed, using as calibrator the average levels of expression of Wt-PCSK9^{Het} or B6SJL mice. Statistical comparisons were performed using one- or two-way ANOVA as appropriate, considering a value of $p \leq 0.05$ as statistically significant and $0.10 > p > 0.05$ as a trend for a significant difference.

3.8. Protein extraction and western blotting analysis

The dissected Hip was mechanically homogenized in RIPA lysis buffer containing 100 mM Tris-HCL, pH 7.5, 150 mM NaCl, 1.0 mM EDTA, 1% sodium deoxycholate, 1% TritonX100, 0.01% SDS, along with protease and phosphatase inhibitor cocktails. The standard Pierce bicinconic acid assay (BCA) was used to quantify the total protein extracted, as previously described (Almoda et al. 2015). After quantification, 5 µg of proteins from each sample were denatured, separated with electrophoresis, and transferred onto polyvinylidene difluoride (PVDF) membranes. The blots were subsequently blocked in 5% non-fat dried milk in tris-buffered saline (TBS) containing 0.1% of tween 20 at RT and incubated overnight at 4°C in the blocking buffer containing the primary antibodies (**Table 2**): mouse anti-synaptophysin (SYN, 1:1000, SYSY) and rabbit anti-ß tubulin (Tub, 1:2000, Cell Sign). On the following day, the membranes were incubated with specific secondary anti-rabbit or anti-mouse IgG-HRP-linked antibodies for 1 h at RT. The membranes were analyzed using the enhanced chemiluminescence system following the manufacturer's protocol (Pierce). Protein signals were quantified using GelPro analyzer and expressed as relative OD normalized to Tub. All data are presented as mean ± SEM. Values were subjected to two-way ANOVA analysis using SPSS, with sex as a covariate. Differences were considered statistically significant at $p < 0.05$.

Aim II

3.9. *In vivo* preliminary screening of novel anti-PCSK9 agents

MR compounds

The MR compounds were synthesized from 2-pyridone derivates with the published method (Giannessi et al., 2023). The cytotoxicity of MR compounds was preliminary *in vitro* evaluated on human HepG2 cells. Finally, tested for its PCSK9 inhibitory activity. The most promising compounds were selected for *in vivo* toxicity evaluation.

For *in vivo* preliminary screening, three putative PCSK9i (MR3, MR532 and MR533; molecular weight 440.39, 402.36 and 444.40 respectively) provided in a powder form by Marco Radi from the Department of Food and Drug Sciences, University of Parma (Italy) were tested. The SBC-115076 (Sigma, cat. n. SML1712) was used as a positive control due to its known inhibitory activity on PCSK9 (WIPO international publication number: WO 2014/150326 A1, Abdel-Meguid et al., 2014). All compounds were diluted in Super Refined™ Diethylene Glycol Monoethyl Ether (DEGEE)-LQ-(MH), CRODA (also known as Transcutol), also used as vehicle in control group.

Animals treatment and toxicity evaluation

Experimental mice were kept in a conventional animal facility with controlled temperature (20 - 24 °C) and humidity (60%) on a light/dark cycle of 12 h. Food and water were available *ad libitum*. A total of 24 healthy male 3 mo C57BL/6J mice (26 – 30g) were trained for three days in an open field (OF) apparatus (50 × 50 × 40 cm), in order to evaluate general motor activity. After basal acquisition phase the mice were randomly divided into five experimental groups: vehicle-treated group n = 4, SBC-115076-treated group n = 5 and MR-treated groups n = 5). From the third day of habituation in OF, each group of mice received a daily subcutaneous injection (SQ inj) for 7 consecutive days of 50 µl of Transcutol (vehicle) or PCSK9i corresponding to a dosage of 4mg/Kg and 40mg/Kg for the positive control SBC-115076 and MR compounds (MR3, MR532 and MR533), respectively.

To assess any potential signs of toxicity induced by the MR compounds, a modified SHIRPA test was used to monitor general health status including locomotion, appearance, behavior, and reflex reactions. Briefly, three days before the first SQ inj and throughout the entire experimental period, body weights were measured; then, mice behavior was evaluated in a cylinder filled with bedding material and scored as follow: activity status (inactive, active, hyperactive), tremor (existing, not existing), eyelid opening, fur appearance (neat, ragged, dull fur), epiphora (existing, not existing), vibrissae movement (existing, not existing), defecation (existing, not existing). Later, the mouse was placed in the OF in order to evaluate motor activity. During a 10 min lasting observation, the analysis

was performed according to following parameters: total distance travelled, mean speed, time spent in the corners and in the center, immediate locomotion after transfer, stereotypies.

All behavioural tests were conducted in a sound-proof room and recorded by ANY-maze video tracking system.

3.10.1 Sacrifice and tissue collection

At the end of the experiment session, 6 h after the last injections, mice were deeply anesthetized with Isoflurane and tissue, including brain and peripheral organs such as gut, kidney, spleen, and part of the liver were dissected out and immediately frozen in liquid nitrogen; the remain portion of the liver was postfixed in 4% PFA for further analysis.

3.10. *Ex vivo* analysis

For the evaluation of MR compounds activity on *Pcsk9* expression, an *ex vivo* analysis was performed. The liver was processed for qPCR as described (Villacampa et al., 2015), total RNA was extracted, and reverse transcribed in cDNA following Promega provided instructions. The amount of cDNA was quantified with iTaq Universal SYBR Green Supermix (Bio-Rad) using a Bio-Rad RT-PCR iCycler. Each PCR reaction was performed in triplicate using 300 nM of each primer (see primers sequence in **Table1**), 10 µL of iTaq Universal SYBR Green Supermix (Bio-Rad), cDNA and nuclease-free water with the following cycling parameters: 2 min at 95 °C and 40 cycles of 5 min at 95 °C and 30 sec at 60 °C, followed by 5 sec at 95°C and 65° to 95° melting curve analysis.

For gene expression analysis, mRNA level of experimental gene target *Pcsk9* was normalized to the housekeeping gene, *Gapdh*. For quantitative evaluation of changes, the comparative ΔΔCt method was performed, using as calibrator the average levels of expression of vehicle mice. Statistical comparisons were performed using the one-way ANOVA, considering a p-value ≤ 0.05 as statistically significant and # $0.10 > p > 0.05$ as a trend for a significant difference.

3.11. Histological analysis

After post fixation in 4% PFA, liver samples were incubated overnight at +4°C in 20% sucrose/PBS sterile solution and embedded in Tissue-Tek OCT (Kaltek, Padua, Italy). Samples were processed for optical microscopy by collecting 7 µm thickness sections using a cryostat. Sections were furtherly fixed with 10% Neutral Buffered Formalin, extensively washed in PBS and then subjected to hematoxylin/eosin staining. Slides were mounted with Eukitt® Quick-hardening mounting medium (Sigma-Aldrich, St. Louis, MO, USA), and coverslips were sealed. Images were acquired with a ZEISS AXIOVERT 200 microscope and visually examined by two different operators.

3.12. Statistical analysis

All data, shown as mean ± standard error of the mean (SEM). Differences between treatment groups were evaluated by one-way ANOVA. A probability value of $p < 0.05$ was considered statistically significant, using the statistical package SPSS (version 26).

4. Results
Aim I

4.1. *In vitro* PCSK9-mediated neuroinflammatory effects

The impact of PCSK9 on Aβ-mediated inflammatory response was first tested *in vitro*, in U373 human astrocytoma cell line. As shown in **Figure 7 A**, the incubation of U373 cells with Aβ fibrils [1 μM] induces an AD-like condition via the upregulation of *IL-6* and *IL-1β* mRNA expression. However, there was no significant change in *TNFα*. Additionally, similar results were obtained by incubating U373 cells with human recombinant PCSK9 [5 μg/ml]. Furthermore, it was shown that under co-incubation conditions recombinant PCSK9 potentiated the pro-inflammatory Aβ fibril effects by significantly increasing *IL6*, *IL-1β* and *TNFα* (**Figure 7 A**).

Since Aβ also stimulates chemokine release from astrocytes *in vitro* (Smits et al., 2002), the release of MCP-1 into the conditioned media was quantified by ELISA assay. The analysis demonstrated that U373 incubation with Aβ fibrils significantly increased the release of MCP-1, and this effect was further enhanced by 24 h pre-incubation with PCSK9 (**Figure 7 B**).

Data from literature reported that the pro-inflammatory response to Aβ in astrocytes is reliant on the overexpression of the scavenger receptor CD36 (Jones et al., 2013). In addition, the interaction between Aβ and CD36 triggers the assembly of a heterotrimeric complex along with TLR4 and TLR6 leading to downstream signaling inducing cytokines release and ROS production. Furthermore, CD36 activates the nucleotide-binding domain, leucine-rich–containing family, pyrin domain–containing-3 (NLRP3), a component of the complex known as the inflammasome, an intermediate step required for the IL-1β maturation process (Sheddy et al., 2013). All these processes influence microglia activation, neuroinflammation and neurodegeneration (Shmuel-Galia et al., 2017).

Based on these premises and the pro-inflammatory effect of PCSK9 described in macrophages (Ding et al., 2018) and astrocytes (**Figure 7**), we evaluated the expression of *CD36* in our experimental conditions. Results demonstrated that *CD36* expression was not changed compared to basal conditions (not shown).

Finally, the expression levels of inflammasome-related genes were analysed by qPCR. Results revealed that *NLRP1* and *NLRP3* as well as the nucleotide-binding domain leucine-rich repeat-containing protein family caspase activation and recruitment domain-containing protein 4 (*NLRC4*) are significantly upregulated by Aβ treatment, whereas incubation with PCSK9 had no significant effect. Of note, the co-incubation with PCSK9 had an additive effect on mRNA levels of *Pyrin*, *NLRP1* and *NLRP3*, and *NLRC4*, although it was statistically significant only for *NLRC4* (**Figure 7**

C). Nevertheless, these findings provide additional support for the role of PCSK9 in promoting the inflammatory response in Aβ fibril exposed-U373 astrocytoma cell line.

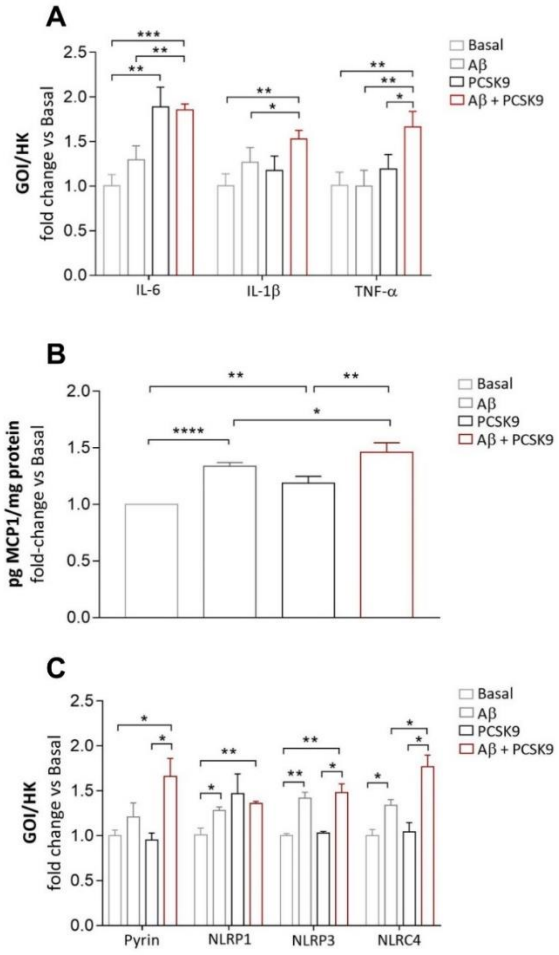

Figure 7. Effects of PCSK9 on Aβ-induced inflammation in U373 astrocytoma cell line. A *IL-6*, *IL1β* and *TNF-α* mRNA expression, with 18S ribosomal RNA (18S) as endogenous control, were measured by qPCR under different experimental conditions: basal, after treatment with Aβ fibrils (1 µM), after treatment with human recombinant PCSK9 (5 µg/ml) and after consecutive incubation of PCSK9 and Aβ fibrils. **B** MCP-1 secretion in conditioned media from U373 cells was measured by ELISA assay under different experimental conditions. **C** Inflammasome-related genes expression, with 18S as endogenous control, were measured by qPCR under different experimental conditions. Experimental conditions were tested in triplicate and data are expressed as mean ± SD. Statistical analyses were performed using the one-way ANOVA with a Tukey's multiple comparison test (see **Table 3** for statistical supplementary information). * $p < 0.05$; ** $p < 0.01$; *** $p < 0.001$; **** $p < 0.0001$.

Table 3: Supplementary statistical report of *in vitro* analyses (**Figure 7**).

Fig.7	Cytokine mRNA (A)	*IL6*	***	F(3,8)=24.05, p=**0.0002**	one-way ANOVA
		IL1B	*	F(3,8)=7.34, p=**0.011**	
		TNFA	**	F(3,8)=10.52, p=**0.003**	
	MCP-1 (B)	MCP-1	**	F(3,4)=27.4, p=**0.004**	one-way ANOVA
	Inflammasome mRNA (C)	*Pyrin*	*	F(3,8)=5.53, p=**0.023**	one-way ANOVA
		NLRP1	ns	F(3,8)=2.75, p=0.112	
		NLRP3	***	F(3,8)=17.61, p=**0.0007**	
		NLRP4	**	F(3,8)=14.15, p=**0.0015**	

4.2. *In vivo* and *ex vivo* effects of PCSK9 genetic ablation in 5XFAD mice

4.2.1. Impact of PCSK9 loss on 5XFAD mouse behavior and cognitive functions

Elevated Plus Maze (EPM)

The EPM was used to assess exploratory and anxiety-like behavior in 10 mo Wt-PCSK9^{Het}, Wt-PCSK9^{KO} (hereinafter mentioned as controls, Ctrls), 5XFAD-PCSK9^{Het}, and 5XFAD-PCSK9^{KO} mice. The motor abilities as well as the innate/spontaneous exploratory behavior were assessed by measuring the distance travelled and total arm entries during test duration; results demonstrated no significant differences between groups (**Figure 8 A, B**).

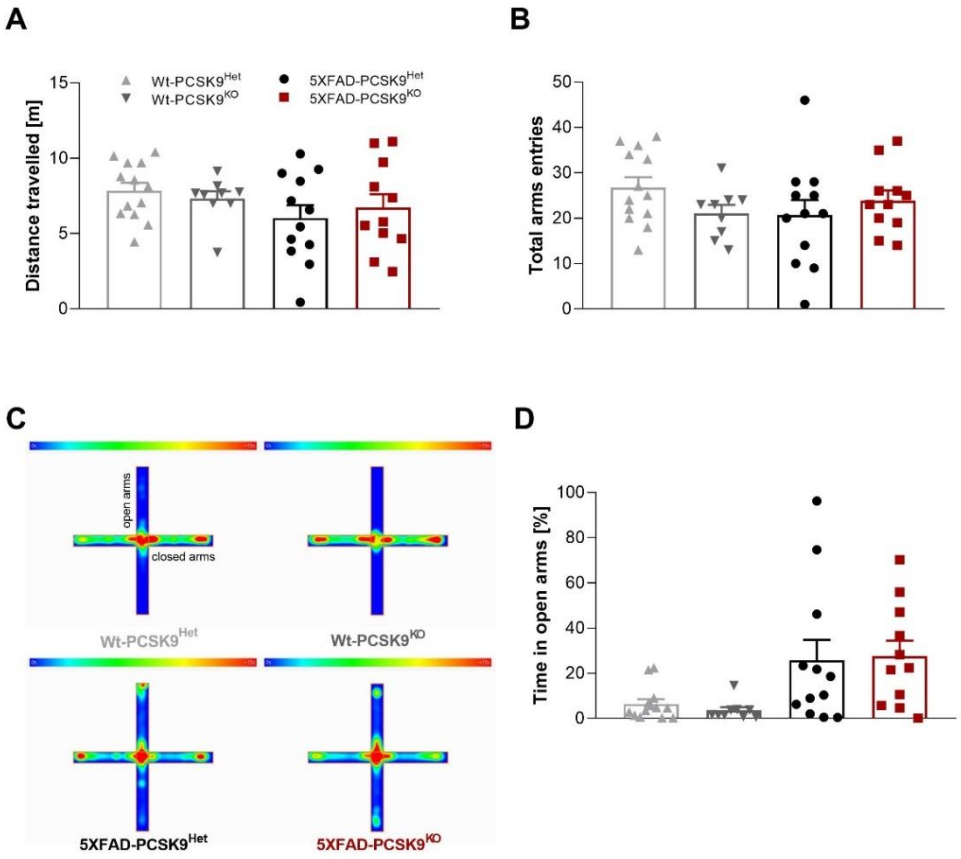

Figure 8. Effect of PCSK9 genetic ablation on motor abilities, exploratory and anxiety-like behavior in EPM. A,B The analysis of distance travelled, as an index of locomotor activity **A**, and total entries in the arms of EPM, as an index of exploratory behavior **B** during test were similar in all experimental groups. **C** Occupancy plot showing the position occupied by experimental groups during test. The color scale represents the average time spent in the different zones of the EPM. **D** The percentage of time spent in open arms of the EPM was significantly higher in AD mice without any effect of PCSK9 deletion. Data are shown as mean ± SEM (**Panels A, B, D**) and analyzed by two-way ANOVA with 5XFAD and PCSK9 expression as factors, and sex as covariate (see **Table 4** for statistical details). Experimental groups: Wt-PCSK9^{Het}, n = 13; Wt-PCSK9^{KO}, n = 9; 5XFAD-PCSK9^{Het}, n = 12; 5XFAD-PCSK9^{KO}, n = 11.

Furthermore, as previously observed by others (Jawhar et al., 2012; Forner et al., 2021), 10 mo 5XFAD mice spent more time in the open arms, an index of decreased anxiety-like behavior (**Figure 8 C, D**, see **Table 4** for statistical information). Additionally, a significantly higher ratio of open arm

entries to total arm entries was observed in 5XFAD mice (data not shown) compared to Ctrls. However, no effect due to PCSK9 loss was found. Detailed statistical report is summarized in **Table 4**.

Morris Water Maze

To unveil the impact of PCSK9 loss in cognitive decline due to AD-like pathology, the MWM task was used. Preliminary data have shown that the spatial learning abilities and memory are significantly impaired in 10 mo 5XFAD mice compared to Wt B6SJL (**Figure 9 A, B**).

Subsequently, the MWM test was conducted to compare the performance of 10 mo Ctrls, 5XFAD-PCSK9^{Het} and 5XFAD-PCSK9^{KO} mice. Swimming motor ability was preserved in these mice; in fact, the mean swimming speed was not different between all tested groups throughout the entire experiment (not shown). The time needed to find the platform (escape latency) was averaged for each day (4 trials/day) to obtain the learning curve of each experimental group. Repeated measure two-way ANOVA analysis demonstrated that the learning curves of the groups were significantly different with a main effect of the 5XFAD factor (see **Table 4** for statistical details).

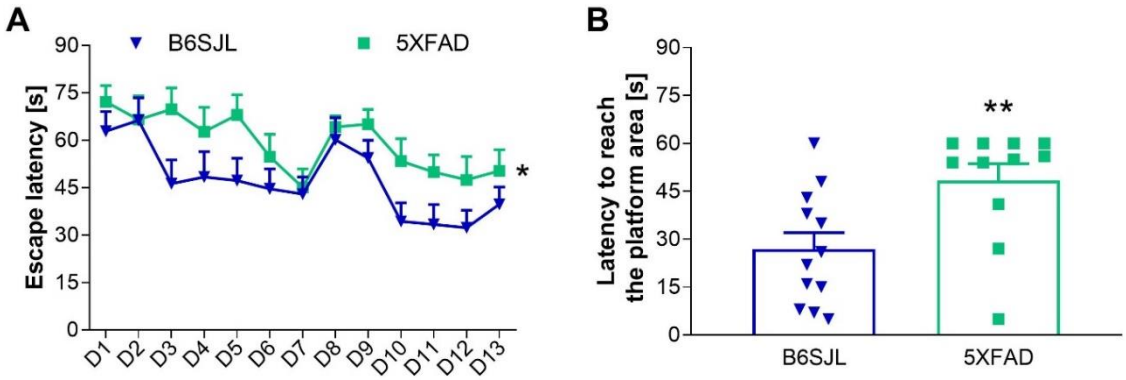

Figure 9: Learning and memory are impaired in 10 mo 5XFAD mice. A Analysis of MWM learning curve. The time needed to find the platform (escape latency) was averaged for each day (4 trials/day) and analyzed by two-way repeated measures ANOVA with training day and genotype as factors, * $p < 0.05$ (see **Table 4** for supplementary statistical information). **B** An increased time to reach the platform in the trained target quadrant (east (E) quadrant) during the probe test in 5XFAD mice was recorded. Statistical analysis according to one-way ANOVA, ** $p < 0.01$ (see **Table 4** for supplementary statistical information). Data are shown as mean ± SEM. Experimental groups: B6SJL, n = 12; 5XFAD, n = 11.

Particularly, 5XFAD-PCSK9^{KO} mice exhibited a significantly reduced escape latency and achieved a level of performance comparable to that of Ctrls (**Figure 10 A**). However, during the reversal test on day 8, when the platform position was changed, the statistical analysis showed a main effect of the 5XFAD factor showing that 5XFAD mouse groups required more time to reach the platform in the new position (see **Table 4** for statistical details). After a 24 h rest period from the last learning session, the four experimental groups were given a 60 sec swim in the pool without the platform for

testing long term memory in the probe test. The percentage of time spent in the E quadrant, the target location, was then recorded. The analysis of the probe test revealed that 5XFAD mice spent significantly less time in the E quadrant, regardless of PCSK9 deficiency (**Figure 10 B**).

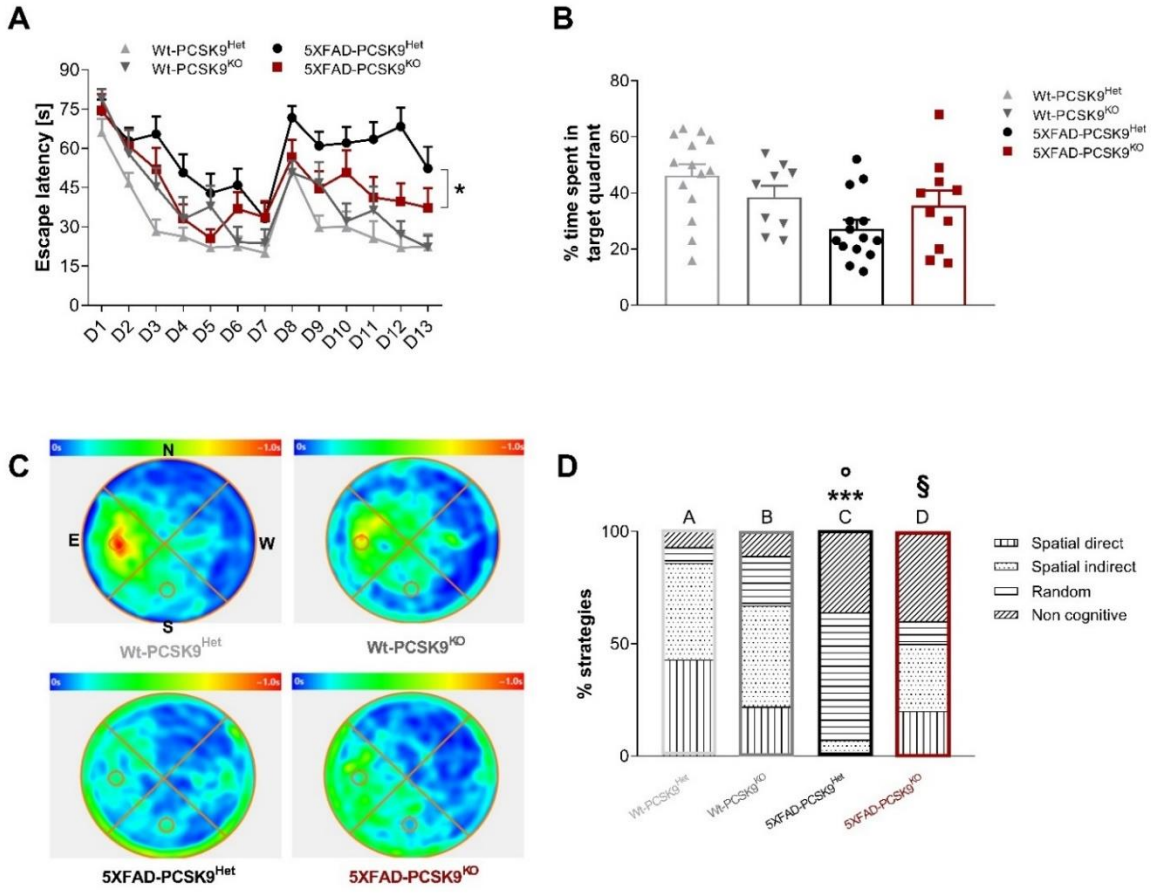

Figure 10. Effect of PCSK9 loss on learning abilities and memory in MWM task. A Analysis of MWM learning curve. The time needed to find the platform (***escape latency***) was averaged for each day (4 trials/day) and analyzed by two-way repeated measures ANOVA with training day and genotype as factors and sex as covariate. The comparison between 5XFAD groups was performed by two-way repeated measures ANOVA (**Table 4** for statistical report): * $p < 0.05$. **B** % of time spent in the target quadrant during 60 sec of probe test was analyzed by a two-way ANOVA with 5XFAD and PCSK9 expression as factors, and sex as covariate (see **Table 4** for supplementary statistical information). **C** Occupancy plots for grouped data. The colour scale represents the average search time during probe test. **D** Analysis of search strategy. Data are analyzed by chi-square test (see **Table 4**): * vs Wt-PCSK9^{Het}; ◦ vs Wt-PCSK9^{KO}; § 5XFAD-PCSK9^{KO}. ◦,§ $p < 0.05$; *** $p < 0.0001$. Data are shown as mean ± SEM (**Panels A-B**). Experimental groups: Wt-PCSK9^{Het}, n = 14; Wt-PCSK9^{KO}, n = 10; 5XFAD-PCSK9^{Het}, n = 15; 5XFAD-PCSK9^{KO}, n = 12. Abbreviations: E, east; N: north; S, south; W, west.

The development of a quadrant and platform position specific preference is shown in **Figure 10 C** by occupancy plots of grouped data. Although no difference was observed in the probe test between the 5XFAD mice, heat maps showed less focused sampling of the maze and reduced dwell time in the target quadrant in the 5XFAD-PCSK9^{Het} group. To evaluate learning quality in the MWM task, we measured the accuracy of swim trajectories displayed by mice to locate the platform during the probe session. Our analysis of search strategies revealed that 5XFAD-PCSK9^{KO} mice exhibited a significant increase in directed strategies and a decrease in non-targeted search approaches (random and non-

cognitive) compared to 5XFAD-PCSK9^{Het} mice (chi-square test p = 0.0437, see **Table 4**) (**Figure 10 D**).

Altogether, these findings demonstrated that the absence of PCSK9 in 5XFAD mice results in enhanced performance in learning and memory tasks, along with an improved search strategy for locating the platform position.

Fear Conditioning

To investigate associative and contextual fear-related memory and the effects of PCSK9 loss in 5XFAD mice, our experimental mice were tested in the FC paradigm. Before testing, the mice were given 2 min to habituate to the test chamber and their behaviour was recorded; obtained results demonstrated that both Ctrls and 5XFAD mice had comparable exploratory activity of the new environment, measured by recording the distance travelled, and spontaneous freezing behavior that amounted to less than 15% of the experimental time (not shown).

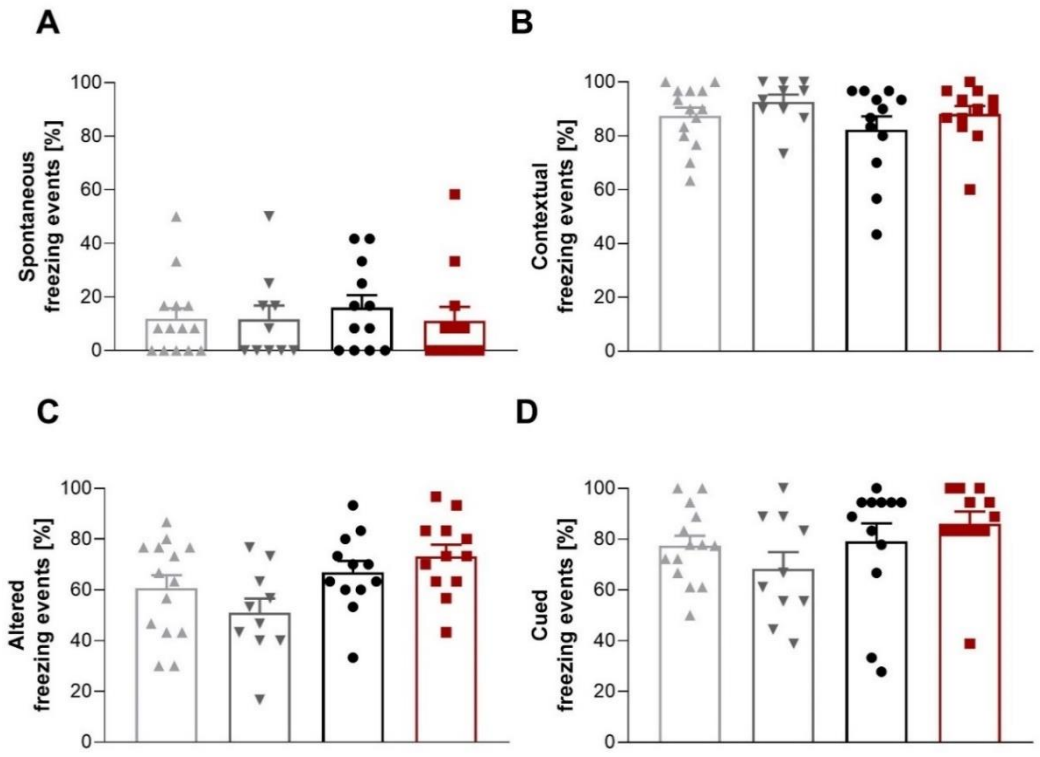

Figure 11. Effect of PCSK9 loss on contextual memory formation in 10 mo AD mice in a FC paradigm. A-D Manually recorded freezing events, measured as the absence of movements except respiration, lasting at least 1 sec and counted every 10 sec during the different session of FC test (data are represented as number of events / total possible events during session * 100). **A** Spontaneous freezing event during 2 min habituation session prior conditioning. **B** Freezing events recorded after 24 h from conditioning **(repeated shock)** in the same conditioning room during 5 min ***contextual session*** **(no shock)**. **C** Freezing events recorded after 3 h from contextual session in a modified environment during 5 min ***altered session*** **(no shock)**. **D** Freezing events recorded in an altered environment during 3 min ***cued session*** **(acoustic tone, no shock)**. Data are shown as mean ± SEM. Experimental groups: Wt-PCSK9^{Het}, n = 14; Wt-PCSK9^{KO}, n = 10; 5XFAD-PCSK9^{Het}, n = 12; 5XFAD-PCSK9^{KO}, n = 12.

In addition, no differences in the number of spontaneous freezing behavior were observed between the experimental groups during pre-conditioning session (see **Figure 11 A**). Then, 24 h after the conditioning, mice were re-exposed to Context A to test contextual memory retrieval; the number of freezing events, measured during 5 min session (contextual), increased for all experimental groups (**Figure 11 B**). These data suggest that contextual associative memory is preserved in 5XFAD mice. Subsequently, 3 h after the context test session, all groups were tested in the altered test session (context B) and showed a global decrease in the number of freezing events compared to the contextual test (**Figure 11 C**). However, an increased number of freezing events was observed in 5XFAD mice without any influence of PCSK9 loss (see **Table 4** for statistical information). Finally, mice were subjected to a cued test session, in which the acoustic tone was administered without any foot shock in context B; results demonstrated that all experimental groups displayed similar freezing behavior indicating a fear memory association.

These data indicate that fear learning and associative memory were intact in 10 mo 5XFAD mice during contextual and cued session. However, the higher freezing behavior during altered session of 5XFAD mice suggests a possible reduced ability to discriminate and dissociate the novel environment from the one where conditioning was assessed, compared to the Ctrls. Moreover, the absence of PCSK9 did not counteract the spatial discrimination impairment observed in 5XFAD mice. See **Table 4** for more statistical information.

Table 4: Statistical supplementary report of *in vivo* analyses (**Figure 8-11**).

Fig.8	**EPM**	distance travelled (A)	ns	**Global analysis:** Sex F(1,44)=0.055, p=0.816; PCSK9 KO F(1,44)=0.020, p=0.889; 5XFAD F(1,44)=4.403, p=0.129, PCSK9*5XFAD F(1,44)=0.514, p=0.477	two-way ANOVA
		total arms entries (B)	ns	**Global analysis:** Sex F(1,44)=3.225, p=0.080; PCSK9 KO F(1,44)=0.031, p=0.861; 5XFAD F(1,44)=0.123, p=0.728, PCSK9*5XFAD F(1,44)=1.402, p=0.243	
		% time spent in open arms (D)	ns	**Global analysis:** Sex F(1,44)=4.387, p=**0.043**; PCSK9 KO F(1,44)=0.193, p=0.663; 5XFAD F(1,44)=11.059, p=**0.002**, PCSK9*5XFAD F(1,44)=0.970, p=0.331	
Fig.9	**MWM**	daily escape latency (A)	*	Sex F(1,20)=0.225, p=0.640; 5XFAD F(1,21)=4.587, p=**0.044**; days of training F(12,252)=6.665, p<**0.001**; Genotype*days of training F(12,252)=0,9138, p=0.534	two-way repeated measure ANOVA
		latency to reach the platform area (B)	**	Sex F(1,20)=1.418, p=0.248 5XFAD F(1,22)=8.393, p=**0.009**	one-way ANOVA
Fig. 10	**MWM**	daily escape latency (A)	*	**Global analysis:** Sex F(1,42)=8.378, p=**0.005**; PCSK9 F(1,42)=1.018, p=0.319; 5XFAD F(1,42)=15.003, p<**0.001**; days of training F(1,42)=7.203, p<**0.001**; days of training*5XFAD*PCSK9 F(1,42)=1.057, p=0.394; 5XFAD*PCSK9 F(1,42)=4.629, p=**0.037**	two-way repeated measure ANOVA

			*	**Analysis in 5XFAD mice:** Sex F(1,21)=4.976, p=**0.037**; PCSK9 F(1,21)=4.737, p=**0.041**; days of training F(11,21)=3.654, p<**0.001**; days of training*PCSK9 F(12,21)=1.271, p=0.236	
		D8-D13 of learning		Days of training (1,43)=38.208, p<**0.001**; genotype (1,43)=9.456, p<**0.001** **Bonferroni post-hoc analysis:** Wt-PCSK9^{Het} vs Wt-PCSK9^{KO}, p=1.000; Wt-PCSK9^{Het} vs 5XFAD-PCSK9^{Het}, p**<0.001;** Wt-PCSK9^{Het} vs 5XFAD-PCSK9^{KO}, p=0.265**;** Wt-PCSK9^{KO} vs 5XFAD-PCSK9^{Het}, p=**0.003**; Wt-PCSK9^{KO} vs 5XFAD-PCSK9^{KO}, p=1.000; 5XFAD-PCSK9^{Het} vs 5XFAD-PCSK9^{KO}, p=0.087	one-way repeated ANOVA
		D8 of learning	ns	**Global analysis:** Sex F(1,46)=2.208, p=0.145; PCSK9 KO F(1,46)=1.901, p=0.175; 5XFAD F(1,46)=7.138, p=**0.011**, PCSK9*5XFAD F(1,46)=2.654, p=0.111	two-way ANOVA
		% time spent in the target quadrant (B)	ns	**Global analysis:** Sex F(1,42)=3.353, p=**0.074**; PCSK9 KO F(1,42)=0.068, p=0.794; 5XFAD F(1,42)=5.454, p=**0.024**, PCSK9*5XFAD F(1,42)=2.216, p=0.144	two-way ANOVA
		% strategies (D)		Wt-PCSK9^{Het} vs Wt-PCSK9^{KO}, p=0.6307; Wt-PCSK9^{Het} vs 5XFAD-PCSK9^{Het}, p=**0.0005**; Wt-PCSK9^{KO} vs 5XFAD-PCSK9^{Het}, p=**0.0241**; Wt-PCSK9^{KO} vs 5XFAD-PCSK9^{KO}, p=0.5261; 5XFAD-PCSK9^{Het} vs 5XFAD-PCSK9^{KO}, p=**0.0437**	chi square test
Fig. 11	**FC**	freezing events (Hab)	ns	**Global analysis:** Sex F(1,47)=0.229, p=0.635; PCSK9 KO F(1,47)=0.229, p=0.634; 5XFAD F(1,47)=0.205, p=0.653, PCSK9*5XFAD F(1,47)=0.363, p=0.550	two-way ANOVA
		freezing events (Contextual)	ns	**Global analysis:** Sex F(1,47)=0.123, p=0.727; PCSK9 KO F(1,47)=2.407, p=0.128; 5XFAD F(1,47)=1.559, p=0.219, PCSK9*5XFAD F(1,47)=0.001, p=0.978	
		freezing events (Altered)	ns	**Global analysis:** Sex F(1,47)=3.273, p=0.077; PCSK9 KO F(1,47)=0.017, p=0.895; 5XFAD F(1,47)=10.497, p=**0.002**, PCSK9*5XFAD F(1,47)=1.185, p=0.282	
		freezing events (Cued)	ns	**Global analysis:** Sex F(1,47)=0.321, p=0.574; PCSK9 KO F(1,47)=0.063, p=0.804; 5XFAD F(1,47)=2.539, p=0.118, PCSK9*5XFAD F(1,47)=2.295, p=0.137	

4.2.2. Aβ pathology

In order to correlate improved cognitive performance with histological markers of AD, the effects of PCSK9 ablation in modulating brain amyloidosis were assessed in 5XFAD mice. Brain sections from 10 mo 5XFAD-PCSK9^{Het} and 5XFAD-PCSK9^{KO} mice were processed by means of IHC; different plaque types were visualized by using different antibodies against Aβ and APP (anti-6E10 Ab) or Aβ42 neurotoxic oligomers (anti-11A1 Ab) and standard ThS staining for β-sheet structures, a marker for fibrillar and compact Aβ. After images capture, quantitative analysis was conducted by measuring the number and size (expressed in area units, μm^2) of $A\beta^+$ plaques. The absence of plaque pathology was confirmed throughout the entire brain in Ctrls mice (not shown).

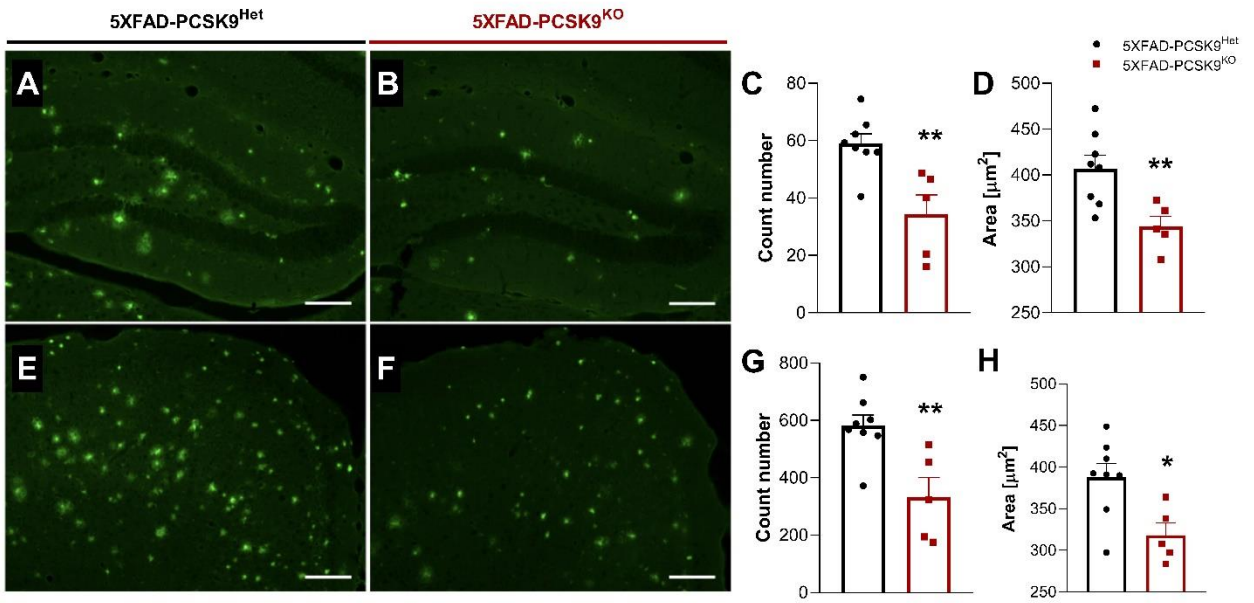

Figure 12. Plaque deposition is reduced in 5XFAD mice in absence of PCSK9. A-B, E-F Representative images showing ThS^+ plaque in DG (**A-B**) and Nctx (**E-F**) of 10 mo 5XFAD-PCSK9^{Het} and 5XFAD-PCSK9^{KO} mice. Scale bar = 200 µm. **C-D, G-H** Quantitative analysis of plaque count (**C,G**) and area (**D,H**) in DG and Nctx of 5XFADPCSK9^{Het} and 5XFAD-PCSK9^{KO} mice. Data are shown as mean ± SEM. Statistical analysis according to two-way ANOVA: * $p < 0.05$, ** $p < 0.01$; sex was used as covariate as appropriate (See **Table 5** for statistical details). Experimental groups: 5XFAD-PCSK9^{Het}, n = 9; 5XFAD-PCSK9^{KO}, n = 5.

ThS^+ aggregates were selectively present in both DG (**Figure 12 A, B**) and Nctx of 5XFAD mice (**Figure 12 E, F**). The quantitative analysis demonstrated a substantial 40 % decrease in the number (**Figure 12 C, G**) as well as in the area (**Figure 12 D, H**) of ThS^+ plaques in both DG and Nctx of 5XFAD-PCSK9^{KO} mice compared to 5XFAD-PCSK9^{Het} mice, clearly demonstrating that PCSK9 loss reduces amyloidosis in 5XFAD mice (detailed statistical report is available in **Table 5**).

Subsequently, in the same brain regions Aβ composition was further characterized by using mouse anti-human Aβ/APP 6E10 and mouse anti-human Aβ 11A1 antibodies. A significant reduction in the number of $6E10^+$ and $11A1^+$ amyloid plaques was observed in both DG and Nctx (DG: -35% and -28%, respectively and Nctx: -40% and -36%, respectively) of 5XFAD-PCSK9^{KO} mice as compared to 5XFAD-PCSK9^{Het} mice. In addition, a considerable decrease in the size of $6E10^+$ plaques in both examined regions was observed in 5XFAD-PCSK9^{KO} mice, whereas the absence of PCSK9 did not affect $11A1^+$ plaque size. The global analysis of plaque distribution indicated that in 5XFAD-PCSK9^{Het} mice, the number and area of ThS^+ and $11A1^+$ plaques were similar and smaller than those of $6E10^+$ plaques (**Figure 13 I-L**). Additionally, in 5XFAD-PCSK9^{KO} mice, despite a global and significant decrease of amyloidosis was observed, the ratio between differently stained plaques remained unaffected (**Figure 13 I-L**). Finally, given the larger amyloidosis in the Nctx compared to the Hip of 5XFAD mice, the ratio between hippocampal and cortical plaque load was evaluated.

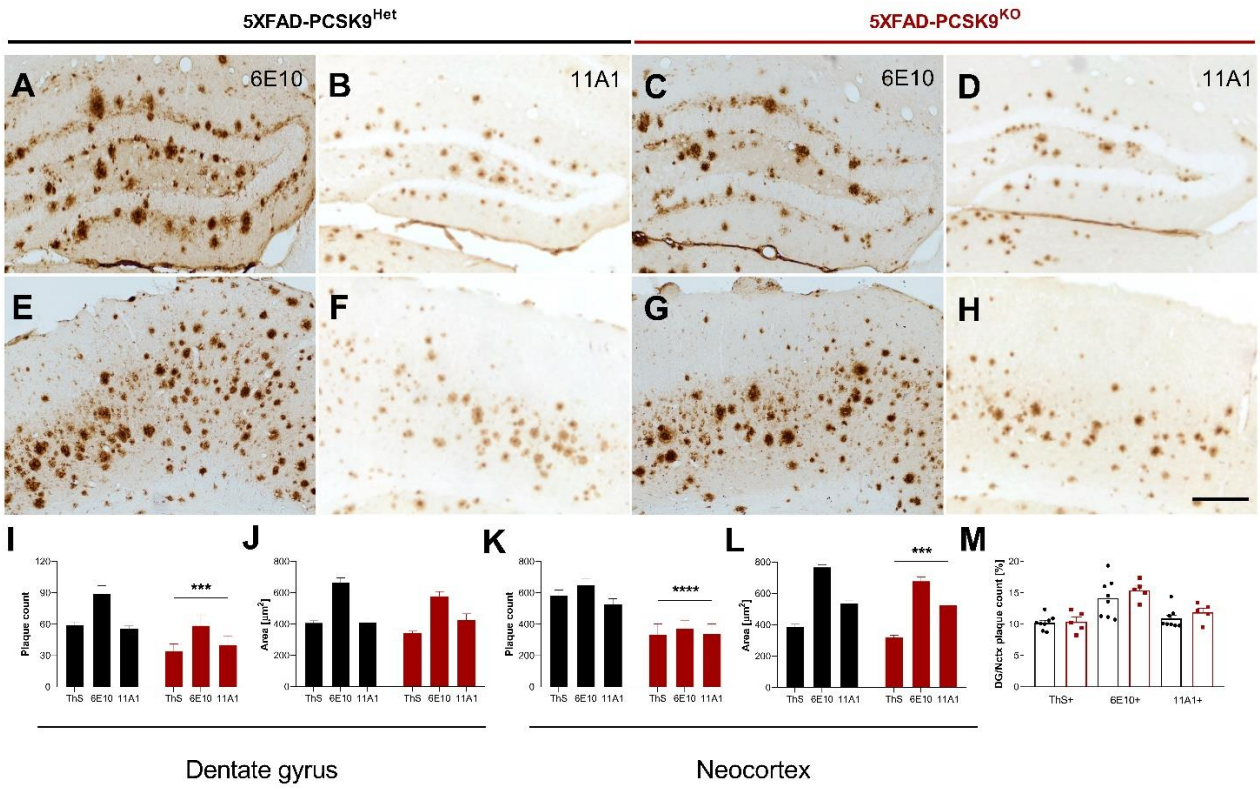

Figure 13. Spatial distribution and quantitative characterization of differently stained plaques within cortical and hippocampal regions. A-H Representative images showing 6E10^{+} and 11A1^{+} plaque in DG and Nctx of 10 mo 5XFAD-PCSK9^{Het} (**A-B; E-F**) and 5XFAD-PCSK9^{KO} (**C-G; G-H**) mice, respectively. Scale bar = 200 µm. **I-L** ThS^{+}, 6E10^{+} and 11A1^{+} amyloid plaque distribution in DG and Nctx of 5XFAD-PCSK9^{Het} (**black bars**) and 5XFAD-PCSK9^{KO} (**red bars**) mice. Data are shown as mean ± SEM. Statistical analysis according to chi-square test (see **Table 5**): *** $p < 0.001$, **** $p < 0.0001$. **M** % of DG/Nctx Aβ^{+} plaques in 5XFAD-PCSK9^{Het} (**black bars**) and 5XFAD-PCSK9^{KO} (**red bars**) mice. Data are shown as mean ± SEM. Statistical analysis according to two-way repeated measure ANOVA or two-way ANOVA as appropriate (see **Table 5** for statistical information). Experimental group: 5XFAD-PCSK9^{Het}, n = 9: 5XFAD-PCSK9^{KO}, n = 5.

PCSK9 loss did not alter the DG/Nctx ratio for the number of Aβ-stained plaques, that was about 10 % for both ThS^{+} and 11A1^{+} and 15 % for 6E10^{+} plaques (**Figure 13 M**).

These results suggest that the spatial and regional distribution of Aβ plaques was maintained even in the absence of PCSK9. Additionally, the amyloid plaque size distribution was evaluated. For this purpose, Aβ^{+} plaques were stratified according to their size into four ranges: ≤ 200, > 200 = 500, > 500 = 1000, and > 1000 µm^2; results demonstrated a significant reduction in the number of 5XFAD-PCSK9^{KO} mice with respect to 5XFAD-PCSK9^{Het} mice in both DG and Nctx, confirming previous analysis (**Figure 14 A-F**). Globally, the absence of PCSK9 did not alter the proportion between different Aβ^{+} size ranges, except for a trend towards a significant effect of PCSK9 loss on the size distribution of ThS^{+} plaques in the Nctx. Finally, we also evaluated the plaque compaction by measuring the diffuseness index ((Area 6E10 – Area ThS) / Area 6E10) (not shown). Our results showed no impact of PCSK9 loss on this parameter in both Nctx and Hip (see statistical report in **Table 5**).

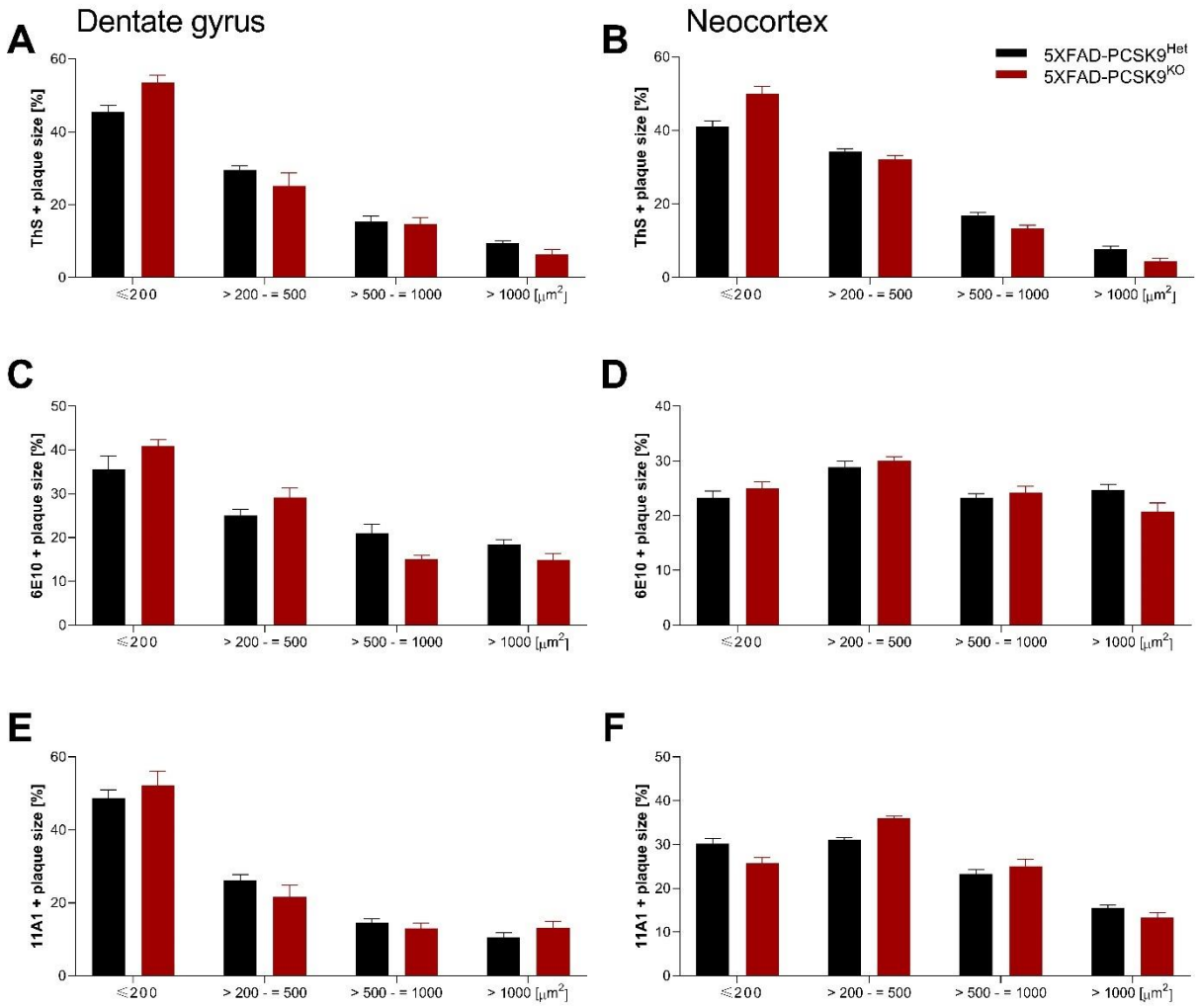

Figure 14. Size distribution of ThS^{+}, 6E10^{+} and 11A1^{+} amyloid plaques in the hippocampal dentate gyrus (A,C,E) and neocortex (B,D,F) of 5XFAD-PCSK9^{Het} (black bars) and 5XFAD-PCSK9^{KO} (red bars) mice. Data are shown as mean ± SEM. Statistical analysis according to chi-square test (for statistical details see in **Table 5**). Experimental group: 5XFAD-PCSK9^{Het}, n = 9; 5XFAD-PCSK9^{KO}, n = 5.

Taken together, these data suggest that the decreased plaque area especially observed in the Nctx (**Figure 13**) is not due to an increased amyloid compaction, but rather a potential delay in development of amyloidosis.

Furthermore, as in the adult mouse brain PCSK9 exhibited higher expression in RE-OP (Seidah et al., 2003), quantitative analysis of amyloidosis was also conducted in the OT area (**Figure 15**). The results showed a significant reduction in the number of 6E10^{+} and 11A1^{+} plaques in 5XFAD-PCSK9^{KO} mice compared to 5XFAD-PCSK9^{Het} mice (**Figure 15 E**) accompanied by a decrease in size (**Figure 15 F**). However, PCSK9 expression did not affect the proportion of plaques in different size ranges consistent with previous analysis (**Figure 15 G, H**). The detailed statistics report is summarized in **Table 5**.

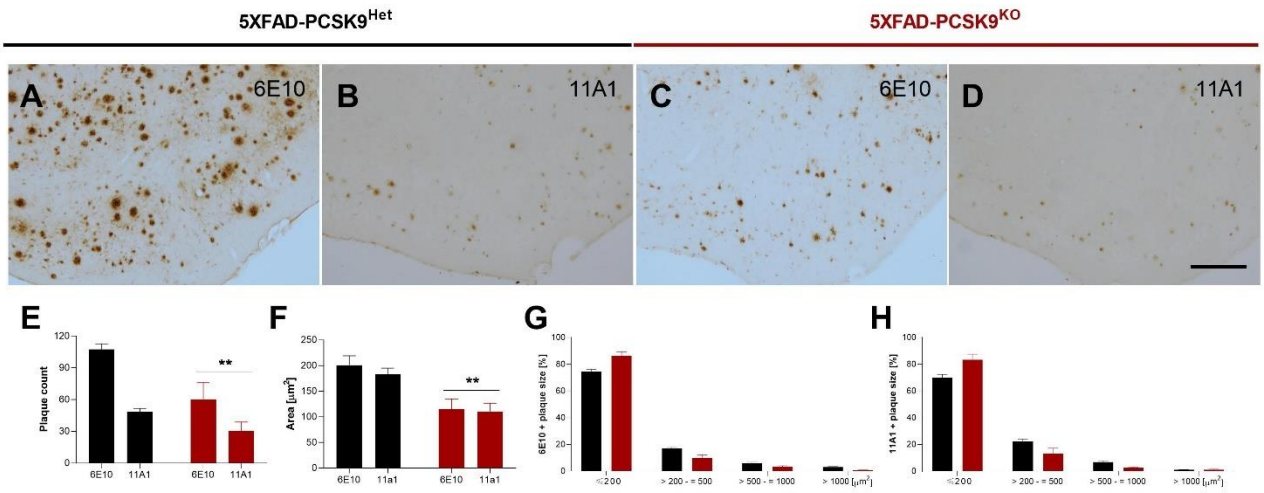

Figure 15. Plaque deposition in OT is reduced in 5XFAD mice in absence of PCSK9. A-D Representative images showing $6E10^{+}$ and $11A1^{+}$ plaque in OT of 10 mo 5XFAD-PCSK9^{Het} (**A, B**) and 5XFAD-PCSK9^{KO} (**C, D**) mice. Scale bar = 200 µm. Quantitative analysis of plaque count (**E**), area (**F**) and size distribution (**G**,**H**) in OT of 10 mo 5XFAD-PCSK9^{Het} and 5XFAD-PCSK9^{KO} mice. Data are shown as mean ± SEM. Statistical analysis according to two-way ANOVA: ** $p < 0.01$; sex was used as covariate as appropriate (See **Table 5** for statistical details). Experimental groups: 5XFAD-PCSK9^{Het}, n = 9; 5XFAD-PCSK9^{KO}, n = 5.

Altogether, these data demonstrate that the lack of PCSK9 significantly reduces the amyloidosis, without affecting its regional distribution or maturation.

4.2.3. β-site APP cleaving enzyme 1 immunoreactivity

The BACE1 enzyme is chiefly located in the brain and is abundantly expressed by neurons. Among its functions, BACE1 acts as a rate-limiting enzyme for Aβ formation and has been displayed to be greatly elevated in the human AD brains and in 9 - 12 mo 5XFAD mice (Zhao et al., 2007). Furthermore, an intense ir was detected in the stratum lucidum (SL) of the CA3 region, which is the terminal field of the mossy fiber pathway (Laird et al., 2005).

To test whether the expression of BACE1 was affected by PCSK9 ablation in 5XFAD mice, a IHC analysis has been conducted. Densitometric analysis did not reveal any significant differences in the ir area in the SL of CA3 between the experimental groups (**Figure 16 E**). Moreover, also morphometric parameter, such as BACE1 ir thickness in SL, showed no significant difference between the experimental groups (**Figure 16 F**). In addition, we also found increased BACE1 ir in presynaptic dystrophic neurites surrounding Aβ plaques, confirming previous reports (Sadleir et al., 2015; Kandalepas et al., 2013). In fact, as shown in higher magnification images, we found BACE1 ir (represented by DAB^{+} spots, brown) close to Congo Red^{+} plaques (red) in 5XFAD mice (**Figure 16 A-D**).

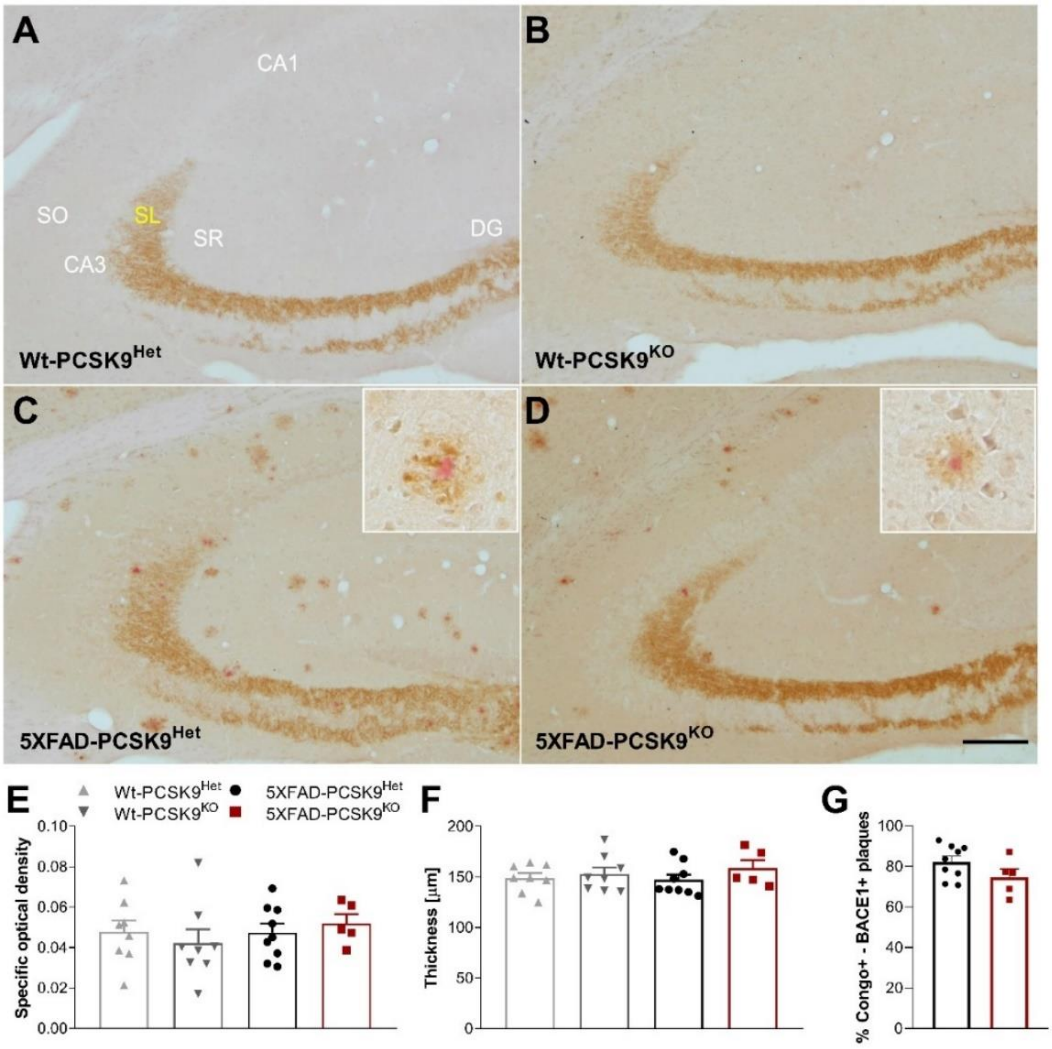

Figure 16. Representative photomicrographs of CA3 field of hippocampus of 10 mo Wt-PCSK9^{Het} (light grey bars), Wt-PCSK9^{KO} (dark grey bars), 5XFAD-PCSK9^{Het} (black bars) and 5XFAD-PCSK9^{KO} (red bars) mice showing immunoreactivity for BACE1 and Congo Red-stained amyloid plaques (A-D). Scale bar = 200 µm. **E-F** Densitometric analysis of BACE1 ir in hippocampal SL of CA3 field by analyzing specific optical area (**E**) and BACE1 ir thickness (**F**). Data are shown as mean ± SEM and compared by two-way ANOVA test (**Table 5**). **G** % of co-stained Congo Red - BACE1^{+} plaques in Nctx of 5XFAD-PCSK9^{Het} (**black bars**) and 5XFAD-PCSK9^{KO} (**red bars**). Data are shown as mean ± SEM and compared by chi square test (**Table 5**). Experimental groups: Wt-PCSK9^{Het}, n = 8; Wt-PCSK9^{KO}, n = 8; 5XFAD-PCSK9^{Het}, n = 10; 5XFAD-PCSK9^{KO}, n = 5. Abbreviations: DG, dentate gyrus; CA3, cornu Ammonis 3; CA1, cornu Ammonis 1; SR, Stratum Radiatum; SL, Stratum Lucidum; SO, Stratum Oriens.

Subsequently, consistent with a global reduction in Aβ pathology, we also observed a significant decrease in the number of BACE1^{+} plaques in Nctx (not shown) of 5XFAD-PCSK9^{KO} mice. Then, BACE1-labelled brain slices were counterstained with Congo Red solution and the number of double positive BACE1^{+} / Congo Red^{+} plaques was manually counted; our results demonstrated that the ratio between the number of double positive Congo Red^{+} - BACE1^{+} plaques / total number of Congo Red^{+} plaques in 5XFAD-PCSK9^{KO} mice was comparable to that of 5XFAD-PCSK9^{Het} mice (**Figure 16 G**) thus suggesting that BACE1 expression is not influenced by PCSK9 loss. Statistical information is available in **Table 5**.

4.2.4. Glial fibrillary acidic protein immunoreactivity

Astrocytes are highly specialized glial cells responsible for maintaining neuronal homeostasis and providing trophic and metabolic support to neurons in the CNS. This includes supplementing cholesterol to adult neurons in physiological conditions. However, in pathological conditions, such as AD, astrocytes undergo astrogliosis, a dynamic process characterized by morphological, molecular, and functional changes. Astrocyte activation is indicated by elevated GFAP expression and linked with increased production and release of paracrine factors that may have either beneficial or detrimental effects on surrounding cells. Astrocytes exhibit close interaction with Aβ plaques and even extend processes into the plaque core, possibly serving as a protective barrier for neurons (Osborn et al., 2016). Nevertheless, these cells can also contribute to neuronal damage through various mechanisms, such as enhancing pro-inflammatory cytokine production.

We, and others, have previously reported a significant increase in astrogliosis in the Ctx of 10 mo 5XFAD mice (Daini et al., 2021; Yoo et al., 2023) and the effects of PCSK9 loss on astrocyte reactivity was here investigated.

In **Figure 17 A-H**, representative images from CC-Cg, DG hilus, CA1 and CA3 fields of the Hip of each experimental group are reported. The semiquantitative analysis revealed a notable increase in GFAP ir in 10 mo 5XFAD mice compared to Ctrls, and PCSK9 loss resulted in a significant reduction only in CC-Cg ($p = 0.045$) (**Figure 17 I**). See **Table 5** for detailed statistical report.

4.2.5. Ionized calcium-binding adapter molecule 1 immunoreactivity

Microglial cells are resident immune cells of the CNS responsible for tight regulation of the brain microenvironment. During brain injury in AD, microglial cells are responsible for phagocytosis and clearance of Aβ and apoptotic cell debris, contributing to their clearance. In addition, activated microglia secrete many soluble factors, including chemoattractants and cytokines, which contribute to various aspects of the immune response to Aβ. Despite the early beneficial effect of their activation, prolonged stimulation induces a chronic inflammatory state that can lead to exacerbation of Aβ deposition and neurodegeneration contributing to disease progression (Miao et al., 2023).

To assess whether the reduced plaque deposition observed in 5XFAD-PCSK9^{KO} mice is also associated with a decrease in neuroinflammation, we studied the reactivity of IBA1^{+} microglia. In **Figure 18 A-H**, representative images of the hilus of Hip and the sCtx of experimental mice are shown. The quantitative analysis demonstrated that the increased IBA1^{+} ir in 5XFAD mice is significantly counteracted by PCSK9 loss in both analysed brain areas ($p = 0.001$ and $p = 0.003$, respectively) (**Figure 18 I**). Furthermore, a significant decrease in the number of microglial cells was

observed in the same brain regions (not shown) (p = 0.001 and p = 0.007, for Hilus and sCtx respectively). See **Table 5** for more statistical details.

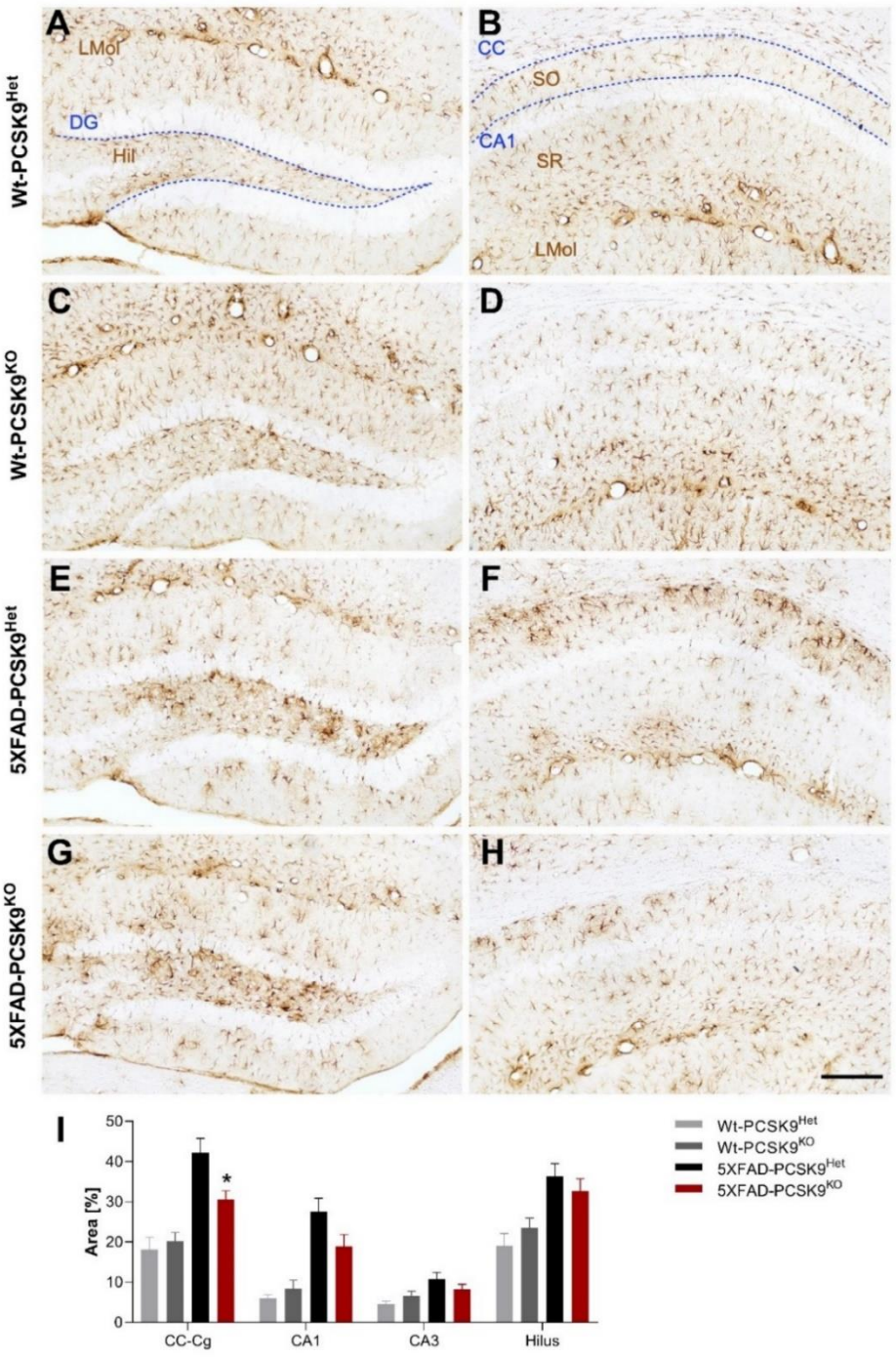

Figure 17. Astrocyte reactivity in AD mice is influenced by PCSK9 loss. A-H Representative photomicrographs of DG (**A, C, E, G**) and CA1 (**B, D, F, H**) fields of hippocampus of 10 mo Wt-PCSK9^{Het} (**A-B** and **light grey bars**), Wt-PCSK9^{KO} (**C-D** and **dark grey bars**), 5XFAD-PCSK9^{Het} (**E-F** and **black bars**) and 5XFAD-PCSK9^{KO} (**G-H** and **red bars**) mice showing GFAP ir. Scale bar = 200 µm. **I** Quantitative analysis of GFAP ir in CC-Cg, Hil, CA1, CA3 fields of Hip of 10 mo mice. Data are shown as mean ± SEM; GFAP ir in different brain areas was compared by two-way repeated measure ANOVA (**Table 5** for statistical information). The analysis in 5XFAD mice was performed by one-way ANOVA (**Table 5**): * $p < 0.05$; Experimental groups: Wt-PCSK9^{Het}, n = 5–6; Wt-PCSK9^{KO}, n = 5–7; 5XFAD-PCSK9^{Het}, n = 9; 5XFAD-PCSK9^{KO}, n = 5). Abbreviations: DG = dentate gyrus; LMol = stratum lacunosum-moleculare; Hil, hilus; CC-Cg,corpus callosum-cingulate cortex; CA1, cornu Ammonis 1; SR, Stratum Radiatum; SL, Stratum Lucidum; SO, Stratum Oriens.

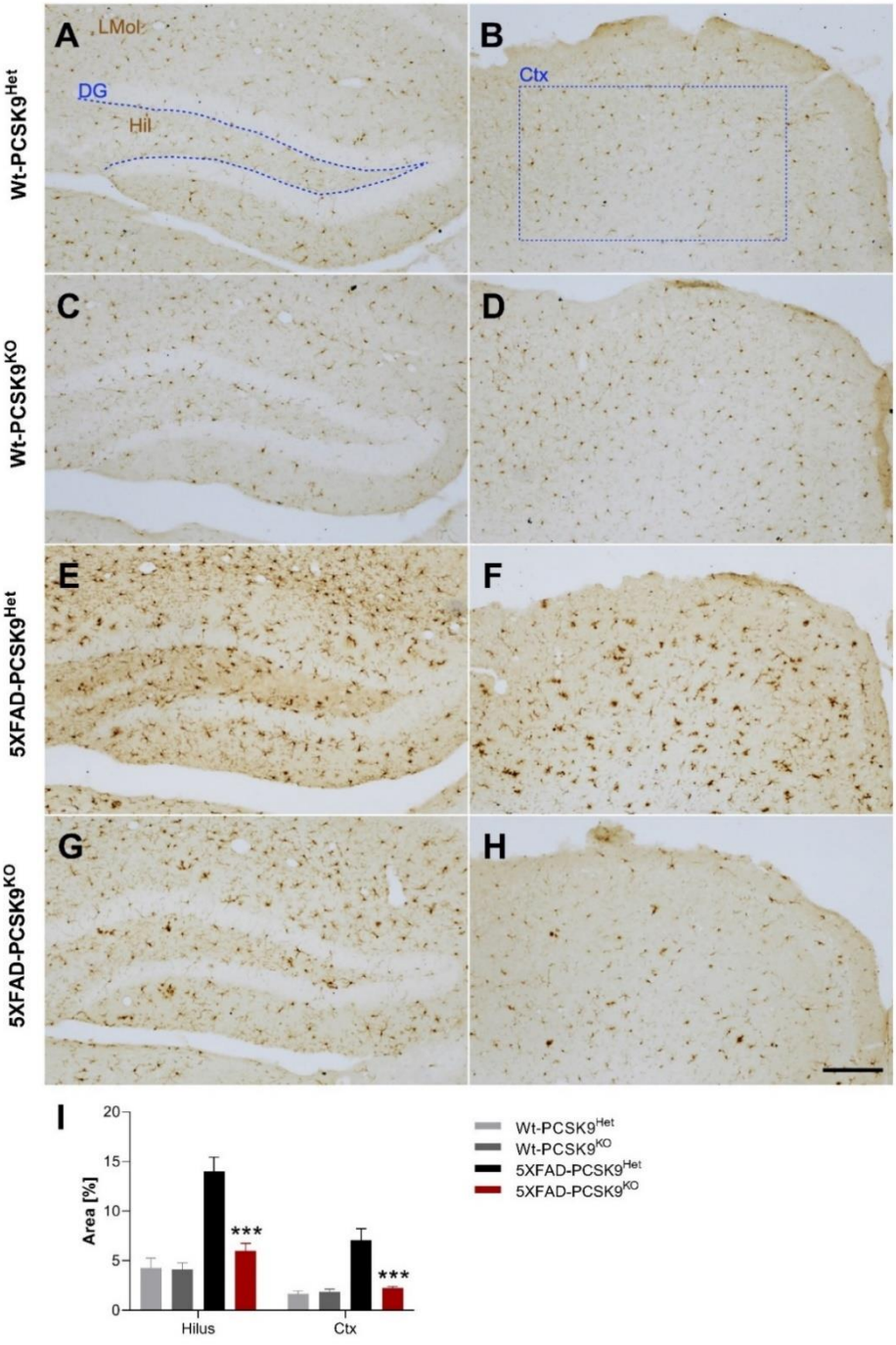

Figure 18. The loss of PCSK9 significantly reduced hippocampal and cortical microgliosis in AD mice. A-H Representative images of brain slices showing IBA1^{+} microglial cells in the hilus of DG (**A,C,E,G**) and Ctx (**B,D,F,H**) of Ctrls (**A-D**) and 5XFAD (**E-H**) mice. Scale bar = 200 µm. **I-J** Quantitative analysis of microgliosis in Ctx and hilar region of Hip. Data are shown as mean ± SEM. Statistical analysis according to two-way repeated measure ANOVA. The analysis was performed in 5XFAD mice by one-way ANOVA (**Table 5**): *** $p < 0.001$. Experimental groups: Wt-PCSK9^{Het}, n = 6; Wt-PCSK9^{KO}, n = 6; 5XFADPCSK9^{Het}, n = 5; 5XFAD-PCSK9^{KO}, n = 5). Abbreviations: DG, dentate gyrus; LMol, stratum lacunosum-moleculare; Hil, hilus; Ctx, cerebral cortex.

4.2.6. Synaptophysin immunoreactivity

Loss of synapses at a fine structural level and reduction in synaptic markers have been well documented in the early and late stages of AD, as well as in AD mouse models; these changes have been shown to correlate with the extent of cognitive deficits (Wu et al., 2021). As specifically concerns 5XFAD mice, a significant reduction of synapses has been observed in 9 and 12 mo mouse brains (Oakley et al., 2006).

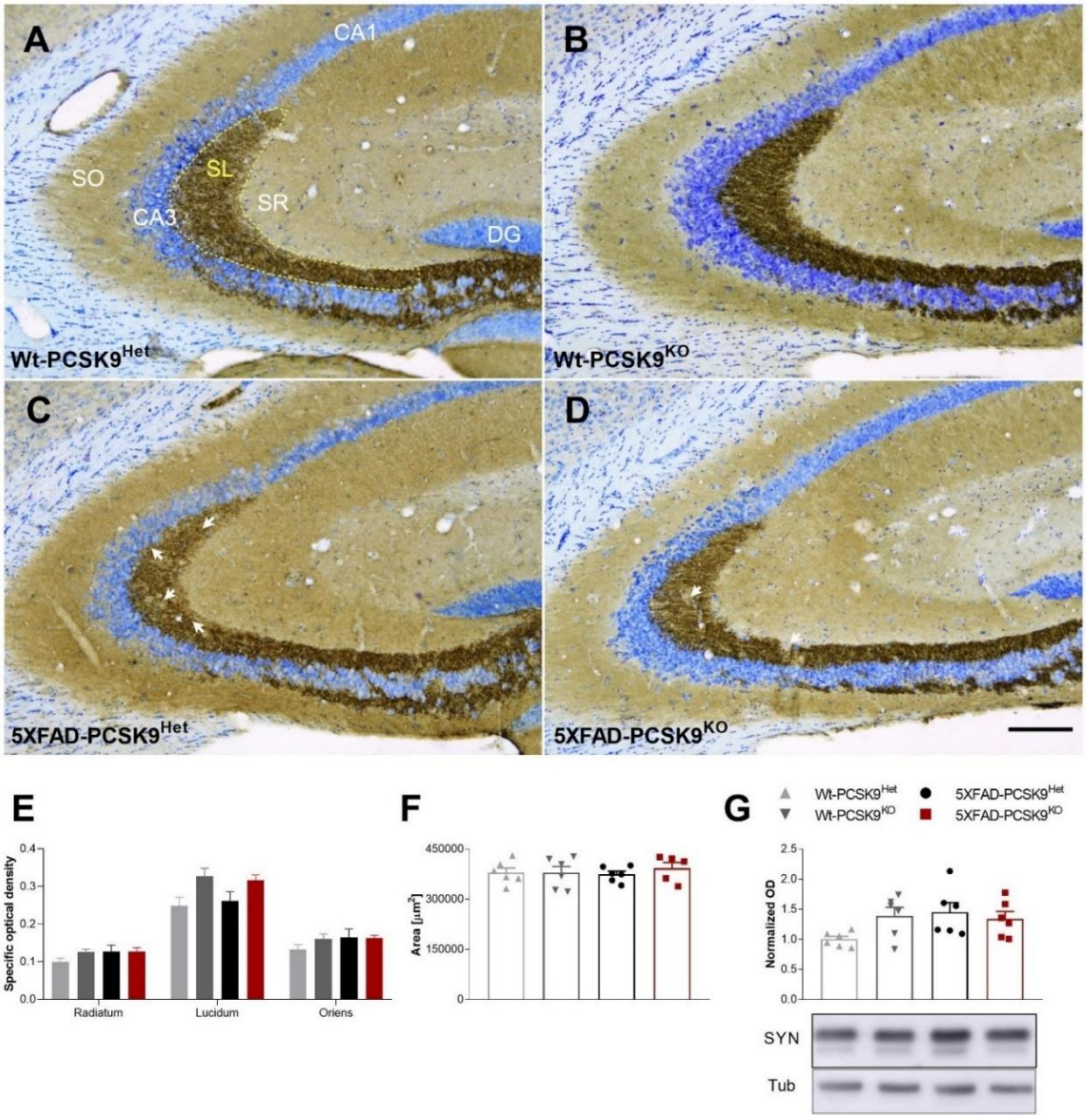

Figure 19. Panels A-D: Representative images of CA3 field of hippocampus of 10 mo Wt-PCSK9^{Het} (A) Wt-PCSK9^{KO} (B), 5XFAD-PCSK9^{Het} (C) and 5XFAD-PCSK9^{KO} (D) mice showing immunoreactivity for SYN. Scale bar = 200 µm. **Panels E-F:** Densitometric analysis of SYN^{+} ir in hippocampal stratum radiatum, stratum lucidum (dashed yellow line) and stratum oriens of CA3 field by analyzing specific optical density (**E**) and total area (**F**). Data are shown as mean ± SEM and compared by two-way repeated measures ANOVA test (specific optical density) and by two-way ANOVA test (CA3-related parameters) (**Table 5** for statistical data). **Panel G:** Representative immunoblots showing hippocampal protein levels of SYN and Tub and relative SYN protein quantification by western blot analysis in hippocampal lysates of Wt-PCSK9^{Het}, Wt-PCSK9^{KO}, 5XFAD-PCSK9^{Het} and 5XFAD-PCSK9^{KO}. Ab-specific optical density (OD) was normalized over β-Tubulin (Tub) signal. Data are shown as mean ± SEM and were analyzed according to two-way ANOVA (n = 6 for each experimental group). Abbreviations: DG, dentate gyrus; CA3, cornu Ammonis 3; CA1, cornu Ammonis 1; SR, Stratum Radiatum, SL, Stratum Lucidum, SO, Stratum Oriens.

To assess whether the improved cognitive abilities, reduced amyloidosis and neuroinflammation in 5XFAD-PCSK9^{KO} mice are accompanied by changes at the synaptic level, we studied SYN ir as an index of synaptic integrity in the CA3 field of the Hip (**Figure 19 A-D**). In all experimental groups, SYN ir was primarily observed in neuropil with dense labelling in dendrites. Densitometric analysis demonstrated a significant effect of PCSK9 factor, responsible for an increased SYN ir intensity ($p = 0.042$) in stratum lucidum (SL), but not in the stratum oriens (SO) or in the stratum radiatum (SR) (**Figure 19 E**). No significant changes in any quantitative morphometric parameter analyzed in SL, such as area (**Figure 19 F**), SYN ir length and thickness, area / thickness ratio, area / CA3 length ratio, SYN^{+} CA3 / SYN ir SL thickness, were detected despite the presence of Aβ deposits (not shown). In addition, protein quantification by western blotting analysis confirmed that SYN expression was unaffected in the Hip of experimental mice (**Figure 19 G**).

Overall, our data suggest that the absence of PCSK9 may influence synaptic structure, as suggested by SYN^{+} ir changes, irrespectively of the presence of AD pathology.

Table 5: Statistical supplementary details for histological analyses (**Figure 12-19**).

Fig.12	**ThS**	All regions - count number		**	**Global analysis:** Sex F(1,19)=6.626, p=**0.028**; PCSK9 KO F(1,10)=11.213, p=**0.007**; plaque count F(1,10)=7.124, p=**0.024**; PCSK9*plaque count F(1,10)=10.337, p=**0.009**	two-way repeated measure ANOVA
		DG count number (C)		**	Sex F(1,10)=3.984, p=**0.073**; PCSK9 KO F(1,10)=10.822, p=**0.008**	one-way ANOVA
		Nctx count number (G)		**	Sex F(1,10)=6.692, p=**0.027**; PCSK9 KO F(1,10)=10.848, p=**0.008**	
		All regions - area		**	**Global analysis:** Sex F(1,10)=2.026, p=0.185; PCSK9 KO F(1,11)=14.126, p=**0.003**; plaque area F(1,11)=2.868, p=0.118; PCSK9*plaque area F(1,11)=0.051, p=0.825	two-way ANOVA
		DG area (D)		**	Sex F(1,10)=0.062, p=0.807; PCSK9 KO F(1,11)=9.929, p=**0.009**	one-way ANOVA
		Nctx area (H)		*	Sex F(1,10)=4.137, p=**0.069**; PCSK9 KO F(1,10)= 6.414, p=**0.029**	
Fig.13	**6E10**	All regions - count number		**	**Global analysis:** Sex F(1,10)=4.827, p=**0.053**; PCSK9 KO F(1,10)=13.360, p=**0.004**; plaque count F(1,10)=13.307, p=**0.004**; PCSK9*plaque count F(1,10)=14.147, p=**0.004**	two-way repeated measure ANOVA
		DG count number		#	Sex F(1,11)=5.389, p=**0.041**; PCSK9 KO F(1,11)=4.161, p=**0.066**	one-way ANOVA
		Nctx count number		**	Sex F(1,10)=4.301, p=**0.065**; PCSK9 KO F(1,10)=14.061, p=**0.004**	
		All regions - area		*	**Global analysis:** Sex F(1,10)=0.906, p=0.364; PCSK9 KO F(1,10)=5.267, p=**0.045**; plaque count F(1,10)=0.953, p=0.352; PCSK9*plaque count F(1,10)=0.001, p=0.975	two-way repeated measure ANOVA
		DG area		ns	Sex F(1,11)=0.177, p=**0.682**; PCSK9 KO F(1,11)=1.425, p=0.148	one-way ANOVA
		Nctx area		*	Sex F(1,10)= 1.284, p=**0.284** PCSK9 KO F(1,10)=5.580, p=**0.040**	
	11A1	All regions - count number		*	**Global analysis:** Sex F(1,11)=4.795, p=**0.051**; PCSK9 KO F(1,11)=6.637, p=**0.026**; plaque count F(1,11)=8.666, p=**0.013**; PCSK9*plaque count F(1,11)=6.972, p=**0.023**	two-way repeated measure ANOVA
		DG count number		#	Sex F(1,11)=3.282, p=**0.097**; PCSK9 KO F(1,11)=3.986, p=**0.071**	one-way ANOVA
		Nctx count number		*	Sex F(1,11)=4.862, p=**0.050**; PCSK9 KO F(1,11)=6.805, p=**0.024**	
		All regions - area		ns	**Global analysis:** Sex F(1,11)=1.075, p=0.322; PCSK9 KO F(1,11)=0.030, p=0.865; plaque count F(1,11)=0.168, p=0.690; PCSK9*plaque count F(1,11)=0.128, p=0.728	two-way repeated measure ANOVA
		DG area		ns	Sex F(1,11)=1.748, p=0.213; PCSK9 KO F(1,11)=0.006, p=0.938	one-way ANOVA
		Nctx area		ns	Sex F(1,11)=0.007, p=0.933; PCSK9 KO F(1,11)=0.285, p=0.604	
	ThS 6E10 11A1	DG	plaque count (I)	*	Sex F(1,10)=5.016, p=**0.049**; PCSK9 KO F(1,10)=6.549, p=**0.028**; plaque type F(2,20)=0.322, p=0.728; sex*plaque type F(2,20)=1.678, p=0.212; PCSK9 KO*plaque type F(2,20)=1.023, p=0.378	two-way repeated measure ANOVA
			area (J)	#	Sex F(1,10)=0.309, p=0.591; PCSK9 KO F(1,11)=3.985, p=**0.071**; plaque type F(2,22)=33.590, p<**0.001**; PCSK9 KO*plaque type F(2,22)=1.350, p=0.280	two-way ANOVA
		Nctx	plaque count (K)	**	Sex F(1,10)=6.515, p=**0.029**; PCSK9 KO F(1,10)=12.04, p=**0.006**; plaque type F(2,20)=1.136, p=0.341; sex*plaque type F(2,20)=0.151, p=0.861; PCSK9 KO*plaque type F(2,20)=1.727, p=0.205	two-way repeated measure ANOVA
			area (L)	**	Sex F(1,10)=2.569, p=0.140; PCSK9 KO F(1,11)=12.241, p=**0.005**; plaque type F(2,22)=202.533, p<**0.001**; PCSK9 KO*plaque type F(2,22)=1.969, p=0.164	two-way ANOVA

		% DG/Nctx plaque count (M)	ns	Sex F (0)=0.051, p=0.827; PCSK9 KO F(1,11)=1.200, p=0.297; plaque type F(2,22)=21.508, p<**0.001**; PCSK9 KO*plaque type F(2,22)=0.330, p=0.722	two-way ANOVA
	Plaque size distribution (I-L)	DG count	ns	p=0.7666	chi square test
		DG area	ns	p=0.0600	
		Nctx count	ns	p=0.4927	
		Nctx area	ns	p=0.2020	
	DG/Nctx plaque count (M)	ThS	ns	p=0.850	
		6E10	ns	p=0.422	
		11A1	ns	p=0.218	
Fig.14	**ThS**	DG (A)	ns	p=0.7684	chi square test
		Nctx (B)	#	p=**0.0616**	
	6E10	DG (C)	ns	p=0.7935	
		Nctx (D)	ns	p=0.5201	
	11A1	DG (E)	ns	p=0.9449	
		Nctx (F)	ns	p=0.3513	
	Diffuseness index	All regions	ns	**Global analysis:** Sex F(1,10)=0.172, p=0.687; PCSK9 KO F(1,11)=1.082, p=0.321; diffuseness index F(1,11)=69.245, p**<0.001**; diffuseness index*PCSK9 KO F(1,11)=0.677, p=0.428	two-way ANOVA
		Nctx	ns	Sex F(1,10)=0.883, p=0.370; PCSK9 KO F(1,12)=0.346, p=0.568	one-way ANOVA
		DG	ns	Sex F(1,10)=0.025, p=0.876; PCSK9 KO F(1,12)=1.679, p=0.222	
Fig.15	**6E10 11A1**	TO	plaque count (E)	**	Sex F(1,11)=5.705, p=**0.036**; PCSK9 KO F(1,11)=10.855, p=**0.007**; plaque type F(1,11)=0.012, p=0.913; sex*plaque type F(1,11)=0.331, p=0.577; PCSK9 KO*plaque type F(1,11)=0.378, p=0.551	two-way repeated measure ANOVA
			area (F)	**	Sex F(1,11)=7.452, p=**0.031**; PCSK9 KO F(1,11)=10.855, p=**0.008**; plaque type F(1,11)=2.512, p=0.141; sex*plaque type F(1,11)=3.8511, p=0.075; PCSK9 KO*plaque type F(1,11)=7.040, p=**0.022**	two-way repeated measure ANOVA
	6E10		size distribution (G)	ns	p=0.5117	chi square test
	11A1		size distribution (H)	ns	p=0.5743	
Fig.16	**BACE1**	SL	Optical density (E)	ns	Sex F (1,25)=1.899, p=0.180; PCSK9 KO F(1,26)=0.008, p=0.932; 5XFAD F(1,26)=0.632, p=0.434; PCSK9 KO*5XFAD F(1,26)=0.734, p=0.399	two-way ANOVA
			BACE1 ir thickness (F)	ns	Sex F (1,26)=0.271, p=0.607; PCSK9 KO F(1,30)=2.060, p=0.163; 5XFAD F(1,30)=0.028, p=0.867; PCSK9 KO*5XFAD F(1,30)=0.574, p=0.455	
		Nctx	All plaque types - Count	***	**Global analysis:** Sex: F(1,11)=5.764, p=**0.035**; PCSK9 KO F(1,11)=15.717, p=**0.002**; plaque type F(2,22)=4.506, p=**0.023**; plaque type*sex F(2,22)=1.430, p=0.261; plaque type*PCSK9 KO F(2,22)=11.082, p<**0.001**	two-way repeated measure ANOVA
			% Congo Red$^+$ - BACE1$^+$ plaques / Congo Red$^+$ plaques (G)	ns	p=0.8598	chi-square test

Fig.17	**GFAP**	All regions	% area	#	**Global analysis:** Sex F(1,19)=0.627, p=0.438; PCSK9 KO F(1,20)=0.638, p=0.434; 5XFAD F(1,20)=24.477, p<**0.001**; brain areas F(3,57)=120.043, p<**0.001**; PCSK9 KO*5XFAD F(1,20)=3.590, p=**0.073**	two-way repeated measure ANOVA
		CC/Cg	% area	*	**Analysis in 5XFAD mice:** Sex F(1,11)=0.007, p=0.934; PCSK9 KO F(1,13)=5.034, p=**0.045**	one-way ANOVA
		CA1		ns	Sex F(1,11)=0.467, p=0.508; PCSK9 KO F(1,13)=2.914, p=0.114	
		CA3		ns	Sex F(1,11)=1.059, p=0.326; PCSK9 KO F(1,13)=1.047, p=0.326	
		Hilus		ns	Sex F(1,11)=0.231, p=0.640; PCSK9 KO F(1,13)=0.575, p=0.463	
Fig.18	**IBA1**	Hilus and Sctx % area		***	**Global analysis:** Sex F(1,17)=0.147, p=0.707; PCSK9 KO F(1,18)=18.671, p<**0.001**; 5XFAD F(1,18)=34.691, p<**0.001**; brain areas F(1,18)=137.061, p<**0.001**; PCSK9 KO*5XFAD F(1,18)=19.209, p<**0.001**	two-way repeated measure ANOVA
				</br>	**Analysis in 5XFAD mice:** Hilus: Sex F(1,7)=0.001, p=0.970 PCSK9 KO F(1,8)=23.531, p=**0.001** sCtx: Sex F(1,7)=0.109, p=0.751 PCSK9 KO F(1,8)=16.958, p=**0.003**	one-way ANOVA
		Hilus and Sctx count		***	**Global analysis:** Sex F(1,17)=0.010, p=0.923; PCSK9 KO F(1,18)=15.796, p<**0.001**; 5XFAD F(1,18)=19.484, p<**0.001**; brain areas F(1,18)=59.628, p<**0.001**; PCSK9 KO*5XFAD F(1,18)=19.794, p<**0.001**	two-way repeated measure ANOVA
				</br>	**Analysis in 5XFAD mice:** Hilus: Sex F(1,7)=0.013, p=0.912 PCSK9 KO F(1,8)=22.729, p=**0.001** sCtx: Sex F(1,7)=0.020, p=0.892 PCSK9 KO F(1,8)=12.871, p=**0.007**	one-way ANOVA
Fig.19	**SYN**	Specific optical density (OD)	All regions (SR, SL, SO)	ns	**Global analysis**: Sex F(1,18)=8.274, p=**0.010**; PCSK9 KO F(1,18)=1.057, p=0.317; hippocampal fields F(2,36)=48.007, p<**0.001**; 5XFAD F(1,18)=0.392, p=0.539; hippocampal fields*sex F(2,36)=1.201, p=0.313, PCSK9 KO*5XFAD F(1,18)=1.451, p=0.244	two-way repeated measure ANOVA
			SR	ns	Sex F(1,18)=6.921, p=**0.017**; PCSK9 KO F(1,18)=0.005, p=0.945; 5XFAD F(1,18)=1.293, p=0.271 PCSK9 KO*5XFAD F(1,18)=1.967, p=0.178	two-way ANOVA
			SL	*	Sex F(1,18)=5.712, p=**0.028**; PCSK9 KO F(1,18)=4.809, p=**0.042**; 5XFAD F(1,18)=0.010, p=0.920; PCSK9 KO*5XFAD F(1,18)=0.572, p=0.459	
			SO	ns	Sex F(1,18)=8.253, p=**0.010**; PCSK9 KO F(1,18)=0.061, p=0.807; 5XFAD F(1,18)=1.197, p=0.288; PCSK9 KO*5XFAD F(1,18)=1.762, p=0.201	
		CA3	Area	ns	Sex F(1,18)=0.097, p=0.759; PCSK9 KO F(1,19)=0.080, p=0.7804; 5XFAD F(1,19)=0.318, p=0.5837; PCSK9*5XFAD F(1,19)=0.3654, p=0.5527	two-way ANOVA
			Length	ns	Sex F(1,18)=0.089, p=0.769; PCSK9 KO F(1,19)=0.864, p=0.364; 5XFAD F(1,19)=0.743, p=0.399; PCSK9*5XFAD F(1,19)=0.005, p=0.947	
			area/thickness ratio	ns	Sex F(1,18)=0.419, p=0.525; PCSK9 KO F(1,19)=0.2293, p=0.637; 5XFAD F(1,19)=0.066, p=0.4259, PCSK9*5XFAD F(1,19)=0.9657, p=0.3381	
			area/CA3 length ratio	ns	Sex F(1,18)=0.078, p=0.784; PCSK9 KO F(1,19)=0.1577, p=0.6957; 5XFAD F(1,19)=0.0027, p=0.9591; PCSK9*5XFAD F(1,19)=0.8586, p=0.3658	

			SYN+CA3/SYN ir SL thickness	*	Sex F(1,18)=0.515, p=0.482; PCSK9 KO F(1,19)=0.110, p=0.744; 5XFAD F(1,19)=2.193, p=0.1550; PCSK9*5XFAD F(1,19)=4.770, p=**0.042**	
		Hip	SYN OD	*	Sex F(1,19)=5.608, p=**0.029**; PCSK9 KO F(1,19)=1.486, p=0.238; 5XFAD F(1,19)=3.010, p=**0.100**; PCSK9*5XFAD F(1,19)=4.721, p=**0.043**	

4.2.7. *Ex-vivo* analysis of neuroinflammation and lipid metabolism gene expression

A preliminary quantification of lipidic / cholesterol metabolism-, microglia-, and cytokine-related gene expressions in 10 mo B6SJL and 5XFAD mice was performed. Obtained results indicated that most of the genes linked to lipid metabolism (*ApoE*, *Lpl*, *Lrp5*), microglia (*P2ry12*, *Ifitm3*, *Cd11b*, *Cx3cr1, Cst7*), and inflammatory mediators (*Il6*, *TnfA*, *Il1B*, *Ccl3*, *Ccl6*) were upregulated in 5XFAD mice with only few exceptions (*Lrp1*, *Hmgcr, Cd36*, *Stmn1*) (**Figure 20**). Notably, the *Hmgcr* expression was increased in 5XFAD mice compared to B6SJL, but the difference was not statistically significant (**Table 6** for statistical report).

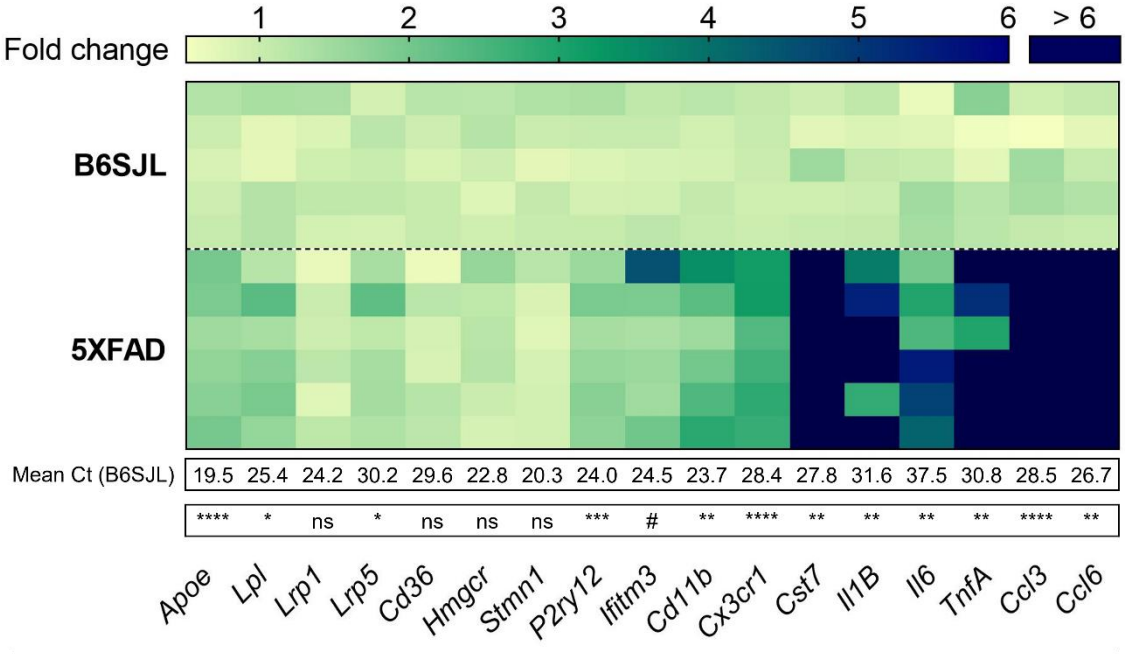

Figure 20. Expression of lipid/cholesterol metabolism-, microglial- and cytokines- related genes in 5XFAD mice. Heatmap of differential gene expression in B6SJL and 5XFAD mice. Data are presented as fold change normalized over B6SJL group mean and calibrated over GAPDH/RER1/CYPA housekeeping genes. Fold changes are visualized through a chromatic scale ranging from **yellow** (<1) to **blue** (6) and **dark blue** (>6). The mean Ct of the group used as calibrator and the results of one-way ANOVA are indicated beneath the heatmap. Data are shown as mean ± SEM and analysed by one-way ANOVA (see **Table 6**); * $p < 0.05$; ** $p < 0.01$, **** $p < 0.0001$, # $0.10 > p > 0.05$ trend for a significant difference. Experimental groups: B6SJL, n = 4-5; 5XFAD, n = 4-6. Abbreviations: *ApoE*, apolipoprotein E; *Lpl*, lipoprotein lipase; *Lrp1*, low-density lipoprotein receptor–related protein 1; *Lrp5*, Low-density lipoprotein receptor–related protein 5; *Cd36*, cluster of differentiation 36; *Hmgcr*, 3-hydroxyl-3-methylglutaryl-coenzyme A reductase; *Stmn1*, Stathmin 1; *P2ry12*, purinergic receptor P2Y; *Ifitm3*, interferon induced transmembrane protein 3; *Cd11b*, cluster of differentiation molecule 11b, *Cx3cr1*, C-X3-C motif chemokine receptor 1; *Cst7*, Cystatin-F; *Il1B*, interleukin-1 Beta, *Il6*, interleukin-6; *TnfA*, tumor necrosis factor alpha; *Ccl3*, chemokine (C-C motif) ligand; *Ccl6*, chemokine (C-C motif) ligand 6.

Subsequently, the effect of PCSK9 absence on these genes in Nctx of both Ctrls and 5XFAD mice was investigated (see **Figure 21** and **Table 6** for statistical report). Regarding lipid metabolism, our analysis revealed a significant increase in *ApoE*, *Lrp5*, and *Lpl* expression, and a slight non-significant decrease in *Cd36* expression in the 5XFAD mice with no impact due to the absence of PCSK9. Additionally, while the *Lrp1* expression remained unchanged, PCSK9 loss induced a trend towards a significant reduction in *Lrp5* expression in 5XFAD mice ($p = 0.0769$). Finally, the expression of the rate-limiting enzyme involved in cholesterol biosynthesis, *Hmgcr*, did not differ between experimental groups.

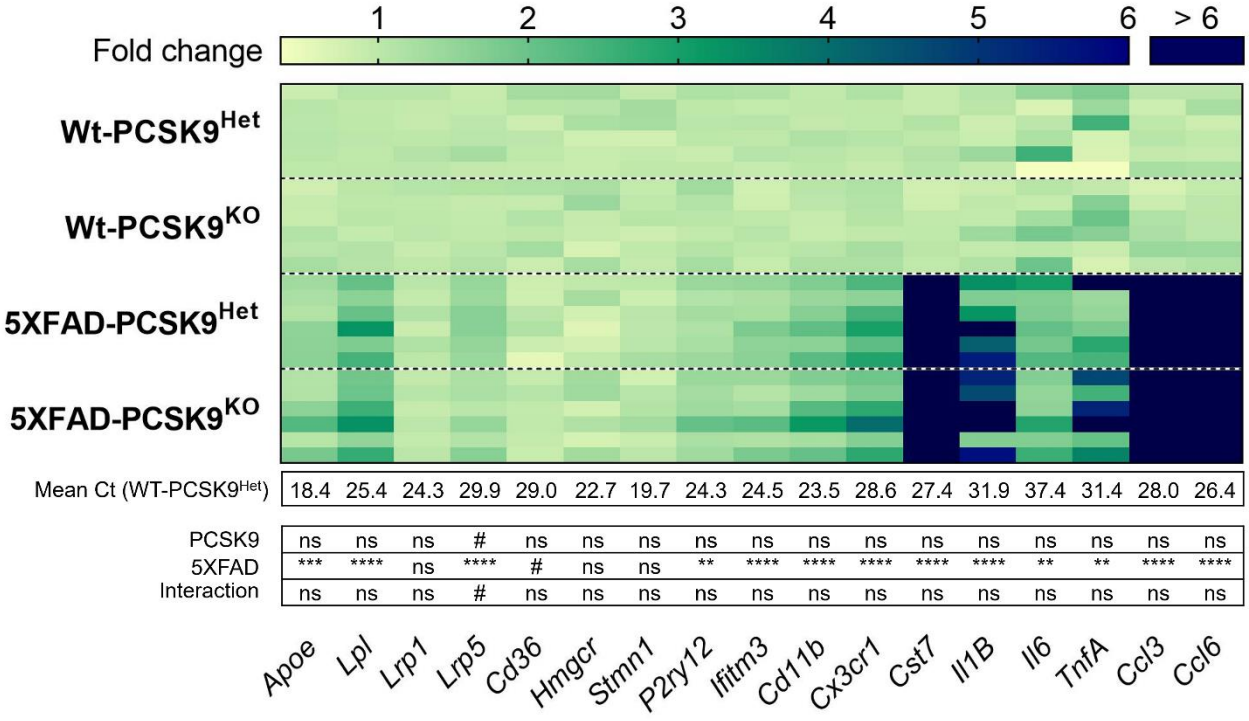

Figure 21. Effect of PCSK9 loss in the expression of lipidic/Cho metabolism-, microglial- and cytokine- related genes in 5XFAD mice. Heatmap of differential gene expression in Wt-PCSK9^{Het}, Wt-PCSK9^{KO}, 5XFAD-PCSK9^{He}t and 5XFAD-PCSK9^{KO} mice. Data are shown as fold change normalized over Wt-PCSK9^{Het} group mean and calibrated over GAPDH/RER1/CYPA housekeeping genes. Fold changes are visualized through a chromatic scale ranging from yellow (<1) to **blue** (6) and **dark blue** (>6). The mean Ct of the group used as calibrator and the results of two-way ANOVA, with PCSK9 and 5XFAD factors and their interaction, are indicated beneath the heatmap; ** $p < 0.01$, *** $p < 0.001$, **** $p < 0.0001$, # $0.10 > p > 0.05$ trend for a significant difference (see **Table 6**) n = 6 for each experimental group. Abbreviations: *ApoE*, apolipoprotein E; *Lpl*, lipoprotein lipase; *Lrp1*, low-density lipoprotein receptor–related protein 1; *Lrp5*, Low-density lipoprotein receptor–related protein 5; *Cd36*, cluster of differentiation 36; *Hmgcr*, 3-hydroxyl-3-methylglutaryl-coenzyme A reductase; *Stmn1*, Stathmin 1; *P2ry12*, purinergic receptor P2Y; *Ifitm3*, interferon induced transmembrane protein 3; *Cd11b*, cluster of differentiation molecule 11b, *Cx3cr1*, C-X3-C motif chemokine receptor 1; *Cst7*, Cystatin-F; *Il1B*, interleukin-1 Beta, *Il6*, interleukin-6; *TnfA*, tumor necrosis factor alpha; *Ccl3*, chemokine (C-C motif) ligand; *Ccl6*, chemokine (C-C motif) ligand 6.

As concerns microglia-associated genes, the expression of *P2ry12* (a marker of homeostatic microglia), *Cd11b*, and *Cx3cr1*, along with *Ifitm3* and *Cst7* (which indicate phagocytic/disease-associated microglia), was upregulated in 5XFAD mice, regardless of PCSK9 loss. Conversely, no

changes in the expression of *Stmn1* were detected (**Figure 21**). Finally, also the expression of pro-inflammatory *Il6, TnfA, Il1B, Ccl3,* and *Ccl6* genes was increased in 5XFAD mice and unaffected by PCSK9 loss (**Figure 21** and **Table 6** for statistical details).

4.2.8. Brain cholesterol and oxysterols quantification

Finally, the effect of the absence of PCSK9 in 5XFAD mice on brain TC and oxysterol levels was assessed. In a preliminary study, we found a 52% reduction in TC in 5XFAD mice compared to B6SJL controls, thus indicating a significant alteration in cerebral cholesterol homeostasis in AD mice (**Figure 22 A**). On the contrary, similar serum TC levels were detected in 5XFAD and B6SJL mice (**Figure 22 C**).

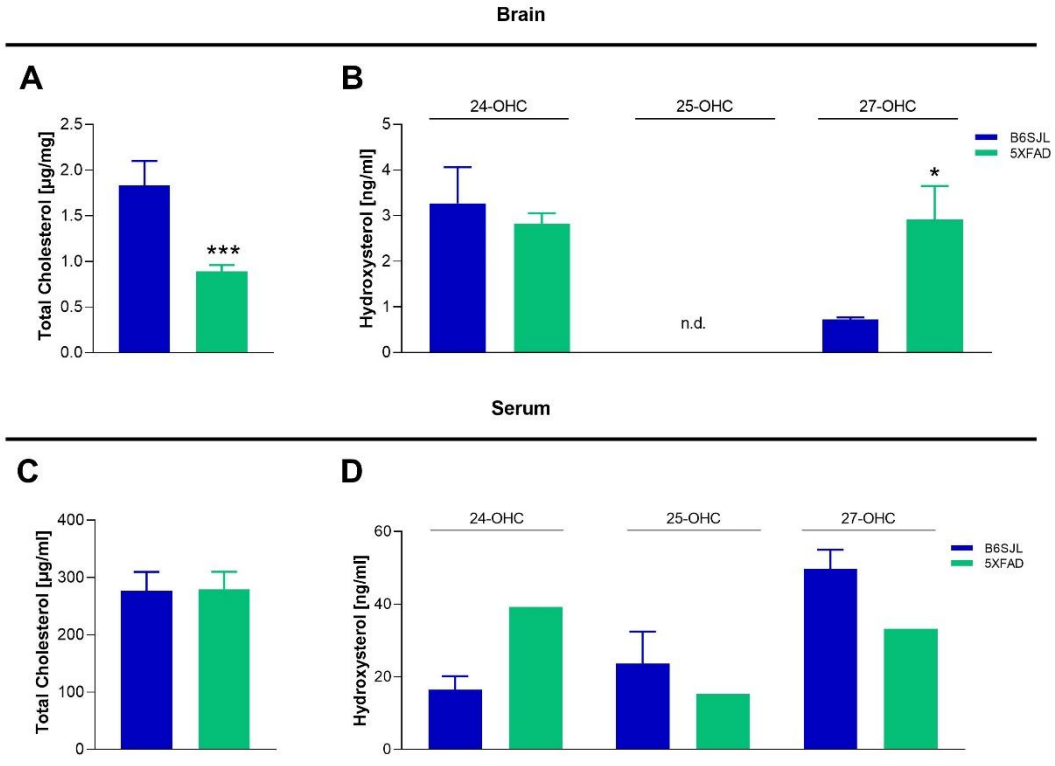

Figure 22. Total cholesterol and hydroxysterol levels in brain (A-B) and sera (C-D) of 10 mo B6SJL and 5XFAD mice. A-B Brain cholesterol and OHC quantifications: A Brain total cholesterol levels are expressed as µg Cho/mg of cerebral tissue. **B** Brain OHC are expressed as ng OHC/mg cerebral tissue. Experimental groups: B6SJL n = 6-3; 5XFAD n = 10-4. **C-D Serum cholesterol and oxysterol quantifications: C** Serum TC levels are expressed as µg Cho/ml. **D** Serum OHC are expressed as ng OHC/ml serum. Experimental groups: B6SJL n = 7-3; 5XFAD n = 11-1. All data are shown as mean ± SEM. Statistical analysis according to one-way ANOVA when applicable is summarized in **Table 6**. A value of $p < 0.05$ was considered statistically significant. Abbreviations: n.d. = non detectable.

Next, TC levels were measured in our experimental groups (**Figure 23**). In the brain, TC content in 5XFAD mice was markedly lower compared to Ctrls and slightly recovered upon PCSK9 loss (**Figure 23 A**). Additionally, the analysis of serum TC indicated a significant impact of both 5XFAD and

PCSK9 factors without interaction (**Figure 23 C**). Moreover, PCSK9 loss had a noteworthy effect in 5XFAD mice ($p < 0.001$) (**Figure 23 C** and **Table 6** for statistical report).

Subsequently, the primary cholesterol-derived oxidative bioactive metabolites 24-, 25- and 27-OHC were quantified in the cerebral tissue and serum of experimental mice. Globally, our analysis demonstrated that only 24- and 27-OHC were detectable in the brain. Specifically, 5XFAD mice exhibited a 4-fold increase in 27-OHC levels when compared to B6SJL controls (**Figure 22 B**). However, brain and serum 24-, 25- and 27-OHC levels were similar between Ctrls, 5XFAD-PCSK9^{Het} and 5XFAD-PCSK9^{KO} mice (**Figure 23 B, D**). Statistical supplementary information is available in **Table 6**.

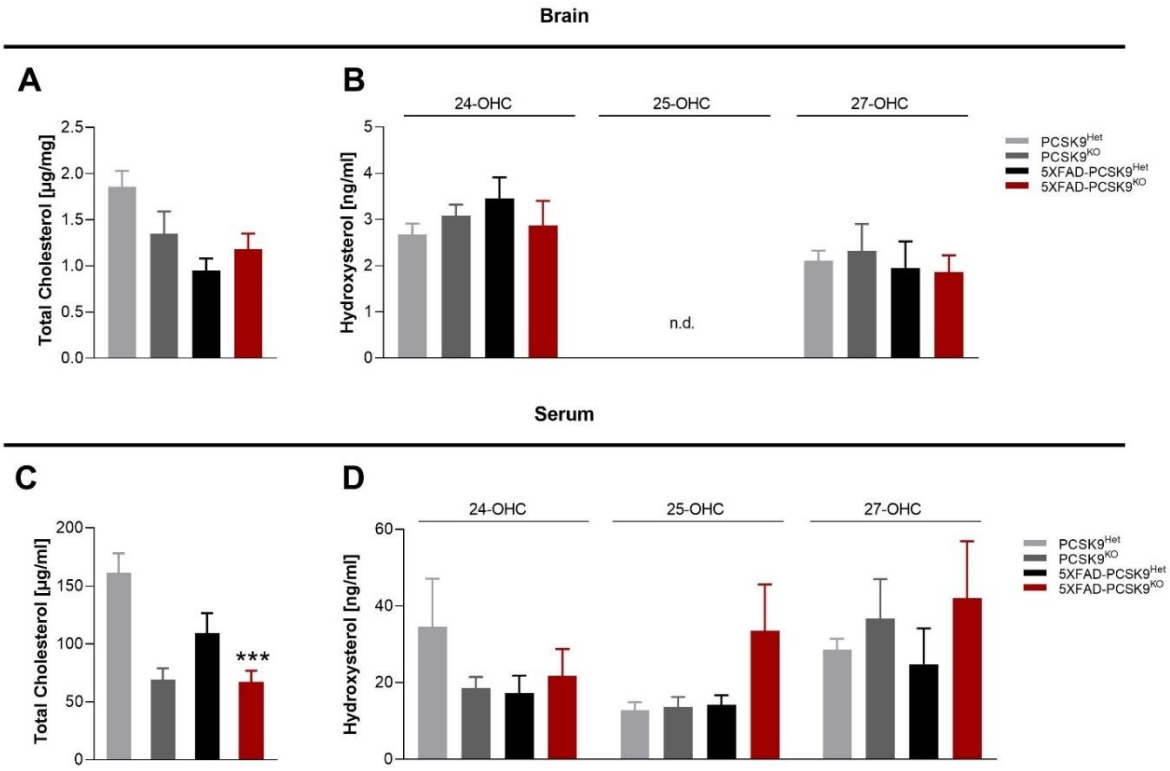

Figure 73. Effect of PCSK9 genetic ablation on total cholesterol and hydroxysterol levels in brain (A-B) and sera (C-D) of 10 mo Wt-PCSK9^{Het}, Wt-PCSK9^{KO}, 5XFAD-PCSK9^{Het} and 5XFAD-PCSK9^{KO} mice. A-B Brain cholesterol and OHC quantifications: A Brain total cholesterol levels are expressed as µg cholesterol/mg of cerebral tissue. **B** Brain OHC are expressed as ng OHC/mg cerebral tissue. Experimental groups: Wt-PCSK9^{Het} n = 12-14; Wt-PCSK9^{KO} n = 10; 5XFAD-PCSK9^{Het} n = 11-12; 5XFAD-PCSK9^{KO} n = 11-12. **C-D Serum cholesterol and OHC quantifications: C** Serum TC levels are expressed as µg Cho/ml. **D** Serum OHC are expressed as ng OHC/ml serum. Experimental groups: Wt-PCSK9^{Het} n = 14-4; Wt-PCSK9^{KO} n = 9-7; 5XFAD-PCSK9^{Het} n = 12-7; 5XFAD-PCSK9^{KO} n = 12-6. All data are shown as mean ± SEM. Statistical analysis according to two-way ANOVA (sex as a covariate) is summarized in **Table 6**. A value of $p < 0.05$ was considered statistically significant. Abbreviations: n.d. = non detectable.

Table 6: Statistical supplementary details for *ex vivo* analyses (**Figure 20-23**).

Fig.20	**lipid/cholesterol metabolism-, microglial- and cytokines- related mRNAs**	Ctx	*ApoE*	****	F(1,10)=50.494; p<**0.0001**	one-way ANOVA
			Lpl	*	F(1,10)=8.796, p=**0.016**	
			Lrp1	ns	F(1,10)=0.398, p=0.544	
			Lrp5	*	F(1,10)=6.552, p=**0.0310**	
			Cd36	ns	F(1,10)=0.073, p=0.793	
			Hmgcr	ns	F(1,11)=2.240, p=0.169	
			Stmn1	ns	F(1,7)=0.619, p=0.461	
			P2ry12	***	F(1,10)=28.560, p=**0.0005**	
			Ifitm3	#	F(1,10)=4.268, p=**0.069**	
			Cd11b	**	F (1,10)=20.939; p=**0.001**	
			Cx3cr1	****	F(1,10)=163.171; p<**0.0001**	
			Cst7	**	F(1,7)=26.961; p=**0.002**	
			Il1B	**	F(1,10)=19.061, p=**0.002**	
			Il6	**	F(1,10)=15.699, p=**0.003**	
			TnfA	**	F(1,10)=19.965, p=**0.002**	
			Ccl3	****	F (1,7)=94.198; p<**0.0001**	
			Ccl6	**	F (1,7)=25.233; p=**0.002**	
Fig.21	**lipid/cholesterol metabolism-, microglial- and cytokines- related mRNAs**	Nctx	*ApoE*	ns	PCSK9 KO F(1,20)=0.1314, p=0.7208; 5XFAD F(1,20)=15.44, p=**0.0008**; PCSK9*5XFAD F(1,20)=0.2725, p=0.6074	two-way ANOVA
			Lpl	ns	PCSK9 KO F(1,20)=0.1618, p=0.6918; 5XFAD F(1,20)=46.79, p<**0.0001**; PCSK9*5XFAD F(1,20)=0.08013, p=0.7800	
			Lrp1	ns	PCSK9 KO F(1,20)=0.9097, p=0.3516; 5XFAD F(1,20)=0.0042, p=0.9489; PCSK9*5XFAD F(1,20)=0.1496, p=0.7030	
			Lrp5	#	PCSK9 KO F(1,20)=3.499, p=**0.0761**; 5XFAD F(1,20)=37.22, p<**0.0001**; PCSK9*5XFAD F(1,20)=3.478, p=**0.0769**	
			Cd36	ns	PCSK9 KO F(1,20)=0.797, p=0.3826; 5XFAD F(1,20)=3.782, p=**0.0660**; PCSK9*5XFAD F(1,20)=0.1273, p=0.7249	
			Hmgcr	ns	PCSK9 KO F(1,23)=1.615, p=0.219; 5XFAD F(1,23)=0.249, p=0.624; PCSK9*5XFAD F(1,23)=0.700, p=0.413	
			Stmn1	ns	PCSK9 KO F(1,20)=0.4456, p=0.5121; 5XFAD F(1,20)=0.4138, p=0.5274; PCSK9*5XFAD F(1,20)=0.3537, p=0.5587	
			P2ry12	#	PCSK9 KO F(1,20)=3.689, p=**0.0691**; 5XFAD F(1,20)=14.47, p=**0.0011**; PCSK9*5XFAD F(1,20)=0.1869, p=0.6702	
			Ifitm3	ns	PCSK9 KO F(1,20)=0.1677, p=0.6865; 5XFAD F(1,20)=25.79, p=**0.0001**; PCSK9*5XFAD F(1,20)=0.2726, p=0.6074	
			Cd11b	ns	PCSK9 KO F(1,20)=0.3005, p=0.5897; 5XFAD F(1,20)=29.43, p<**0.0001**; PCSK9*5XFAD F(1,20)= 0.2737, p=0.6066	
			Cx3cr1	ns	PCSK9 KO F(1,20)=0.2408, p=0.6290; 5XFAD F(1,20)=41.67, p<**0.0001**; PCSK9*5XFAD F(1,20)=0.0048, p=0.9454	
			Cst7	ns	PCSK9 KO F(1,20)=0.0351, p=0.8533; 5XFAD F(1,20)=33.84, p<**0.001**; PCSK9*5XFAD F(1,20)=0.0459, p=0.8324	
			Il1B	ns	PCSK9 KO F(1,20)=1.408, p=0.2494; 5XFAD F(1,20)=40.18, p<**0.0001**; PCSK9*5XFAD F(1,20)=1.34, p=0.2606	

			Il6	ns	PCSK9 KO F(1,20)=0.0003, p=0.9868; 5XFAD F(1,20)=10.58, p=**0.0040**; PCSK9*5XFAD F(1,20)=0.3234, p=0.5759	
			TnfA	ns	PCSK9 KO F(1,20)=1.827, p=0.1915; 5XFAD F(1,20)=14.18, p=**0.0012**; PCSK9*5XFAD F(1,20)=1.518, p=0.2322	
			Ccl3	ns	PCSK9 KO F(1,20)=0.0108, p=0.9183; 5XFAD F(1,20)=39.84, p<**0.0001**; PCSK9*5XFAD F(1,20)=0.008, p=0.9284	
			Ccl6	ns	PCSK9 KO F(1,20)=0.1542, p=0.6987; 5XFAD F(1,20)=54.68, p<**0.0001**; PCSK9*5XFAD F(1,20)=0.1225, p=0.7300	
Fig. 22	**Total cholesterol**	Brain (A)		***	Sex F(1,13)=2.077, p=0.173; 5XFAD F(1,13)=17.436, p<**0.001**	one-way ANOVA
		Serum (C)		ns	Sex F(1,15)=7.004, p=**0.018** 5XFAD F(1,15)=0.001, p=0.978	one-way ANOVA
	Hydroxysterols	Brain (B)	24-OHC	ns	Sex F(1,4)=3.070, p=0.155; 5XFAD F(1,5)=0.404, p=0.553	one-way ANOVA
			27-OHC	*	Sex F(1,3)=0.006, p=0.941 5XFAD F(1,4)=8.707, p=**0.042**	one-way ANOVA
		Serum (D)	24-OHC	not applicable		
			25-OHC	not applicable		
			27-OHC	not applicable		
Fig.23	**Total cholesterol**	Brain (A)		#	Sex F(1,38)=2.070, p=0.158; PCSK9 KO F(1,38)=0.603, p=0.442; 5XFAD F(1,38)=8.497, p=**0.006**; PCSK9*5XFAD F(1,38)=4.056, p=**0.051**	two-way ANOVA
		Serum (C)		***	Sex F(1,38)=6.322, p=**0.016**; PCSK9 KO F(1,38)=23.006, p<**0.001**; 5XFAD F(1,38)=3.343, p=**0.075**; PCSK9*5XFAD F(1,38)=0.699, p=0.408	two-way ANOVA
				***	**Analysis in 5XFAD mice:** Sex F(1,19)=15.363, p<**0.001;** PCSK9 KO F(1,19)=17.040, p<**0.001**	one-way ANOVA
	Hydroxysterols	Brain (B)	24-OHC	ns	Sex F(1,43)=1.259, p=0.268; PCSK9 KO F(1,44)=0.052, p=0.821; 5XFAD F(1,44)=0.528, p=0.471, PCSK9*5XFAD F(1,44)=1626, p=0.209	two-way ANOVA
			27-OHC	ns	Sex F(1,41)=1.605, p=0.212; PCSK9 KO F(1,42)=**0.022**, p=0.883; 5XFAD F(1,42)=0.482, p=0.491, PCSK9*5XFAD F(1,41)=0.122, p=0.729	
		Serum (D)	24-OHC	ns	Sex F(1,20)=0.341, p=0.566; PCSK9 KO F(1,21)=0.277, p=0.604; 5XFAD F(1,21)=0.209, p=0.653, PCSK9*5XFAD F(1,21)=1.771, p=0.198	two-way ANOVA
			25-OHC	ns	Sex F(1,19)=0.187, p=0.671; PCSK9 KO F(1,20)=0.890, p=0.357; 5XFAD F(1,20)=0.661, p=0.426, PCSK9*5XFAD F(1,20)=0.033, p=0.858	
			27-OHC	ns	Sex F(1,19)=0.597, p=0.44; PCSK9 KO F(1,20)=0.203, p=0.657; 5XFAD F(1,20)=0.287, p=0.598, PCSK9*5XFAD F(1,20)=0.022, p=0.884	

4.3. *In vivo* effect of 2-pyridone derivative compounds

A synthetic procedure for obtaining 2-pyridone derivative molecules was recently published (Giannessi et al. 2023). These molecules were preliminarily tested *in vitro* on human HepG2 cells to assess their cytotoxicity and their effect on PCSK9 inhibition and LDLR expression (Giannessi et al., 2023). The compound 5c (hereinafter referred to as **MR compound 3, MR3**) showed a significant inhibitory effect on both proPCSK9 and mature PCSK9 expression. Furthermore, although the **MR3** compound demonstrated only a moderate effect on its own, it showed an additive effect on LDLR levels and a dose-dependent reduction of *Pcsk9* mRNA levels when co-incubated with the positive control Simvastatin (Giannessi et al. 2023). Although its mechanism of action is still unknown, it has been hypothesized that MR3 could specifically interfere with PCSK9 transcription.

The newly synthesized class of PCSK9i, including **MR3**, **MR532**, and **MR533**, were selected for *in vivo* tolerability evaluation due to the positive preliminary results *in vitro*.

4.3.1. *In vivo* analysis of selected MRs tollerability

MR3, **MR532** and **MR533** were administered to Wt C57BL/6J mice to preliminarily evaluate the *in vivo* tolerability with respect of positive control SBC-115076, a commercially available PCSK9 modulator (Xu et al., 2019). The latter compound is known to inhibit the PCSK9-LDLR interaction and was shown to be safe in 3 mo male C57Bl6/J mice at 4 mg/Kg dosage (WIPO international publication number: **WO 2014/150326 A1**, Abdel-Meguid et al., 2014).

To evaluate the *in vivo* safety of selected compounds, each MR was SQ injected at dose of 40 mg/kg, ten times the dosage of SBC-115076, for 7 consecutive days. Body weight was daily recorded throughout the entire experimental period and weight variation was measured and compared to vehicle-treated group.

The average daily weight variation from first observation day (Basal-D1) of each group reported in **Figure 24 A** showed no significant alterations (see **Table 7** for statistical information). A body weight variation below 5% suggests the absence of critical suffering, according to the Federation of European Laboratory Animal Science Associations (FELASA) guidelines that define a body-weight reduction of 20% or more as severe suffering (Baumans et al., 1994).

The total distance travelled in OF by experimental mice was recorded in 10 min test daily; as shown in **Figure 24 B**, no significant differences in average distance travelled were found between groups; in addition, the global reduction in spontaneous exploration due to repeated exposure to OF arena was not influenced by any treatment suggesting the absence of toxic effects due to PCSK9i.

Moreover, no difference was detected on other locomotion parameters such as mean speed and % time exploration of corners and arena center, representing indexes of anxiety (data not shown); no other altered behaviors were observed during 10 min of free OF exploration.

Throughout the experimental period, mice were also subjected to a modified SHIRPA test (see **Material and Methods** for details). All animals, regardless of treatment group, have shown a good health status for whole observation period; mice were active and responsive to stimulations by operator; no changes in urination and defecation, fur sheen, tremors and abnormal secretions were detected.

Finally, after sacrifice, macroscopic alterations and weight of brain, spleen, liver, kidney, and gut were evaluated. No abnormalities were observed in PCSK9i receiving mouse groups with respect to vehicle-treated group. In particular, livers had normal morphology and no signs of hepatomegaly or necrosis were reported (see representative images in **Figure 24 C**).

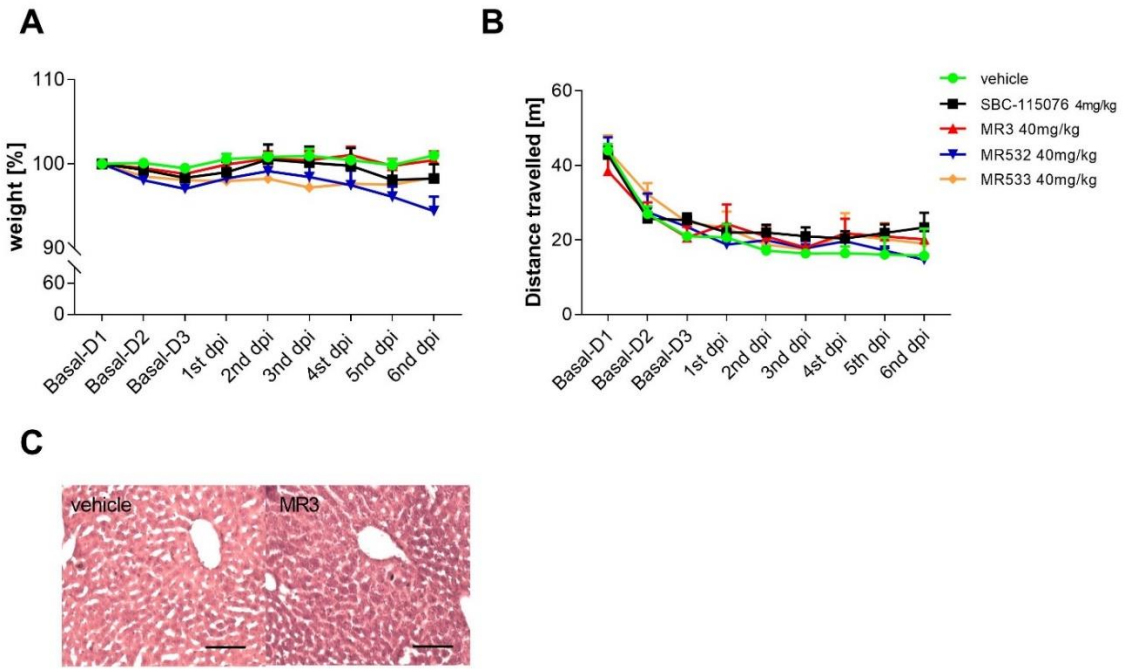

Figure 24. Effects of subacute iPCSK9 treatment in 3 mo male C56Bl6/J mice. A-B The analysis of body weight changes (**A**) and spontaneous locomotor activity (**B**) in OF were similar in all experimental groups - vehicle (**green line**), SBC-115076 (**black**), MR3 (**red line**), MR532 (**blue line**) and MR533 (**orange line**) - showing the absence of toxicity due to subacute injections of three compounds. Data are shown as mean ± SEM. Experimental groups: Vehicle, n = 5; SBC-115076, n = 6; MR3, n = 6; MR532, n = 6; MR533, n = 6. The analyses were performed by two-way repeated measure ANOVA (see **Table 7** for statistical report). **C** Representative images of vehicle and MR3 liver section. The histological analysis of hepatic tissues did not evidence any signs of toxicity. Abbreviations: D, Day; dpi, day post injection.

4.3.2. *Ex vivo* analysis

After *in vivo* safety evaluation, mice were sacrificed and *Pcsk9* mRNA was quantified in liver of treated mice. Analysis revealed no significant changes in the expression of hepatic *Pcsk9* (**Figure 25**).

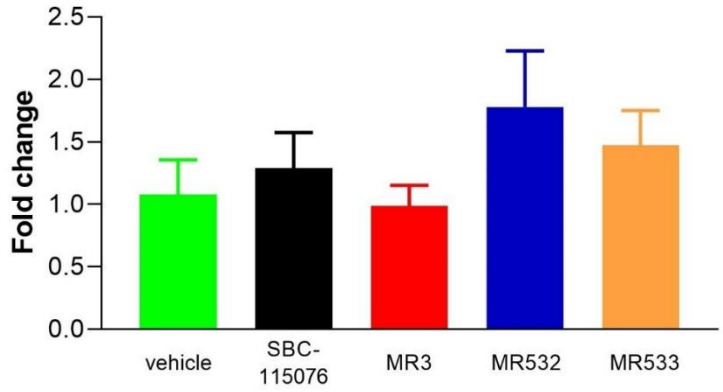

Figure 25. *Pcsk9* expression in the liver of mice treated with vehicle (green bar), SBC-115076 (black bar), MR3 (red bar), MR532 (blue bar) and MR533 (orange bar). Data are presented as fold change normalized over vehicle group mean and calibrated over GAPDH housekeeping gene and are shown as mean ± SEM. Experimental groups: Vehicle, n = 4; SBC-115076, n = 5; MR3, n = 5; MR532, n = 5; MR533, n = 5. Statistical comparisons were performed using one-way ANOVA (see **Table 7** for statistical report).

Overall, these data suggest that the SQ inj of 40 mg/kg of newly synthetized MRs for 7 days did not induce any sign of toxicity and was well tolerated by treated mice. However, the mechanism of action of MRs *in vivo* is still under investigation.

Table 7: Statistical supplementary details of *in vivo* tolerability and *ex vivo* analyses (**Figure 24-25**).

Fig.24	**OF**	weight % (A)	ns	Treatment F(4,18)=1.095, p=0.389; weight (8,144)=3.752, p=0.069; treatment*weight F(32,18)=1.513, p=0.240	one-way repeated measure ANOVA
		distance travelled (B)	ns	Treatment F(4,17)=0.320, p=0.861; distance (8,136)=34.719, p<0.001; treatment*distance F(32,17)=0.552, p=0.700	
Fig.25	***Pcsk9* mRNA**		ns	p=4116	one-way ANOVA

5. Discussion

Aim I

In addition to the well-known pathological hallmarks involving Aβ and phospho-tau aggregation, AD patients are characterized by neuroinflammation and metabolic abnormalities. A growing body of evidence from genetic studies links lipid dyshomeostasis and AD. In fact, genes involved in cholesterol metabolism have been identified as risk factors for disease onset and progression. Furthermore, the presence of cerebrovascular and cardiovascular disorders, diabetes, dyslipidemia, and hypertension has been associated with an increased risk of developing AD (Reitz et al., 2014). The pathogenesis of AD is characterized by a complex network of dysregulated mechanisms. Altered cholesterol homeostasis in the CNS can lead to oxidative stress, neuroinflammation, synaptic and neuronal dysfunction, and ultimately cognitive decline (McFarlane and Kedziora-Kornatowska, 2020).

PCSK9 is a well-known protein in the cardiovascular field that regulates the lifecycle of LDLR on the surface of liver cells, leading to its lysosomal degradation. Abnormal PCSK9 levels can cause an elevation of plasma circulating LDL-C levels, resulting in hypercholesterolemia. Recent studies have highlighted several extrahepatic effects of PCSK9 that occur in various tissues, including the brain. PCSK9 was first characterized in the brain as a regulator of neurodevelopment and apoptosis (Wu et al., 2014; Bingham et al., 2006; Seidah et al., 2003). Recently, PCSK9 has gained attention for its potential involvement in several CNS diseases, including AD. However, the available genetic data are limited and conflicting. For instance, Picard and colleagues observed that two specific variants of PCSK9 were associated with higher levels of PCSK9 in the frontal cortex and were linked to an increased risk of late-onset AD only in female subjects (Picard et al., 2019). More convincing data came from human biological samples; recently higher levels of PCSK9 were found in CSF of AD patients (Courtemanche et al., 2018; Zimetti et al., 2017), especially in those carrying the *APOEε4* variant (Zimetti et al., 2017).

Available evidence supporting the beneficial effects of PCSK9 inhibition on Aβ pathology and cognitive functions is restricted to animal models that only partially mimic the AD phenotype, such as high-fat diet rats (Abuelezz and Hendawy, 2021; Arunsak et al., 2020), or the use of monoclonal antibodies that only target peripheral PCSK9 due to their inability to cross the BBB (Mazura et al., 2022). On the other hand, the potential detrimental effect of PCSK9 has been investigated *in vitro*. The overexpression of PCSK9 in human neuroblastoma cells was found to exacerbate neurotoxicity induced by AD-like conditions resulting from exposure to Aβ fibrils (Papotti et al., 2022).

Present study shows for the first time the role of PCSK9 in modulating the neuroinflammatory response by upregulating several key inflammatory markers, such as proinflammatory cytokines and secretion of the chemokine MCP-1, in human U373 astrocytoma cells after exposure to Aβ fibrils. The impact of PCSK9 deletion on AD-like pathology *in vivo* and behavior was investigated in a severe AD mouse model, the 5XFAD mouse. In this study, 5XFAD mice lacking PCSK9, generated specifically for this purpose, were compared with 5XFAD mice expressing PCSK9 and respective Wt Ctrls. The new model was behaviorally characterized starting at 10 months of age, which is a period of full plaque maturation in 5XFAD mice. No alterations in motor or spontaneous exploratory behavior were observed in any 5XFAD mouse group compared to Ctrls. As previously reported by others, 5XFAD mice displayed reduced anxiety-like behavior in the EPM task, an effect which was maintained in the absence of PCSK9 (Jawhar et al., 2012; Forner et al., 2021).

Notably, complete ablation of PCSK9 in 10 mo 5XFAD mice resulted in several protective effects, including improvements in spatial learning and memory as tested by the MWM task. Moreover, the absence of PCSK9 impacted neuropathological outcomes as well as microglial density, distribution, and morphology. Specifically, the impaired hippocampus-dependent performance of a spatial memory task in 10 mo 5XFAD mice was significantly improved by the absence of PCSK9. During the initial cue-guided training period (D1-D7), all mice performed similarly and learned equally. However, differences in performance began to emerge as the training period was extended and task was made more difficult by changing the position of the platform and increasing the time between trials. At D8, despite a similar task was required, the 5XFAD groups regardless of the presence of PCSK9, showed higher time to reach the platform in the new position with respect to the Ctrls. However, in the second training period (D8-D13), only 5XFAD mice without PCSK9 were able to efficiently locate the new position of the hidden platform using spatially directed strategies, similar to the Ctrls. These findings are consistent with recent studies showing cognitive impairments in the high-fat cholesterol diet rat model of AD-like condition, by Abuelezz and Hendawy (2021), and in 6 mo 5XFAD mice by Mazura et al. (2022) after 10 weeks of systemic PCSK9 inhibition through monoclonal anti-PCSK9 antibody injection.

Gephine and colleagues recently investigated spatial pattern separation processes, which allow the creation of distinct episodic memories by encoding similar but different spatial information without interference and found an altered discrimination ability in 6 mo 5XFAD mice (Gephine et al., 2024). Since the MWM reversal test has been proposed to probe spatial pattern separation (Garthe and Kempermann 2013), present data confirm Gephine et al. study and suggest that PCSK9 may play a role in spatial pattern separation functions, possibly involving an effect on hippocampal neurogenesis (Clelland et al., 2009) as also reported in 5XFAD mice (Moon et al., 2014).

Our experimental model based on a global deletion of PCSK9 gene does not allow to determine whether the beneficial effects of PCSK9 deletion derive from its inhibition in the CNS and/or in peripheral tissues. Interestingly, recent data have revealed an increased expression of PCSK9 in AD (Picard et al., 2019). Therefore, it can be speculated that the observed changes are a direct consequence of PCSK9 loss in the CNS. However, it cannot be excluded that peripheral PCSK9 loss may also have an indirect influence (Mazura et al., 2022).
Taken together, present behavioral data demonstrate that inhibiting PCSK9 preserves hippocampal-dependent spatial learning abilities and memory in the 5XFAD model of AD.

In agreement with the recent evidence on the involvement of PCSK9 in promoting the deposition of Aβ (Abuelezz and Hendawy, 2021; Apaijai et al., 2019; Arunsak et al., 2020), our results show that its absence significantly reduces Aβ-related pathology. In fact, the deletion of PCSK9 significantly reduced the number and area of ThS^{+} and $6E10^{+}$ plaques, as well as the number of $11A1^{+}$ plaques in the cortico-hippocampal regions of 5XFAD mice, without affecting the regional distribution or the size distribution of amyloid plaques. Also in the olfactory tubercle area, where PCSK9 expression remains sustained in adult mice (Seidah et al., 2003), the analysis revealed a decrease in the count and area of $6E10^{+}$ and $11A1^{+}$ plaques in 5XFAD-$PCSK9^{KO}$ mice compared to 5XFAD-$PCSK9^{Het}$ mice. Overall, present evidence shows that the cognitive improvement observed in 5XFAD mice lacking PCSK9 is accompanied by a significant reduction of amyloid pathology.
This effect is unlikely to depend on changes in global BACE1 expression or its accumulation in peri-plaque dystrophic neurites. Although recent research has found that PCSK9 inhibition leads to a decrease in hippocampal *BACE1* expression in rats with high-fat cholesterol diet-induced AD-like conditions (Abuelezz and Hendawy, 2021), the role of PCSK9 in modulating BACE1 activity remains controversial. Different experimental conditions have shown both an increase and a decrease in BACE1 activity (Liu et al., 2010). Despite the significant and expected reduction in BACE1 plaque-associated dystrophic neurites in Nctx of 5XFAD-$PCSK9^{KO}$, consistent with the previously observed reduction in amyloidosis, the percentage of Congo Red^{+}-$BACE1^{+}$ plaques was comparable between 5XFAD mice with and without PCSK9.

In AD, Aβ can induce a neuroinflammatory response through a direct activation of microglia and the release of cytokines, for instance, by activating the NFkB-mediated signaling pathway (Combs et al., 2001). Previous *in vivo* data have demonstrated the role of PCSK9 in atherosclerotic plaque inflammation, which may involve TLR4 signaling (Tang et al., 2017). Moreover, emerging evidence has also implicated PCSK9 in neuroinflammation, namely through a role in coordinating the induction of the NFκB pathway and the activation of astrocytes and microglia (Abuelezz and

Hendawy, 2021; Apaijai et al., 2019). Our *in vitro* data indicate that recombinant PCSK9 worsened the AD-like condition induced by Aβ fibrils in the U373 astrocytoma cell line by increasing proinflammatory cytokine expression. Similarly, the absence of PCSK9 in 5XFAD mice reduced microglial reactivity, a key indicator of brain inflammation, in cortico-hippocampal regions to levels comparable to those of Ctrls, in terms of global $IBA1^+$ ir and the number of microglial cells. These findings tally well with recent studies indicating that in rats with brain ischemia-reperfusion injury, pretreatment with PCSK9i reduced astrocytes and microglia activation (Apaijai et al., 2019). In addition, PCSK9 inhibition has been shown to reduce activation of human T cells induced by oxidized LDL (Liu and Frostegard, 2018) and macrophage inflammatory response (Badimon et al., 2021).
Our *ex vivo* analysis, limited to transcripts, showed a significant increase in the expression of homeostatic genes, such as *P2ry12*, *Cd11b*, and *Cx3cr1*, as well as phagocytic/disease-associated genes of microglia, such as *Ifitm3* and *Cst7*, in the cortex of 10 mo 5XFAD mice, consistent with previous studies (Landel et al., 2014). However, the absence of PCSK9 did not modulate this effect. Our analysis showed only a minor decrease in *Cd36* expression in relation to AD-like pathology, but not PCSK9 loss, which was also confirmed by our *in vitro* experiments in astrocytes. Since increased *Cd36* expression has been associated with increased $A\beta_{1\text{-}42}$ uptake in the brain and decreased Aβ plaque burden in the Hip of 5XFAD mice (Koronyo et al., 2015; Koronyo-Hamaoui et al., 2019; Lucin et al., 2013), our data support the hypothesis that reduced amyloid plaque deposition in the absence of PCSK9 is not a consequence of accelerated Aβ phagocytosis. It should be noted that the analysis of the effect of genetic ablation of PCSK9 on microglial gene expression was conducted on the entire cerebral cortex, which is the brain region most affected by Aβ pathology in 5XFAD mice, and thus possible cell type and/or brain area specific alterations cannot be excluded.

The analysis of $GFAP^+$ ir, a marker of astrogliosis, in 5XFAD mice did not show significant effects of PCSK9 loss, except for CC-Cg. It is important to note that GFAP ir does not label all astrocytic populations, particularly in areas such as the cerebral cortex. Therefore, our data do not rule out the possibility that PCSK9 loss may have protective effect on other astrocytic populations. In addition, $GFAP^+$ astrocytes are known to contain subpopulations with different functional roles, including A1 neurotoxic astrocytes, which are the major astrocytic subtype that mediates astrocytic toxicity in AD (Lau et al., 2021). Further studies using A1-specific markers may reveal alterations in astrocytic subpopulations that were not identified in the present analysis.

As shown in mice lacking LRP1, lower neuronal cholesterol content is associated with neuronal loss in specific brain regions (Liu et al., 2010). Accordingly, *in vitro* studies showed that PCSK9 reduced cholesterol content and uptake in both astrocytes and neurons and potentiated Aβ neurotoxicity. In

particular, PCSK9 acts by degrading the APOERs at the synaptic level and impedes the correct supply of cholesterol to neurons, possibly leading to neurodegeneration (Papotti et al., 2022).
Our *in vivo* studies support the proposal of the impact of PCSK9 on brain cholesterol metabolism. Specifically, PCSK9 loss partially recovered the marked reduction of TC levels observed in 10 mo 5XFAD mice compared to Ctrls. Similarly, the quantification of serum TC levels demonstrated a significant effect of PCSK9 loss in 5XFAD mice. However, the most relevant oxidative bioactive metabolites of cholesterol did not show changes between the experimental groups. Therefore, present data suggest that the improved cognitive performance, reduced amyloidosis, and neuroinflammation caused by PCSK9 deletion in 5XFAD mice could only be partially explained by a restoration of lipid homeostasis. Accordingly, also the expression of lipid-related genes was unaffected by PCSK9 loss, with minor exceptions. In fact, both *ApoE* and *Lpl* were increased in 5XFAD mice without any interference by PCSK9 loss. Yet, cell-specific changes may occur in 5XFAD mice in the absence of PCSK9, as previously shown (Papotti et al., 2022). For these reasons, future studies investigating the differential effect of PCSK9 loss on cholesterol content in primary astrocytes and neurons from 5XFAD mice would be of great interest.

In conclusion, based on present and previous data, the pharmacological inhibition of PCSK9 may be an innovative strategy for AD treatment. Yet, the available data are few and most of published studies have not been conducted on animal models, like obese rats, that are not specific for AD; in addition, most of PCSK9i, such as monoclonal antibodies developed for hypercholesterolemia treatment, are not able to cross the BBB and therefore only act peripherally (Arunsak et al., 2020; Mazura et al., 2022). Preclinical studies, like the one presented here, are, therefore, highly warranted.

Aim II

To overcome the drawbacks of anti-PCSK9 biological drugs, a new class of small lipophilic molecules for AD treatment are being developed. Here, three newly synthesized small lipophilic compounds, MR3, MR532, and MR533, derivatives of 2-pyridone, were selected for their efficacy in PCSK9 inhibition and absence of cytotoxic effects *in vitro* on human HepG2 cells. In particular, MR3 exhibited potent inhibition activity on PCSK9 even at low doses (Giannessi et al., 2023).

All of these compounds demonstrated a good *in vivo* tolerability profile, showing no relevant effects on indices of mouse wellness, such as body weight, locomotion, and exploration activity. Additionally, there were no signs of suffering measured by the SHIRPA protocol. Moreover, no signs of hepatic toxicity were noticed in comparison with vehicle-treated mice.

The *ex vivo* analysis revealed no significant change in *Pcsk9* expression in the liver, as well as no change in plasma TC level compared to the vehicle group (Giannessi et al., 2023). This lack of effect may be due to an insufficient dosage, length of treatment, or poor biodistribution. Indeed, an effect could be better detected in mice fed with high-fat diet.

Given the fact that compound MR3 has shown strong inhibition activity on PCSK9, a significant additive effect with Simvastatin in inducing of LDLR expression *in vitro*, and a good tolerability *in vivo*, dedicated experiments will be necessary to test the effectiveness of this anti-PCSK9 compound.

References

Agarwal, M., & Khan, S. (2020). Plasma Lipids as Biomarkers for Alzheimer's Disease: A Systematic Review. *Cureus*, *12*(12), e12008.

Abdel-Meguid S.S. , Elshourbagy N., Meyers H., Mousa S.A., Anti-proprotein convertase subtilisin kexin type 9 (anti-PCSK9) compounds and methods of using the same in the treatment and/or prevention of cardiovascular diseases, WO 2014/150326 A1, 25 September 2014.

Abuelezz, S. A., & Hendawy, N. (2021). HMGB1/RAGE/TLR4 axis and glutamate as novel targets for PCSK9 inhibitor in high fat cholesterol diet induced cognitive impairment and amyloidosis. *Life sciences*, *273*, 119310.

Adorni, M. P., Cipollari, E., Favari, E., Zanotti, I., Zimetti, F., Corsini, A., Ricci, C., Bernini, F., & Ferri, N. (2017). Inhibitory effect of PCSK9 on Abca1 protein expression and cholesterol efflux in macrophages. *Atherosclerosis*, 256, 1–6.

Adorni, M. P., Ruscica, M., Ferri, N., Bernini, F., & Zimetti, F. (2019). Proprotein Convertase Subtilisin/Kexin Type 9, Brain Cholesterol Homeostasis and Potential Implication for Alzheimer's Disease. *Frontiers in aging neuroscience*, *11*, 120.

Ajayi, A. M., John, K. A., Emmanuel, I. B., Chidebe, E. O., & Adedapo, A. D. A. (2021). High-fat diet-induced memory impairment and anxiety-like behavior in rats attenuated by peel extract of *Ananas comosus* fruit via atheroprotective, antioxidant and anti-inflammatory actions. *Metabolism open*, *9*, 100077.

Alecu, I., & Bennett, S. A. L. (2019). Dysregulated Lipid Metabolism and Its Role in α-Synucleinopathy in Parkinson's Disease. *Frontiers in neuroscience*, 13, 328.

Alexandrov, P., Cui, J. G., Zhao, Y., & Lukiw, W. J. (2005). 24S-hydroxycholesterol induces inflammatory gene expression in primary human neural cells. *Neuroreport*, 16(9), 909–913.

Allinson, T. M., Parkin, E. T., Turner, A. J., & Hooper, N. M. (2003). ADAMs family members as amyloid precursor protein alpha-secretases. *Journal of neuroscience research*, 74(3), 342–352.

Almolda, B., de Labra, C., Barrera, I., Gruart, A., Delgado-Garcia, J. M., Villacampa, N., Vilella, A., Hofer, M. J., Hidalgo, J., Campbell, I. L., González, B., & Castellano, B. (2015). Alterations in microglial phenotype and hippocampal neuronal function in transgenic mice with astrocyte-targeted production of interleukin-10. *Brain, behavior, and immunity*, 45, 80–97.

Altmann, A., Tian, L., Henderson, V. W., Greicius, M. D., & Alzheimer's Disease Neuroimaging Initiative Investigators (2014). Sex modifies the APOE-related risk of developing Alzheimer disease. *Annals of neurology*, 75(4), 563–573.

Apaijai, N., Moisescu, D. M., Palee, S., McSweeney, C. M., Saiyasit, N., Maneechote, C., Boonnag, C., Chattipakorn, N., & Chattipakorn, S. C. (2019). Pretreatment With PCSK9 Inhibitor Protects

the Brain Against Cardiac Ischemia/Reperfusion Injury Through a Reduction of Neuronal Inflammation and Amyloid Beta Aggregation. *Journal of the American Heart Association*, 8(2), e010838.

Arélin, K., Kinoshita, A., Whelan, C. M., Irizarry, M. C., Rebeck, G. W., Strickland, D. K., & Hyman, B. T. (2002). LRP and senile plaques in Alzheimer's disease: colocalization with apolipoprotein E and with activated astrocytes. *Brain research. Molecular brain research*, *104*(1), 38–46.

Arunsak, B., Pratchayasakul, W., Amput, P., Chattipakorn, K., Tosukhowong, T., Kerdphoo, S., Jaiwongkum, T., Thonusin, C., Palee, S., Chattipakorn, N., & Chattipakorn, S. C. (2020). Proprotein convertase subtilisin/kexin type 9 (PCSK9) inhibitor exerts greater efficacy than atorvastatin on improvement of brain function and cognition in obese rats. *Archives of biochemistry and biophysics*, 689, 108470.

Badimon, L., Luquero, A., Crespo, J., Peña, E., & Borrell-Pages, M. (2021). PCSK9 and LRP5 in macrophage lipid internalization and inflammation. *Cardiovascular research*, *117*(9), 2054–2068.

Bajaj, N. S., Patel, N., Kalra, R., Ahmad, A., Venkatraman, A., Arora, G., & Arora, P. (2018). Neurological effects of proprotein convertase subtilisin/kexin type 9 inhibitors: direct comparisons. *European heart journal. Quality of care & clinical outcomes*, *4*(2), 132–141.

Balducci, C., Frasca, A., Zotti, M., La Vitola, P., Mhillaj, E., Grigoli, E., Iacobellis, M., Grandi, F., Messa, M., Colombo, L., Molteni, M., Trabace, L., Rossetti, C., Salmona, M., & Forloni, G. (2017). Toll-like receptor 4-dependent glial cell activation mediates the impairment in memory establishment induced by β-amyloid oligomers in an acute mouse model of Alzheimer's disease. *Brain, behavior, and immunity*, *60*, 188–197.

Bales, K. R., Verina, T., Cummins, D. J., Du, Y., Dodel, R. C., Saura, J., Fishman, C. E., DeLong, C. A., Piccardo, P., Petegnief, V., Ghetti, B., & Paul, S. M. (1999). Apolipoprotein E is essential for amyloid deposition in the APP(V717F) transgenic mouse model of Alzheimer's disease. *Proceedings of the National Academy of Sciences of the United States of America*, *96*(26), 15233–15238.

Baumans V, Brain PF, Bruge´re H, et al. Pain and distress in laboratory rodents and lagomorphs: report of the Federation of European Laboratory Animal Science Associations (FELASA) Working Group on Pain and Distress accepted by the FELASA Board of Management November 1992. *Lab Anim* 1994; 28: 97–112. 18.

Bellenguez, C., Küçükali, F., Jansen, I. E., Kleineidam, L., Moreno-Grau, S., Amin, N., Naj, A. C., Campos-Martin, R., Grenier-Boley, B., Andrade, V., Holmans, P. A., Boland, A., Damotte, V., van der Lee, S. J., Costa, M. R., Kuulasmaa, T., Yang, Q., de Rojas, I., Bis, J. C., Yaqub, A., …

Lambert, J. C. (2022). New insights into the genetic etiology of Alzheimer's disease and related dementias. *Nature genetics*, 54(4), 412–436.

Benjannet, S., Rhainds, D., Essalmani, R., Mayne, J., Wickham, L., Jin, W., Asselin, M. C., Hamelin, J., Varret, M., Allard, D., Trillard, M., Abifadel, M., Tebon, A., Attie, A. D., Rader, D. J., Boileau, C., Brissette, L., Chrétien, M., Prat, A., & Seidah, N. G. (2004). NARC-1/PCSK9 and its natural mutants: zymogen cleavage and effects on the low-density lipoprotein (LDL) receptor and LDL cholesterol. *The Journal of biological chemistry*, *279*(47), 48865–48875.

Berghoff, S. A., Spieth, L., Sun, T., Hosang, L., Schlaphoff, L., Depp, C., Düking, T., Winchenbach, J., Neuber, J., Ewers, D., Scholz, P., van der Meer, F., Cantuti-Castelvetri, L., Sasmita, A. O., Meschkat, M., Ruhwedel, T., Möbius, W., Sankowski, R., Prinz, M., Huitinga, I., … Saher, G. (2021). Microglia facilitate repair of demyelinated lesions via post-squalene sterol synthesis. *Nature neuroscience*, 24(1), 47–60.

Bianchi, P., Ciani, E., Guidi, S., Trazzi, S., Felice, D., Grossi, G., Fernandez, M., Giuliani, A., Calzà, L., & Bartesaghi, R. (2010). Early pharmacotherapy restores neurogenesis and cognitive performance in the Ts65Dn mouse model for Down syndrome. *The Journal of neuroscience : the official journal of the Society for Neuroscience*, 30(26), 8769–8779.

Bingham, B., Shen, R., Kotnis, S., Lo, C. F., Ozenberger, B. A., Ghosh, N., Kennedy, J. D., Jacobsen, J. S., Grenier, J. M., DiStefano, P. S., Chiang, L. W., & Wood, A. (2006). Proapoptotic effects of NARC 1 (= PCSK9), the gene encoding a novel serine proteinase. *Cytometry. Part A : the journal of the International Society for Analytical Cytology*, *69*(11), 1123–1131.

Blasco, H., Veyrat-Durebex, C., Bocca, C., Patin, F., Vourc'h, P., Kouassi Nzoughet, J., Lenaers, G., Andres, C. R., Simard, G., Corcia, P., & Reynier, P. (2017). Lipidomics Reveals Cerebrospinal-Fluid Signatures of ALS. *Scientific reports*, 7(1), 17652.

Borah, K., Rickman, O. J., Voutsina, N., Ampong, I., Gao, D., Baple, E. L., Dias, I. H., Crosby, A. H., & Griffiths, H. R. (2020). A quantitative LC-MS/MS method for analysis of mitochondrial -specific oxysterol metabolism. *Redox biology*, 36, 101595.

Bouscary, A., Quessada, C., René, F., Spedding, M., Turner, B. J., Henriques, A., Ngo, S. T., & Loeffler, J. P. (2021). Sphingolipids metabolism alteration in the central nervous system: Amyotrophic lateral sclerosis (ALS) and other neurodegenerative diseases. *Seminars in cell & developmental biology*, 112, 82–91.

Bu G. (2009). Apolipoprotein E and its receptors in Alzheimer's disease: pathways, pathogenesis and therapy. *Nature reviews. Neuroscience*, *10*(5), 333–344.

Buckley, R. F., Mormino, E. C., Rabin, J. S., Hohman, T. J., Landau, S., Hanseeuw, B. J., Jacobs, H. I. L., Papp, K. V., Amariglio, R. E., Properzi, M. J., Schultz, A. P., Kirn, D., Scott, M. R., Hedden,

T., Farrell, M., Price, J., Chhatwal, J., Rentz, D. M., Villemagne, V. L., Johnson, K. A., … Sperling, R. A. (2019). Sex Differences in the Association of Global Amyloid and Regional Tau Deposition Measured by Positron Emission Tomography in Clinically Normal Older Adults. *JAMA neurology*, 76(5), 542–551.

Buckley, R. F., Scott, M. R., Jacobs, H. I. L., Schultz, A. P., Properzi, M. J., Amariglio, R. E., Hohman, T. J., Mayblyum, D. V., Rubinstein, Z. B., Manning, L., Hanseeuw, B. J., Mormino, E. C., Rentz, D. M., Johnson, K. A., & Sperling, R. A. (2020). Sex Mediates Relationships Between Regional Tau Pathology and Cognitive Decline. *Annals of neurology*, 88(5), 921–932.

Burns, S., Selman, A., Sehar, U., Rawat, P., Reddy, A. P., & Reddy, P. H. (2022). Therapeutics of Alzheimer's Disease: Recent Developments. *Antioxidants (Basel, Switzerland)*, *11*(12), 2402.

Busquets, O., Ettcheto, M., Pallàs, M., Beas-Zarate, C., Verdaguer, E., Auladell, C., Folch, J., & Camins, A. (2017). Long-term exposition to a high fat diet favors the appearance of β-amyloid depositions in the brain of C57BL/6J mice. A potential model of sporadic Alzheimer's disease. *Mechanisms of ageing and development*, *162*, 38–45.

Campioni, S., Mannini, B., Zampagni, M., Pensalfini, A., Parrini, C., Evangelisti, E., Relini, A., Stefani, M., Dobson, C. M., Cecchi, C., & Chiti, F. (2010). A causative link between the structure of aberrant protein oligomers and their toxicity. *Nature chemical biology*, 6(2), 140–147.

Canuel, M., Sun, X., Asselin, M. C., Paramithiotis, E., Prat, A., & Seidah, N. G. (2013). Proprotein convertase subtilisin/kexin type 9 (PCSK9) can mediate degradation of the low density lipoprotein receptor-related protein 1 (LRP-1). *PloS one*, *8*(5), e64145.

Castellano, J. M., Kim, J., Stewart, F. R., Jiang, H., DeMattos, R. B., Patterson, B. W., Fagan, A. M., Morris, J. C., Mawuenyega, K. G., Cruchaga, C., Goate, A. M., Bales, K. R., Paul, S. M., Bateman, R. J., & Holtzman, D. M. (2011). Human apoE isoforms differentially regulate brain amyloid-β peptide clearance. *Science translational medicine*, *3*(89), 89ra57.

Ce, O., Rs, P., Ab, W., S, D., Cj, W., Qm, M., & D, L. (2018). Potential Link Between Proprotein Convertase Subtilisin/Kexin Type 9 and Alzheimer's Disease. *International journal of biomedical investigation*, *1*(1), 106.

Chaibva, M., Gao, X., Jain, P., Campbell, W. A., 4th, Frey, S. L., & Legleiter, J. (2018). Sphingomyelin and GM1 Influence Huntingtin Binding to, Disruption of, and Aggregation on Lipid Membranes. *ACS omega*, 3(1), 273–285.

Chaudhary, R., Garg, J., Shah, N., & Sumner, A. (2017). PCSK9 inhibitors: A new era of lipid lowering therapy. *World journal of cardiology*, *9*(2), 76–91.

Chen, G. F., Xu, T. H., Yan, Y., Zhou, Y. R., Jiang, Y., Melcher, K., & Xu, H. E. (2017). Amyloid beta: structure, biology and structure-based therapeutic development. *Acta pharmacologica Sinica*, *38*(9), 1205–1235.

Chen, X., Wu, S., Chen, C., Xie, B., Fang, Z., Hu, W., Chen, J., Fu, H., & He, H. (2017). Omega-3 polyunsaturated fatty acid supplementation attenuates microglial-induced inflammation by inhibiting the HMGB1/TLR4/NF-κB pathway following experimental traumatic brain injury. *Journal of neuroinflammation*, 14(1), 143.

Chew, H., Solomon, V. A., & Fonteh, A. N. (2020). Involvement of Lipids in Alzheimer's Disease Pathology and Potential Therapies. *Frontiers in physiology*, 11, 598.

Chia, R., Sabir, M. S., Bandres-Ciga, S., Saez-Atienzar, S., Reynolds, R. H., Gustavsson, E., Walton, R. L., Ahmed, S., Viollet, C., Ding, J., Makarious, M. B., Diez-Fairen, M., Portley, M. K., Shah, Z., Abramzon, Y., Hernandez, D. G., Blauwendraat, C., Stone, D. J., Eicher, J., Parkkinen, L., … Scholz, S. W. (2021). Genome sequencing analysis identifies new loci associated with Lewy body dementia and provides insights into its genetic architecture. *Nature genetics*, 53(3), 294–303.

Choi, G. E., Lee, S. J., Lee, H. J., Ko, S. H., Chae, C. W., & Han, H. J. (2017). Membrane-Associated Effects of Glucocorticoid on BACE1 Upregulation and Aβ Generation: Involvement of Lipid Raft-Mediated CREB Activation. *The Journal of neuroscience : the official journal of the Society for Neuroscience*, *37*(35), 8459–8476.

Ciudad, S., Puig, E., Botzanowski, T., Meigooni, M., Arango, A. S., Do, J., Mayzel, M., Bayoumi, M., Chaignepain, S., Maglia, G., Cianferani, S., Orekhov, V., Tajkhorshid, E., Bardiaux, B., & Carulla, N. (2020). Aβ(1-42) tetramer and octamer structures reveal edge conductivity pores as a mechanism for membrane damage. *Nature communications*, *11*(1), 3014.

Clelland, C. D., Choi, M., Romberg, C., Clemenson, G. D., Jr, Fragniere, A., Tyers, P., Jessberger, S., Saksida, L. M., Barker, R. A., Gage, F. H., & Bussey, T. J. (2009). A functional role for adult hippocampal neurogenesis in spatial pattern separation. *Science (New York, N.Y.)*, 325(5937), 210–213.

Cohen, J. C., Boerwinkle, E., Mosley, T. H., Jr, & Hobbs, H. H. (2006). Sequence variations in PCSK9, low LDL, and protection against coronary heart disease. *The New England journal of medicine*, *354*(12), 1264–1272.

Combs, C. K., Karlo, J. C., Kao, S. C., & Landreth, G. E. (2001). beta-Amyloid stimulation of microglia and monocytes results in TNFalpha-dependent expression of inducible nitric oxide synthase and

neuronal apoptosis. *The Journal of neuroscience : the official journal of the Society for Neuroscience*, 21(4), 1179–1188

Costet, P., Krempf, M., & Cariou, B. (2008). PCSK9 and LDL cholesterol: unravelling the target to design the bullet. *Trends in biochemical sciences*, *33*(9), 426–434.

Courtemanche, H., Bigot, E., Pichelin, M., Guyomarch, B., Boutoleau-Bretonnière, C., Le May, C., Derkinderen, P., & Cariou, B. (2018). PCSK9 Concentrations in Cerebrospinal Fluid Are Not Specifically Increased in Alzheimer's Disease. *Journal of Alzheimer's disease: JAD*, *62*(4), 1519–1525.

Crisby, M., Rahman, S. M., Sylvén, C., Winblad, B., & Schultzberg, M. (2004). Effects of high cholesterol diet on gliosis in apolipoprotein E knockout mice. Implications for Alzheimer's disease and stroke. *Neuroscience letters*, *369*(2), 87–92.

Crivelli, S. M., Giovagnoni, C., Visseren, L., Scheithauer, A. L., de Wit, N., den Hoedt, S., Losen, M., Mulder, M. T., Walter, J., de Vries, H. E., Bieberich, E., & Martinez-Martinez, P. (2020). Sphingolipids in Alzheimer's disease, how can we target them?. *Advanced drug delivery reviews*, 159, 214–231.

Cunnane, S. C., Schneider, J. A., Tangney, C., Tremblay-Mercier, J., Fortier, M., Bennett, D. A., & Morris, M. C. (2012). Plasma and brain fatty acid profiles in mild cognitive impairment and Alzheimer's disease. *Journal of Alzheimer's disease* : JAD, 29(3), 691–697.

Czubowicz, K., Jęśko, H., Wencel, P., Lukiw, W. J., & Strosznajder, R. P. (2019). The Role of Ceramide and Sphingosine-1-Phosphate in Alzheimer's Disease and Other Neurodegenerative Disorders. *Molecular neurobiology*, 56(8), 5436–5455.

Dafnis, I., Raftopoulou, C., Mountaki, C., Megalou, E., Zannis, V. I., & Chroni, A. (2018). ApoE isoforms and carboxyl-terminal-truncated apoE4 forms affect neuronal BACE1 levels and Aβ production independently of their cholesterol efflux capacity. *The Biochemical journal*, *475*(10), 1839–1859.

Daini, E., Secco, V., Liao, W., Zoli, M., & Vilella, A. (2021). A regional and cellular analysis of the early intracellular and extracellular accumulation of Aβ in the brain of 5XFAD mice. *Neuroscience letters*, *754*, 135869.

De Bem, A. F., Krolow, R., Farias, H. R., de Rezende, V. L., Gelain, D. P., Moreira, J. C. F., Duarte, J. M. D. N., & de Oliveira, J. (2021). Animal Models of Metabolic Disorders in the Study of Neurodegenerative Diseases: An Overview. *Frontiers in neuroscience*, *14*, 604150.

De Oliveira, J., Engel, D. F., de Paula, G. C., Dos Santos, D. B., Lopes, J. B., Farina, M., Moreira, E. L. G., & de Bem, A. F. (2020). High Cholesterol Diet Exacerbates Blood-Brain Barrier

Disruption in LDLr-/- Mice: Impact on Cognitive Function. *Journal of Alzheimer's disease : JAD*, *78*(1), 97–115.

De Roeck, A., Van Broeckhoven, C., & Sleegers, K. (2019). The role of ABCA7 in Alzheimer's disease: evidence from genomics, transcriptomics and methylomics. *Acta neuropathologica*, *138*(2), 201–220.

De Rojas, I., Moreno-Grau, S., Tesi, N., Grenier-Boley, B., Andrade, V., Jansen, I. E., Pedersen, N. L., Stringa, N., Zettergren, A., Hernández, I., Montrreal, L., Antúnez, C., Antonell, A., Tankard, R. M., Bis, J. C., Sims, R., Bellenguez, C., Quintela, I., González-Perez, A., Calero, M., … Ruiz, A. (2021). Common variants in Alzheimer's disease and risk stratification by polygenic risk scores. *Nature communications*, *12*(1), 3417.

Del Puppo, M., Kienle, M. G., Petroni, M. L., Crosignani, A., & Podda, M. (1998). Serum 27-hydroxycholesterol in patients with primary biliary cirrhosis suggests alteration of cholesterol catabolism to bile acids via the acidic pathway. *Journal of lipid research*, 39(12), 2477–2482.

Deng, S. J., Shen, Y., Gu, H. M., Guo, S., Wu, S. R., & Zhang, D. W. (2020). The role of the C-terminal domain of PCSK9 and SEC24 isoforms in PCSK9 secretion. *Biochimica et biophysica acta. Molecular and cell biology of lipids*, *1865*(6), 158660.

Di Pardo, A., Monyror, J., Morales, L. C., Kadam, V., Lingrell, S., Maglione, V., Wozniak, R. W., & Sipione, S. (2020). Mutant huntingtin interacts with the sterol regulatory element-binding proteins and impairs their nuclear import. *Human molecular genetics*, 29(3), 418–431.

Díaz, M., Fabelo, N., Ferrer, I., & Marín, R. (2018). "Lipid raft aging" in the human frontal cortex during nonpathological aging: gender influences and potential implications in Alzheimer's disease. *Neurobiology of aging*, 67, 42–52.

Diekstra, F. P., Saris, C. G., van Rheenen, W., Franke, L., Jansen, R. C., van Es, M. A., van Vught, P. W., Blauw, H. M., Groen, E. J., Horvath, S., Estrada, K., Rivadeneira, F., Hofman, A., Uitterlinden, A. G., Robberecht, W., Andersen, P. M., Melki, J., Meininger, V., Hardiman, O., Landers, J. E., … Veldink, J. H. (2012). Mapping of gene expression reveals CYP27A1 as a susceptibility gene for sporadic ALS. *PloS one*, 7(4), e35333.

Ding, Z., Liu, S., Wang, X., Theus, S., Deng, X., Fan, Y., Zhou, S., & Mehta, J. L. (2018). PCSK9 regulates expression of scavenger receptors and ox-LDL uptake in macrophages. *Cardiovascular research*, 114(8), 1145–1153.

Dodart, J. C., Mathis, C., Bales, K. R., Paul, S. M., & Ungerer, A. (2000). Behavioral deficits in APP(V717F) transgenic mice deficient for the apolipoprotein E gene. *Neuroreport*, *11*(3), 603–607.

Donahue, J. E., Flaherty, S. L., Johanson, C. E., Duncan, J. A., 3rd, Silverberg, G. D., Miller, M. C., Tavares, R., Yang, W., Wu, Q., Sabo, E., Hovanesian, V., & Stopa, E. G. (2006). RAGE, LRP-1, and amyloid-beta protein in Alzheimer's disease. *Acta neuropathologica*, *112*(4), 405–415.

Dubuc, G., Chamberland, A., Wassef, H., Davignon, J., Seidah, N. G., Bernier, L., & Prat, A. (2004). Statins upregulate PCSK9, the gene encoding the proprotein convertase neural apoptosis-regulated convertase-1 implicated in familial hypercholesterolemia. *Arteriosclerosis, thrombosis, and vascular biology*, *24*(8), 1454–1459.

Edwards F. A. (2019). A Unifying Hypothesis for Alzheimer's Disease: From Plaques to Neurodegeneration. *Trends in neurosciences*, *42*(5), 310–322.

Evison, B. J., Palmer, J. T., Lambert, G., Treutlein, H., Zeng, J., Nativel, B., Chemello, K., Zhu, Q., Wang, J., Teng, Y., Tang, W., Xu, Y., Rathi, A. K., Kumar, S., Suchowerska, A. K., Parmar, J., Dixon, I., Kelly, G. E., & Bonnar, J. (2020). A small molecule inhibitor of PCSK9 that antagonizes LDL receptor binding via interaction with a cryptic PCSK9 binding groove. *Bioorganic & medicinal chemistry*, *28*(6), 115344.

Evola, M., Hall, A., Wall, T., Young, A., & Grammas, P. (2010). Oxidative stress impairs learning and memory in apoE knockout mice. *Pharmacology, biochemistry, and behavior*, *96*(2), 181–186.

Famer, D., Meaney, S., Mousavi, M., Nordberg, A., Björkhem, I., & Crisby, M. (2007). Regulation of alpha- and beta-secretase activity by oxysterols: cerebrosterol stimulates processing of APP via the alpha-secretase pathway. *Biochemical and biophysical research communications*, 359(1), 46–50.

Fan, T. Y., Yang, Y. X., Zeng, Q. X., Wang, X. L., Wei, W., Guo, X. X., Zhao, L. P., Song, D. Q., Wang, Y. X., Wang, L., & Hong, B. (2021). Structure-activity relationship and biological evaluation of berberine derivatives as PCSK9 down-regulating agents. *Bioorganic chemistry*, *113*, 104994.

Fantini, J., Di Scala, C., Yahi, N., Troadec, J. D., Sadelli, K., Chahinian, H., & Garmy, N. (2014). Bexarotene blocks calcium-permeable ion channels formed by neurotoxic Alzheimer's β-amyloid peptides. *ACS chemical neuroscience*, 5(3), 216–224.

Farmer, B. C., Walsh, A. E., Kluemper, J. C., & Johnson, L. A. (2020). Lipid Droplets in Neurodegenerative Disorders. *Frontiers in neuroscience*, *14*, 742.

Ferré-González, L., Balaguer, Á., Roca, M., Ftara, A., Lloret, A., & Cháfer-Pericás, C. (2024). Author Correction: Brain areas lipidomics in female transgenic mouse model of Alzheimer's disease. *Scientific reports*, 14(1), 2100.

Filippov, V., Song, M. A., Zhang, K., Vinters, H. V., Tung, S., Kirsch, W. M., Yang, J., & Duerksen-Hughes, P. J. (2012). Increased ceramide in brains with Alzheimer's and other neurodegenerative diseases. *Journal of Alzheimer's disease : JAD*, 29(3), 537–547.

Fitz, N. F., Cronican, A., Pham, T., Fogg, A., Fauq, A. H., Chapman, R., Lefterov, I., & Koldamova, R. (2010). Liver X receptor agonist treatment ameliorates amyloid pathology and memory deficits caused by high-fat diet in APP23 mice. *The Journal of neuroscience : the official journal of the Society for Neuroscience*, *30*(20), 6862–6872.

Flores-Leon, M., & Outeiro, T. F. (2023). More than meets the eye in Parkinson's disease and other synucleinopathies: from proteinopathy to lipidopathy. *Acta neuropathologica*, 146(3), 369–385.

Forner, S., Kawauchi, S., Balderrama-Gutierrez, G., Kramár, E. A., Matheos, D. P., Phan, J., Javonillo, D. I., Tran, K. M., Hingco, E., da Cunha, C., Rezaie, N., Alcantara, J. A., Baglietto-Vargas, D., Jansen, C., Neumann, J., Wood, M. A., MacGregor, G. R., Mortazavi, A., Tenner, A. J., LaFerla, F. M., … Green, K. N. (2021). Systematic phenotyping and characterization of the 5xFAD mouse model of Alzheimer's disease. *Scientific data*, 8(1), 270.

France-Lanord, V., Brugg, B., Michel, P. P., Agid, Y., & Ruberg, M. (1997). Mitochondrial free radical signal in ceramide-dependent apoptosis: a putative mechanism for neuronal death in Parkinson's disease. *Journal of neurochemistry*, 69(4), 1612–1621.

Fu, T., Guan, Y., Xu, J., & Wang, Y. (2017). APP, APLP2 and LRP1 interact with PCSK9 but are not required for PCSK9-mediated degradation of the LDLR in vivo. *Biochimica et biophysica acta. Molecular and cell biology of lipids*, *1862*(9), 883–889.

Fünfschilling, U., Saher, G., Xiao, L., Möbius, W., & Nave, K. A. (2007). Survival of adult neurons lacking cholesterol synthesis in vivo. *BMC neuroscience*, *8*, 1.

Galper, J., Dean, N. J., Pickford, R., Lewis, S. J. G., Halliday, G. M., Kim, W. S., & Dzamko, N. (2022). Lipid pathway dysfunction is prevalent in patients with Parkinson's disease. *Brain : a journal of neurology*, 145(10), 3472–3487.

Gamba, P., Giannelli, S., Staurenghi, E., Testa, G., Sottero, B., Biasi, F., Poli, G., & Leonarduzzi, G. (2021). The Controversial Role of 24-S-Hydroxycholesterol in Alzheimer's Disease. *Antioxidants (Basel, Switzerland)*, *10*(5), 740.

Gamba, P., Staurenghi, E., Testa, G., Giannelli, S., Sottero, B., & Leonarduzzi, G. (2019). A Crosstalk Between Brain Cholesterol Oxidation and Glucose Metabolism in Alzheimer's Disease. *Frontiers in neuroscience*, 13, 556.

Gao, Y., Ye, S., Tang, Y., Tong, W., & Sun, S. (2023). Brain cholesterol homeostasis and its association with neurodegenerative diseases. *Neurochemistry international*, 171, 105635.

Genaro-Mattos, T. C., Anderson, A., Allen, L. B., Korade, Z., & Mirnics, K. (2019). Cholesterol Biosynthesis and Uptake in Developing Neurons. *ACS chemical neuroscience*, 10(8), 3671–3681.

Gencer, B., Mach, F., Guo, J., Im, K., Ruzza, A., Wang, H., Kurtz, C. E., Pedersen, T. R., Keech, A. C., Ott, B. R., Sabatine, M. S., Giugliano, R. P., & FOURIER Investigators (2020). Cognition After Lowering LDL-Cholesterol With Evolocumab. *Journal of the American College of Cardiology*, *75*(18), 2283–2293.

Gephine, L., Roux, C. M., Freret, T., Boulouard, M., & Leger, M. (2024). Vulnerability of Spatial Pattern Separation in 5xFAD Alzheimer's Disease Mouse Model. *Journal of Alzheimer's disease : JAD*, 97(4), 1889–1900.

Giannessi, L., Lupo, M. G., Rossi, I., Martina, M. G., Vilella, A., Bodria, M., Giuliani, D., Zimetti, F., Zanotti, I., Potì, F., Bernini, F., Ferri, N., & Radi, M. (2024). Identification of 4-amino-2-Pyridones as new potent PCSK9 inhibitors: From phenotypic hit discovery to in vivo tolerability. *European journal of medicinal chemistry*, 265, 116063.

Giugliano, R. P., Mach, F., Zavitz, K., Kurtz, C., Schneider, J., Wang, H., Keech, A., Pedersen, T. R., Sabatine, M. S., Sever, P. S., Honarpour, N., Wasserman, S. M., Ott, B. R., & EBBINGHAUS Investigators (2017). Design and rationale of the EBBINGHAUS trial: A phase 3, double-blind, placebo-controlled, multicenter study to assess the effect of evolocumab on cognitive function in patients with clinically evident cardiovascular disease and receiving statin background lipid-lowering therapy-A cognitive study of patients enrolled in the FOURIER trial. *Clinical cardiology*, *40*(2), 59–65.

Hamilton, L. K., Dufresne, M., Joppé, S. E., Petryszyn, S., Aumont, A., Calon, F., Barnabé-Heider, F., Furtos, A., Parent, M., Chaurand, P., & Fernandes, K. J. (2015). Aberrant Lipid Metabolism in the Forebrain Niche Suppresses Adult Neural Stem Cell Proliferation in an Animal Model of Alzheimer's Disease. *Cell stem cell*, *17*(4), 397–411.

Han, W., Ji, T., Mei, B., & Su, J. (2011). Peptide p3 may play a neuroprotective role in the brain. *Medical hypotheses*, 76(4), 543–546.

Han, X., M Holtzman, D., McKeel, D. W., Jr, Kelley, J., & Morris, J. C. (2002). Substantial sulfatide deficiency and ceramide elevation in very early Alzheimer's disease: potential role in disease pathogenesis. *Journal of neurochemistry*, 82(4), 809–818.

Harvey, P. D., Sabbagh, M. N., Harrison, J. E., Ginsberg, H. N., Chapman, M. J., Manvelian, G., Moryusef, A., Mandel, J., & Farnier, M. (2018). No evidence of neurocognitive adverse events associated with alirocumab treatment in 3340 patients from 14 randomized Phase 2 and 3

controlled trials: a meta-analysis of individual patient data. *European heart journal*, *39*(5), 374–381.

Hascalovici, J. R., Vaya, J., Khatib, S., Holcroft, C. A., Zukor, H., Song, W., Arvanitakis, Z., Bennett, D. A., & Schipper, H. M. (2009). Brain sterol dysregulation in sporadic AD and MCI: relationship to heme oxygenase-1. *Journal of neurochemistry*, *110*(4), 1241–1253.

Hatters, D. M., Peters-Libeu, C. A., & Weisgraber, K. H. (2006). Apolipoprotein E structure: insights into function. *Trends in biochemical sciences*, 31(8), 445–454.

Heneka, M. T., Carson, M. J., El Khoury, J., Landreth, G. E., Brosseron, F., Feinstein, D. L., Jacobs, A. H., Wyss-Coray, T., Vitorica, J., Ransohoff, R. M., Herrup, K., Frautschy, S. A., Finsen, B., Brown, G. C., Verkhratsky, A., Yamanaka, K., Koistinaho, J., Latz, E., Halle, A., Petzold, G. C., … Kummer, M. P. (2015). Neuroinflammation in Alzheimer's disease. *The Lancet. Neurology*, *14*(4), 388–405.

Heverin, M., Bogdanovic, N., Lütjohann, D., Bayer, T., Pikuleva, I., Bretillon, L., Diczfalusy, U., Winblad, B., & Björkhem, I. (2004). Changes in the levels of cerebral and extracerebral sterols in the brain of patients with Alzheimer's disease. *Journal of lipid research*, *45*(1), 186–193.

Hollingworth, P., Harold, D., Sims, R., Gerrish, A., Lambert, J. C., Carrasquillo, M. M., Abraham, R., Hamshere, M. L., Pahwa, J. S., Moskvina, V., Dowzell, K., Jones, N., Stretton, A., Thomas, C., Richards, A., Ivanov, D., Widdowson, C., Chapman, J., Lovestone, S., Powell, J., … Williams, J. (2011). Common variants at ABCA7, MS4A6A/MS4A4E, EPHA1, CD33 and CD2AP are associated with Alzheimer's disease. *Nature genetics*, *43*(5), 429–435.

Horton, J. D., Cohen, J. C., & Hobbs, H. H. (2009). PCSK9: a convertase that coordinates LDL catabolism. *Journal of lipid research*, *50 Suppl*(Suppl), S172–S177.

Horton, J. D., Goldstein, J. L., & Brown, M. S. (2002). SREBPs: activators of the complete program of cholesterol and fatty acid synthesis in the liver. *The Journal of clinical investigation*, *109*(9), 1125–1131.

Horton, J. D., Shah, N. A., Warrington, J. A., Anderson, N. N., Park, S. W., Brown, M. S., & Goldstein, J. L. (2003). Combined analysis of oligonucleotide microarray data from transgenic and knockout mice identifies direct SREBP target genes. *Proceedings of the National Academy of Sciences of the United States of America*, *100*(21), 12027–12032.

Huang, Y. A., Zhou, B., Wernig, M., & Südhof, T. C. (2017). ApoE2, ApoE3, and ApoE4 Differentially Stimulate APP Transcription and Aβ Secretion. *Cell*, *168*(3), 427–441.e21.

Hudry, E., Van Dam, D., Kulik, W., De Deyn, P. P., Stet, F. S., Ahouansou, O., Benraiss, A., Delacourte, A., Bougnères, P., Aubourg, P., & Cartier, N. (2010). Adeno-associated virus gene

therapy with cholesterol 24-hydroxylase reduces the amyloid pathology before or after the onset of amyloid plaques in mouse models of Alzheimer's disease. *Molecular therapy : the journal of the American Society of Gene Therapy*, 18(1), 44–53.

Huse, J. T., Liu, K., Pijak, D. S., Carlin, D., Lee, V. M., & Doms, R. W. (2002). Beta-secretase processing in the trans-Golgi network preferentially generates truncated amyloid species that accumulate in Alzheimer's disease brain. *The Journal of biological chemistry*, 277(18), 16278–16284.

Jaén, R. I., Povo-Retana, A., Rosales-Mendoza, C., Capillas-Herrero, P., Sánchez-García, S., Martín-Sanz, P., Mojena, M., Prieto, P., & Boscá, L. (2022). Functional Crosstalk between PCSK9 Internalization and Pro-Inflammatory Activation in Human Macrophages: Role of Reactive Oxygen Species Release. *International journal of molecular sciences*, *23*(16), 9114.

Jang, H., Arce, F. T., Ramachandran, S., Capone, R., Azimova, R., Kagan, B. L., Nussinov, R., & Lal, R. (2010). Truncated beta-amyloid peptide channels provide an alternative mechanism for Alzheimer's Disease and Down syndrome. *Proceedings of the National Academy of Sciences of the United States of America*, 107(14), 6538–6543.

Jawhar, S., Trawicka, A., Jenneckens, C., Bayer, T. A., & Wirths, O. (2012). Motor deficits, neuron loss, and reduced anxiety coinciding with axonal degeneration and intraneuronal Aβ aggregation in the 5XFAD mouse model of Alzheimer's disease. *Neurobiology of aging*, 33(1), 196.e29–196.e1.96E40.

Jiang, Q., Lee, C. Y., Mandrekar, S., Wilkinson, B., Cramer, P., Zelcer, N., Mann, K., Lamb, B., Willson, T. M., Collins, J. L., Richardson, J. C., Smith, J. D., Comery, T. A., Riddell, D., Holtzman, D. M., Tontonoz, P., & Landreth, G. E. (2008). ApoE promotes the proteolytic degradation of Abeta. *Neuron*, *58*(5), 681–693.

Jonas, M. C., Costantini, C., & Puglielli, L. (2008). PCSK9 is required for the disposal of non-acetylated intermediates of the nascent membrane protein BACE1. *EMBO reports*, *9*(9), 916–922.

Jones, L., Holmans, P. A., Hamshere, M. L., Harold, D., Moskvina, V., Ivanov, D., Pocklington, A., Abraham, R., Hollingworth, P., Sims, R., Gerrish, A., Pahwa, J. S., Jones, N., Stretton, A., Morgan, A. R., Lovestone, S., Powell, J., Proitsi, P., Lupton, M. K., Brayne, C., … Williams, J. (2010). Genetic evidence implicates the immune system and cholesterol metabolism in the aetiology of Alzheimer's disease. *PloS one*, *5*(11), e13950.

Jones, R. S., Minogue, A. M., Connor, T. J., & Lynch, M. A. (2013). Amyloid-β-induced astrocytic phagocytosis is mediated by CD36, CD47 and RAGE. *Journal of neuroimmune pharmacology : the official journal of the Society on NeuroImmune Pharmacology*, 8(1), 301–311.

Jorissen, E., Prox, J., Bernreuther, C., Weber, S., Schwanbeck, R., Serneels, L., Snellinx, A., Craessaerts, K., Thathiah, A., Tesseur, I., Bartsch, U., Weskamp, G., Blobel, C. P., Glatzel, M., De Strooper, B., & Saftig, P. (2010). The disintegrin/metalloproteinase ADAM10 is essential for the establishment of the brain cortex. *The Journal of neuroscience : the official journal of the Society for Neuroscience*, 30(14), 4833–4844.

Kandalepas, P. C., Sadleir, K. R., Eimer, W. A., Zhao, J., Nicholson, D. A., & Vassar, R. (2013). The Alzheimer's β-secretase BACE1 localizes to normal presynaptic terminals and to dystrophic presynaptic terminals surrounding amyloid plaques. *Acta neuropathologica*, 126(3), 329–352.

Kanekiyo, T., Xu, H., & Bu, G. (2014). ApoE and Aβ in Alzheimer's disease: accidental encounters or partners?. *Neuron*, 81(4), 740–754.

Kang, D. E., Pietrzik, C. U., Baum, L., Chevallier, N., Merriam, D. E., Kounnas, M. Z., Wagner, S. L., Troncoso, J. C., Kawas, C. H., Katzman, R., & Koo, E. H. (2000). Modulation of amyloid beta-protein clearance and Alzheimer's disease susceptibility by the LDL receptor-related protein pathway. *The Journal of clinical investigation*, *106*(9), 1159–1166.

Kang, S., Jeong, H., Baek, J. H., Lee, S. J., Han, S. H., Cho, H. J., Kim, H., Hong, H. S., Kim, Y. H., Yi, E. C., Seo, S. W., Na, D. L., Hwang, D., & Mook-Jung, I. (2016). PiB-PET Imaging-Based Serum Proteome Profiles Predict Mild Cognitive Impairment and Alzheimer's Disease. *Journal of Alzheimer's disease : JAD*, *53*(4), 1563–1576.

Kao, Y. C., Ho, P. C., Tu, Y. K., Jou, I. M., & Tsai, K. J. (2020). Lipids and Alzheimer's Disease. *International journal of molecular sciences*, *21*(4), 1505.

Khezri, M. R., Mohebalizadeh, M., & Ghasemnejad-Berenji, M. (2023). Therapeutic potential of ADAM10 modulation in Alzheimer's disease: a review of the current evidence. *Cell communication and signaling: CCS*, *21*(1), 60.

Kinney, J. W., Bemiller, S. M., Murtishaw, A. S., Leisgang, A. M., Salazar, A. M., & Lamb, B. T. (2018). Inflammation as a central mechanism in Alzheimer's disease. *Alzheimer's & dementia (New York, N. Y.)*, *4*, 575–590.

Knopman, D. S., Amieva, H., Petersen, R. C., Chételat, G., Holtzman, D. M., Hyman, B. T., Nixon, R. A., & Jones, D. T. (2021). Alzheimer disease. *Nature reviews. Disease primers*, *7*(1), 33.

Knowles, T. P., Vendruscolo, M., & Dobson, C. M. (2014). The amyloid state and its association with protein misfolding diseases. Nature reviews. *Molecular cell biology*, 15(6), 384–396.

Koran, M. E. I., Wagener, M., Hohman, T. J., & Alzheimer's Neuroimaging Initiative (2017). Sex differences in the association between AD biomarkers and cognitive decline. *Brain imaging and behavior*, 11(1), 205–213.

Koronyo, Y., Salumbides, B. C., Sheyn, J., Pelissier, L., Li, S., Ljubimov, V., Moyseyev, M., Daley, D., Fuchs, D. T., Pham, M., Black, K. L., Rentsendorj, A., & Koronyo-Hamaoui, M. (2015). Therapeutic effects of glatiramer acetate and grafted CD115^{+} monocytes in a mouse model of Alzheimer's disease. *Brain : a journal of neurology*, 138(Pt 8), 2399–2422.

Koronyo-Hamaoui, M., Sheyn, J., Hayden, E. Y., Li, S., Fuchs, D. T., Regis, G. C., Lopes, D. H. J., Black, K. L., Bernstein, K. E., Teplow, D. B., Fuchs, S., Koronyo, Y., & Rentsendorj, A. (2020). Peripherally derived angiotensin converting enzyme-enhanced macrophages alleviate Alzheimer-related disease. *Brain : a journal of neurology*, 143(1), 336–358.

Koudinov, A. R., & Koudinova, N. V. (2005). Cholesterol homeostasis failure as a unifying cause of synaptic degeneration. *Journal of the neurological sciences*, *229-230*, 233–240.

Koudinov, A., Kezlya, E., Koudinova, N., & Berezov, T. (2009). Amyloid-beta, tau protein, and oxidative changes as a physiological compensatory mechanism to maintain CNS plasticity under Alzheimer's disease and other neurodegenerative conditions. *Journal of Alzheimer's disease : JAD*, *18*(2), 381–400.

Koutsodendris, N., Nelson, M. R., Rao, A., & Huang, Y. (2022). Apolipoprotein E and Alzheimer's Disease: Findings, Hypotheses, and Potential Mechanisms. *Annual review of pathology*, *17*, 73–99.

Kuzmich, N., Andresyuk, E., Porozov, Y., Tarasov, V., Samsonov, M., Preferanskaya, N., Veselov, V., & Alyautdin, R. (2022). PCSK9 as a Target for Development of a New Generation of Hypolipidemic Drugs. *Molecules (Basel, Switzerland)*, *27*(2), 434.

Kysenius, K., Muggalla, P., Mätlik, K., Arumäe, U., & Huttunen, H. J. (2012). PCSK9 regulates neuronal apoptosis by adjusting ApoER2 levels and signaling. *Cellular and molecular life sciences : CMLS*, *69*(11), 1903–1916.

Laird, F. M., Cai, H., Savonenko, A. V., Farah, M. H., He, K., Melnikova, T., Wen, H., Chiang, H. C., Xu, G., Koliatsos, V. E., Borchelt, D. R., Price, D. L., Lee, H. K., & Wong, P. C. (2005). BACE1, a major determinant of selective vulnerability of the brain to amyloid-beta amyloidogenesis, is essential for cognitive, emotional, and synaptic functions. *The Journal of neuroscience : the official journal of the Society for Neuroscience*, 25(50), 11693–11709.

Lambert, G., Sjouke, B., Choque, B., Kastelein, J. J., & Hovingh, G. K. (2012). The PCSK9 decade. *Journal of lipid research*, 53(12), 2515–2524.

Landel, V., Baranger, K., Virard, I., Loriod, B., Khrestchatisky, M., Rivera, S., Benech, P., & Féron, F. (2014). Temporal gene profiling of the 5XFAD transgenic mouse model highlights the importance of microglial activation in Alzheimer's disease. *Molecular neurodegeneration*, 9, 33.

Ledeen, R. W., & Wu, G. (2008). Nuclear sphingolipids: metabolism and signaling. *Journal of lipid research*, 49(6), 1176–1186.

Leoni, V., Masterman, T., Patel, P., Meaney, S., Diczfalusy, U., & Björkhem, I. (2003). Side chain oxidized oxysterols in cerebrospinal fluid and the integrity of blood-brain and blood-cerebrospinal fluid barriers. *Journal of lipid research*, *44*(4), 793–799.

Leoni, V., Shafaati, M., Salomon, A., Kivipelto, M., Björkhem, I., & Wahlund, L. O. (2006). Are the CSF levels of 24S-hydroxycholesterol a sensitive biomarker for mild cognitive impairment?. *Neuroscience letters*, 397(1-2), 83–87.

Liao, F., Hori, Y., Hudry, E., Bauer, A. Q., Jiang, H., Mahan, T. E., Lefton, K. B., Zhang, T. J., Dearborn, J. T., Kim, J., Culver, J. P., Betensky, R., Wozniak, D. F., Hyman, B. T., & Holtzman, D. M. (2014). Anti-ApoE antibody given after plaque onset decreases Aβ accumulation and improves brain function in a mouse model of Aβ amyloidosis. *The Journal of neuroscience : the official journal of the Society for Neuroscience*, *34*(21), 7281–7292.

Lin, B., Hasegawa, Y., Takane, K., Koibuchi, N., Cao, C., & Kim-Mitsuyama, S. (2016). High-Fat-Diet Intake Enhances Cerebral Amyloid Angiopathy and Cognitive Impairment in a Mouse Model of Alzheimer's Disease, Independently of Metabolic Disorders. *Journal of the American Heart Association*, *5*(6), e003154.

Liu, A., & Frostegård, J. (2018). PCSK9 plays a novel immunological role in oxidized LDL-induced dendritic cell maturation and activation of T cells from human blood and atherosclerotic plaque. *Journal of internal medicine*, 10.1111/joim.12758. Advance online publication.

Liu, C. C., Liu, C. C., Kanekiyo, T., Xu, H., & Bu, G. (2013). Apolipoprotein E and Alzheimer disease: risk, mechanisms and therapy. *Nature reviews. Neurology*, *9*(2), 106–118.

Liu, C., Chen, J., Chen, H., Zhang, T., He, D., Luo, Q., Chi, J., Hong, Z., Liao, Y., Zhang, S., Wu, Q., Cen, H., Chen, G., Li, J., & Wang, L. (2022). PCSK9 Inhibition: From Current Advances to Evolving Future. *Cells*, *11*(19), 2972.

Liu, M., Wu, G., Baysarowich, J., Kavana, M., Addona, G. H., Bierilo, K. K., Mudgett, J. S., Pavlovic, G., Sitlani, A., Renger, J. J., Hubbard, B. K., Fisher, T. S., & Zerbinatti, C. V. (2010). PCSK9 is not involved in the degradation of LDL receptors and BACE1 in the adult mouse brain. *Journal of lipid research*, *51*(9), 2611–2618.

Liu, Y., Xu, X., Dou, H., Hua, Y., Xu, J., & Hui, X. (2015). Apolipoprotein E knockout induced inflammatory responses related to microglia in neonatal mice brain via astrocytes. *International journal of clinical and experimental medicine*, 8(1), 737–743.

Locchi, F., Dall'olio, R., Gandolfi, O., & Rimondini, R. (2008). Olanzapine counteracts stress-induced anxiety-like behavior in rats. *Neuroscience letters*, 438(2), 146–149.

Loving, B. A., & Bruce, K. D. (2020). Lipid and Lipoprotein Metabolism in Microglia. *Frontiers in physiology*, *11*, 393.

Lucin, K. M., O'Brien, C. E., Bieri, G., Czirr, E., Mosher, K. I., Abbey, R. J., Mastroeni, D. F., Rogers, J., Spencer, B., Masliah, E., & Wyss-Coray, T. (2013). Microglial beclin 1 regulates retromer trafficking and phagocytosis and is impaired in Alzheimer's disease. *Neuron*, 79(5), 873–886.

Luo, J., Yang, H., & Song, B. L. (2020). Mechanisms and regulation of cholesterol homeostasis. *Nature reviews. Molecular cell biology*, *21*(4), 225–245.

Ma, S. L., Ng, H. K., Baum, L., Pang, J. C., Chiu, H. F., Woo, J., Tang, N. L., & Lam, L. C. (2002). Low-density lipoprotein receptor-related protein 8 (apolipoprotein E receptor 2) gene polymorphisms in Alzheimer's disease. *Neuroscience letters*, 332(3), 216–218.

Macchi, C., Ferri, N., Sirtori, C. R., Corsini, A., Banach, M., & Ruscica, M. (2021). Proprotein Convertase Subtilisin/Kexin Type 9: A View beyond the Canonical Cholesterol-Lowering Impact. *The American journal of pathology*, *191*(8), 1385–1397.

Macías-García, D., Periñán, M. T., Muñoz-Delgado, L., Jimenez-Jaraba, M. V., Labrador-Espinosa, M. Á., Jesús, S., Buiza-Rueda, D., Méndez-Del Barrio, C., Adarmes-Gómez, A., Gómez-Garre, P., & Mir, P. (2021). Serum lipid profile among sporadic and familial forms of Parkinson's disease. *NPJ Parkinson's disease*, 7(1), 59.

Mahley R. W. (2016). Central Nervous System Lipoproteins: ApoE and Regulation of Cholesterol Metabolism. *Arteriosclerosis, thrombosis, and vascular biology*, *36*(7), 1305–1315.

Malchiodi-Albedi, F., Paradisi, S., Matteucci, A., Frank, C., & Diociaiuti, M. (2011). Amyloid oligomer neurotoxicity, calcium dysregulation, and lipid rafts. *International journal of Alzheimer's disease*, *2011*, 906964.

Marchi, C., Adorni, M. P., Caffarra, P., Ronda, N., Spallazzi, M., Barocco, F., Galimberti, D., Bernini, F., & Zimetti, F. (2019). ABCA1- and ABCG1-mediated cholesterol efflux capacity of cerebrospinal fluid is impaired in Alzheimer's disease. *Journal of lipid research*, *60*(8), 1449–1456.

Mariosa, D., Hammar, N., Malmström, H., Ingre, C., Jungner, I., Ye, W., Fang, F., & Walldius, G. (2017). Blood biomarkers of carbohydrate, lipid, and apolipoprotein metabolisms and risk of amyotrophic lateral sclerosis: A more than 20-year follow-up of the Swedish AMORIS cohort. *Annals of neurology*, 81(5), 718–728.

Marquer, C., Devauges, V., Cossec, J. C., Liot, G., Lécart, S., Saudou, F., Duyckaerts, C., Lévêque-Fort, S., & Potier, M. C. (2011). Local cholesterol increase triggers amyloid precursor protein-Bace1 clustering in lipid rafts and rapid endocytosis. *FASEB journal : official publication of the Federation of American Societies for Experimental Biology*, *25*(4), 1295–1305.

Martín, V., Fabelo, N., Santpere, G., Puig, B., Marín, R., Ferrer, I., & Díaz, M. (2010). Lipid alterations in lipid rafts from Alzheimer's disease human brain cortex. *Journal of Alzheimer's disease : JAD*, 19(2), 489–502.

Martinez, Z., Zhu, M., Han, S., & Fink, A. L. (2007). GM1 specifically interacts with alpha-synuclein and inhibits fibrillation. *Biochemistry*, 46(7), 1868–1877.

Mazura, A. D., Ohler, A., Storck, S. E., Kurtyka, M., Scharfenberg, F., Weggen, S., Becker-Pauly, C., & Pietrzik, C. U. (2022). PCSK9 acts as a key regulator of Aβ clearance across the blood-brain barrier. *Cellular and molecular life sciences: CMLS*, *79*(4), 212.

McFarlane, O., & Kędziora-Kornatowska, K. (2020). Cholesterol and Dementia: A Long and Complicated Relationship. *Current aging science*, *13*(1), 42–51.

Mencarelli, C., & Martinez-Martinez, P. (2013). Ceramide function in the brain: when a slight tilt is enough. *Cellular and molecular life sciences: CMLS*, 70(2), 181–203.

Mesa-Herrera, F., Taoro-González, L., Valdés-Baizabal, C., Diaz, M., & Marín, R. (2019). Lipid and Lipid Raft Alteration in Aging and Neurodegenerative Diseases: A Window for the Development of New Biomarkers. *International journal of molecular sciences*, 20(15), 3810.

Methia, N., André, P., Hafezi-Moghadam, A., Economopoulos, M., Thomas, K. L., & Wagner, D. D. (2001). ApoE deficiency compromises the blood brain barrier especially after injury. *Molecular medicine (Cambridge, Mass.)*, *7*(12), 810–815.

Miao, J., Ma, H., Yang, Y., Liao, Y., Lin, C., Zheng, J., Yu, M., & Lan, J. (2023). Microglia in Alzheimer's disease: pathogenesis, mechanisms, and therapeutic potentials. *Frontiers in aging neuroscience*, 15, 1201982.

Michaels, T. C. T., Šarić, A., Curk, S., Bernfur, K., Arosio, P., Meisl, G., Dear, A. J., Cohen, S. I. A., Dobson, C. M., Vendruscolo, M., Linse, S., & Knowles, T. P. J. (2020). Dynamics of oligomer populations formed during the aggregation of Alzheimer's Aβ42 peptide. *Nature chemistry*, 12(5), 445–451.

Mielke, M. M., Bandaru, V. V., Haughey, N. J., Xia, J., Fried, L. P., Yasar, S., Albert, M., Varma, V., Harris, G., Schneider, E. B., Rabins, P. V., Bandeen-Roche, K., Lyketsos, C. G., & Carlson, M. C. (2012). Serum ceramides increase the risk of Alzheimer disease: the Women's Health and Aging Study II. *Neurology*, 79(7), 633–641.

Mielke, M. M., Haughey, N. J., Bandaru, V. V., Schech, S., Carrick, R., Carlson, M. C., Mori, S., Miller, M. I., Ceritoglu, C., Brown, T., Albert, M., & Lyketsos, C. G. (2010). Plasma ceramides are altered in mild cognitive impairment and predict cognitive decline and hippocampal volume loss. *Alzheimer's & dementia : the journal of the Alzheimer's Association*, 6(5), 378–385.

Min, S. W., Cho, S. H., Zhou, Y., Schroeder, S., Haroutunian, V., Seeley, W. W., Huang, E. J., Shen, Y., Masliah, E., Mukherjee, C., Meyers, D., Cole, P. A., Ott, M., & Gan, L. (2010). Acetylation of tau inhibits its degradation and contributes to tauopathy. *Neuron*, 67(6), 953–966.

Momtazi-Borojeni, A. A., Sabouri-Rad, S., Gotto, A. M., Pirro, M., Banach, M., Awan, Z., Barreto, G. E., & Sahebkar, A. (2019). PCSK9 and inflammation: a review of experimental and clinical evidence. *European heart journal. Cardiovascular pharmacotherapy*, 5(4), 237–245.

Moon, M., Cha, M. Y., & Mook-Jung, I. (2014). Impaired hippocampal neurogenesis and its enhancement with ghrelin in 5XFAD mice. *Journal of Alzheimer's disease : JAD*, 41(1), 233–241.

Mori, T., Paris, D., Town, T., Rojiani, A. M., Sparks, D. L., Delledonne, A., Crawford, F., Abdullah, L. I., Humphrey, J. A., Dickson, D. W., & Mullan, M. J. (2001). Cholesterol accumulates in senile plaques of Alzheimer disease patients and in transgenic APP(SW) mice. *Journal of neuropathology and experimental neurology*, *60*(8), 778–785.

Morley, J. E., Farr, S. A., Banks, W. A., Johnson, S. N., Yamada, K. A., & Xu, L. (2010). A physiological role for amyloid-beta protein:enhancement of learning and memory. *Journal of Alzheimer's disease : JAD*, 19(2), 441–449.

Mortensen, M. B., & Nordestgaard, B. G. (2020). Elevated LDL cholesterol and increased risk of myocardial infarction and atherosclerotic cardiovascular disease in individuals aged 70-100 years: a contemporary primary prevention cohort. *Lancet (London, England)*, 396(10263), 1644–1652.

Mulder, M., Jansen, P. J., Janssen, B. J., van de Berg, W. D., van der Boom, H., Havekes, L. M., de Kloet, R. E., Ramaekers, F. C., & Blokland, A. (2004). Low-density lipoprotein receptor-knockout mice display impaired spatial memory associated with a decreased synaptic density in the hippocampus. *Neurobiology of disease*, *16*(1), 212–219.

Mulder, M., Koopmans, G., Wassink, G., Al Mansouri, G., Simard, M. L., Havekes, L. M., Prickaerts, J., & Blokland, A. (2007). LDL receptor deficiency results in decreased cell proliferation and presynaptic bouton density in the murine hippocampus. *Neuroscience research*, *59*(3), 251–256.

Neu, S. C., Pa, J., Kukull, W., Beekly, D., Kuzma, A., Gangadharan, P., Wang, L. S., Romero, K., Arneric, S. P., Redolfi, A., Orlandi, D., Frisoni, G. B., Au, R., Devine, S., Auerbach, S., Espinosa, A., Boada, M., Ruiz, A., Johnson, S. C., Koscik, R., … Toga, A. W. (2017). Apolipoprotein E Genotype and Sex Risk Factors for Alzheimer Disease: A Meta-analysis. *JAMA neurology*, 74(10), 1178–1189.

Nieweg, K., Schaller, H., & Pfrieger, F. W. (2009). Marked differences in cholesterol synthesis between neurons and glial cells from postnatal rats. *Journal of neurochemistry*, 109(1), 125–134.

Nikolaev, A., McLaughlin, T., O'Leary, D. D., & Tessier-Lavigne, M. (2009). APP binds DR6 to trigger axon pruning and neuron death via distinct caspases. *Nature*, 457(7232), 981–989.

Nilsson, N. I. V., Picard, C., Labonté, A., Köbe, T., Meyer, P. F., Villeneuve, S., Auld, D., Poirier, J., For The Prevent-Ad Research Group, & Alzheimer's Disease Neuroimaging Initiative (2021). Association of a Total Cholesterol Polygenic Score with Cholesterol Levels and Pathological Biomarkers across the Alzheimer's Disease Spectrum. *Genes*, *12*(11), 1805.

Nishikido, T., & Ray, K. K. (2019). Non-antibody Approaches to Proprotein Convertase Subtilisin Kexin 9 Inhibition: siRNA, Antisense Oligonucleotides, Adnectins, Vaccination, and New Attempts at Small-Molecule Inhibitors Based on New Discoveries. *Frontiers in cardiovascular medicine*, *5*, 199.

Oakley, H., Cole, S. L., Logan, S., Maus, E., Shao, P., Craft, J., Guillozet-Bongaarts, A., Ohno, M., Disterhoft, J., Van Eldik, L., Berry, R., & Vassar, R. (2006). Intraneuronal beta-amyloid aggregates, neurodegeneration, and neuron loss in transgenic mice with five familial Alzheimer's disease mutations: potential factors in amyloid plaque formation. *The Journal of neuroscience : the official journal of the Society for Neuroscience*, 26(40), 10129–10140.

Oblak, A. L., Lin, P. B., Kotredes, K. P., Pandey, R. S., Garceau, D., Williams, H. M., Uyar, A., O'Rourke, R., O'Rourke, S., Ingraham, C., Bednarczyk, D., Belanger, M., Cope, Z. A., Little, G. J., Williams, S. G., Ash, C., Bleckert, A., Ragan, T., Logsdon, B. A., Mangravite, L. M., … Lamb, B. T. (2021). Comprehensive Evaluation of the 5XFAD Mouse Model for Preclinical Testing Applications: A MODEL-AD Study. *Frontiers in aging neuroscience*, 13, 713726.

O'Connell, E. M., & Lohoff, F. W. (2020). Proprotein Convertase Subtilisin/Kexin Type 9 (PCSK9) in the Brain and Relevance for Neuropsychiatric Disorders. *Frontiers in neuroscience*, *14*, 609.

Odnoshivkina, U. G., Kuznetsova, E. A., & Petrov, A. M. (2022). 25-Hydroxycholesterol as a Signaling Molecule of the Nervous System. *Biochemistry. Biokhimiia*, 87(6), 524–537.

Oku, Y., Murakami, K., Irie, K., Hoseki, J., & Sakai, Y. (2017). Synthesized Aβ42 Caused Intracellular Oxidative Damage, Leading to Cell Death, via Lysosome Rupture. *Cell structure and function*, *42*(1), 71–79.

Oliver, D. M. A., & Reddy, P. H. (2019). Molecular Basis of Alzheimer's Disease: Focus on Mitochondria. *Journal of Alzheimer's disease : JAD*, *72*(s1), S95–S116.

Olsen, B. N., Schlesinger, P. H., Ory, D. S., & Baker, N. A. (2012). Side-chain oxysterols: from cells to membranes to molecules. *Biochimica et biophysica acta*, *1818*(2), 330–336.

Osborn, L. M., Kamphuis, W., Wadman, W. J., & Hol, E. M. (2016). Astrogliosis: An integral player in the pathogenesis of Alzheimer's disease. *Progress in neurobiology*, 144, 121–141.

Panza, F., D'Introno, A., Colacicco, A. M., Capurso, C., Pichichero, G., Capurso, S. A., Capurso, A., & Solfrizzi, V. (2006). Lipid metabolism in cognitive decline and dementia. *Brain research reviews*, *51*(2), 275–292.

Papotti, B., Adorni, M. P., Marchi, C., Zimetti, F., Ronda, N., Panighel, G., Lupo, M. G., Vilella, A., Giuliani, D., Ferri, N., & Bernini, F. (2022). PCSK9 Affects Astrocyte Cholesterol Metabolism and Reduces Neuron Cholesterol Supplying In Vitro: Potential Implications in Alzheimer's Disease. *International journal of molecular sciences*, *23*(20), 12192.

Pärn, A., Olsen, D., Tuvikene, J., Kaas, M., Borisova, E., Bilgin, M., Elhauge, M., Vilstrup, J., Madsen, P., Ambrozkiewicz, M. C., Goz, R. U., Timmusk, T., Tarabykin, V., Gustafsen, C., & Glerup, S. (2023). PCSK9 deficiency alters brain lipid composition without affecting brain development and function. *Frontiers in molecular neuroscience*, *15*, 1084633.

Paxinos, G., Franklin, K.B.J., 2019. Paxinos and Franklin's the Mouse Brain in Stereotaxic Coordinates.

Petrilli, W. L., Adam, G. C., Erdmann, R. S., Abeywickrema, P., Agnani, V., Ai, X., Baysarowich, J., Byrne, N., Caldwell, J. P., Chang, W., DiNunzio, E., Feng, Z., Ford, R., Ha, S., Huang, Y., Hubbard, B., Johnston, J. M., Kavana, M., Lisnock, J. M., Liang, R., … Imbriglio, J. E. (2020). From Screening to Targeted Degradation: Strategies for the Discovery and Optimization of Small Molecule Ligands for PCSK9. *Cell chemical biology*, *27*(1), 32–40.e3.

Petrov, A. M., Kasimov, M. R., & Zefirov, A. L. (2016). Brain Cholesterol Metabolism and Its Defects: Linkage to Neurodegenerative Diseases and Synaptic Dysfunction. *Acta naturae*, 8(1), 58–73.

Pfundstein, G., Nikonenko, A. G., & Sytnyk, V. (2022). Amyloid precursor protein (APP) and amyloid β (Aβ) interact with cell adhesion molecules: Implications in Alzheimer's disease and normal physiology. *Frontiers in cell and developmental biology*, *10*, 969547.

Picard, C., Poirier, A., Bélanger, S., Labonté, A., Auld, D., Poirier, J., & PREVENT-AD Research Group (2019). Proprotein convertase subtilisin/kexin type 9 (PCSK9) in Alzheimer's disease: A genetic and proteomic multi-cohort study. *PloS one*, *14*(8), e0220254.

Pike C. J. (2017). Sex and the development of Alzheimer's disease. *Journal of neuroscience research*, 95(1-2), 671–680.

Podbielska, M., Ariga, T., & Pokryszko-Dragan, A. (2022). Sphingolipid Players in Multiple Sclerosis: Their Influence on the Initiation and Course of the Disease. *International journal of molecular sciences*, 23(10), 5330.

Poirier, S., & Mayer, G. (2013). The biology of PCSK9 from the endoplasmic reticulum to lysosomes: new and emerging therapeutics to control low-density lipoprotein cholesterol. *Drug design, development and therapy*, 7, 1135–1148.

Poirier, S., Mayer, G., Benjannet, S., Bergeron, E., Marcinkiewicz, J., Nassoury, N., Mayer, H., Nimpf, J., Prat, A., & Seidah, N. G. (2008). The proprotein convertase PCSK9 induces the degradation of low density lipoprotein receptor (LDLR) and its closest family members VLDLR and ApoER2. *The Journal of biological chemistry*, *283*(4), 2363–2372.

Poirier, S., Prat, A., Marcinkiewicz, E., Paquin, J., Chitramuthu, B. P., Baranowski, D., Cadieux, B., Bennett, H. P., & Seidah, N. G. (2006). Implication of the proprotein convertase NARC-1/PCSK9 in the development of the nervous system. *Journal of neurochemistry*, *98*(3), 838–850.

Porsteinsson, A. P., Isaacson, R. S., Knox, S., Sabbagh, M. N., & Rubino, I. (2021). Diagnosis of Early Alzheimer's Disease: Clinical Practice in 2021. *The journal of prevention of Alzheimer's disease*, *8*(3), 371–386.

Postina, R., Schroeder, A., Dewachter, I., Bohl, J., Schmitt, U., Kojro, E., Prinzen, C., Endres, K., Hiemke, C., Blessing, M., Flamez, P., Dequenne, A., Godaux, E., van Leuven, F., & Fahrenholz, F. (2004). A disintegrin-metalloproteinase prevents amyloid plaque formation and hippocampal defects in an Alzheimer disease mouse model. *The Journal of clinical investigation*, *113*(10), 1456–1464.

Prakash, P., Manchanda, P., Paouri, E., Bisht, K., Sharma, K., Wijewardhane, P. R., Randolph, C. E., Clark, M. G., Fine, J., Thayer, E. A., Crockett, A., Gasmi, N., Stanko, S., Prayson, R. A., Zhang, C., Davalos, D., & Chopra, G. (2023). Amyloid β Induces Lipid Droplet-Mediated Microglial Dysfunction in Alzheimer's Disease. *bioRxiv : the preprint server for biology*, 2023.06.04.543525.

Prasanthi, J. R., Huls, A., Thomasson, S., Thompson, A., Schommer, E., & Ghribi, O. (2009). Differential effects of 24-hydroxycholesterol and 27-hydroxycholesterol on beta-amyloid precursor protein levels and processing in human neuroblastoma SH-SY5Y cells. *Molecular neurodegeneration*, 4, 1.

Prince, J. A., Zetterberg, H., Andreasen, N., Marcusson, J., & Blennow, K. (2004). APOE epsilon4 allele is associated with reduced cerebrospinal fluid levels of Abeta42. *Neurology*, *62*(11), 2116–2118.

Puzzo, D., Privitera, L., Fa', M., Staniszewski, A., Hashimoto, G., Aziz, F., Sakurai, M., Ribe, E. M., Troy, C. M., Mercken, M., Jung, S. S., Palmeri, A., & Arancio, O. (2011). Endogenous amyloid-

β is necessary for hippocampal synaptic plasticity and memory. *Annals of neurology*, 69(5), 819–830.

Qiu, C., Kivipelto, M., & von Strauss, E. (2009). Epidemiology of Alzheimer's disease: occurrence, determinants, and strategies toward intervention. *Dialogues in clinical neuroscience*, 11(2), 111–128.

Qiu, L., Lewis, A., Como, J., Vaughn, M. W., Huang, J., Somerharju, P., Virtanen, J., & Cheng, K. H. (2009). Cholesterol modulates the interaction of beta-amyloid peptide with lipid bilayers. *Biophysical journal*, *96*(10), 4299–4307.

Rabinovici G. D. (2019). Late-onset Alzheimer Disease. *Continuum (Minneapolis, Minn.)*, *25*(1), 14–33.

Rahman, A., Jackson, H., Hristov, H., Isaacson, R. S., Saif, N., Shetty, T., Etingin, O., Henchcliffe, C., Brinton, R. D., & Mosconi, L. (2019). Sex and Gender Driven Modifiers of Alzheimer's: The Role for Estrogenic Control Across Age, Race, Medical, and Lifestyle Risks. *Frontiers in aging neuroscience*, 11, 315.

Rahman, S. M., Van Dam, A. M., Schultzberg, M., & Crisby, M. (2005). High cholesterol diet results in increased expression of interleukin-6 and caspase-1 in the brain of apolipoprotein E knockout and wild type mice. *Journal of neuroimmunology*, *169*(1-2), 59–67.

Rashid, S., Curtis, D. E., Garuti, R., Anderson, N. N., Bashmakov, Y., Ho, Y. K., Hammer, R. E., Moon, Y. A., & Horton, J. D. (2005). Decreased plasma cholesterol and hypersensitivity to statins in mice lacking Pcsk9. *Proceedings of the National Academy of Sciences of the United States of America*, *102*(15), 5374–5379.

Raulin, A. C., Doss, S. V., Trottier, Z. A., Ikezu, T. C., Bu, G., & Liu, C. C. (2022). ApoE in Alzheimer's disease: pathophysiology and therapeutic strategies. *Molecular neurodegeneration*, 17(1), 72.

Rebiai, R., Givogri, M. I., Gowrishankar, S., Cologna, S. M., Alford, S. T., & Bongarzone, E. R. (2021). Synaptic Function and Dysfunction in Lysosomal Storage Diseases. *Frontiers in cellular neuroscience*, 15, 619777.

Refolo, L. M., Malester, B., LaFrancois, J., Bryant-Thomas, T., Wang, R., Tint, G. S., Sambamurti, K., Duff, K., & Pappolla, M. A. (2000). Hypercholesterolemia accelerates the Alzheimer's amyloid pathology in a transgenic mouse model. *Neurobiology of disease*, *7*(4), 321–331.

Reitz, C., & Mayeux, R. (2014). Alzheimer disease: epidemiology, diagnostic criteria, risk factors and biomarkers. *Biochemical pharmacology*, 88(4), 640–651.

Ricci, C., Ruscica, M., Camera, M., Rossetti, L., Macchi, C., Colciago, A., Zanotti, I., Lupo, M. G., Adorni, M. P., Cicero, A. F. G., Fogacci, F., Corsini, A., & Ferri, N. (2018). PCSK9 induces a pro-inflammatory response in macrophages. *Scientific reports*, *8*(1), 2267.

Rigillo, G., Vilella, A., Benatti, C., Schaeffer, L., Brunello, N., Blom, J. M. C., Zoli, M., & Tascedda, F. (2018). LPS-induced histone H3 phospho(Ser10)-acetylation(Lys14) regulates neuronal and microglial neuroinflammatory response. *Brain, behavior, and immunity*, 74, 277–290.

Robinson, J. G., Farnier, M., Krempf, M., Bergeron, J., Luc, G., Averna, M., Stroes, E. S., Langslet, G., Raal, F. J., El Shahawy, M., Koren, M. J., Lepor, N. E., Lorenzato, C., Pordy, R., Chaudhari, U., Kastelein, J. J., & ODYSSEY LONG TERM Investigators (2015). Efficacy and safety of alirocumab in reducing lipids and cardiovascular events. *The New England journal of medicine*, *372*(16), 1489–1499.

Rom, S., Heldt, N. A., Gajghate, S., Seliga, A., Reichenbach, N. L., & Persidsky, Y. (2020). Hyperglycemia and advanced glycation end products disrupt BBB and promote occludin and claudin-5 protein secretion on extracellular microvesicles. *Scientific reports*, *10*(1), 7274.

Rouser, G., & Yamamoto, A. (1968). Curvilinear regression course of human brain lipid composition changes with age. *Lipids*, 3(3), 284–287.

Rousselet, E., Marcinkiewicz, J., Kriz, J., Zhou, A., Hatten, M. E., Prat, A., & Seidah, N. G. (2011). PCSK9 reduces the protein levels of the LDL receptor in mouse brain during development and after ischemic stroke. *Journal of lipid research*, *52*(7), 1383–1391.

Rudajev, V., & Novotny, J. (2022). Cholesterol as a key player in amyloid β-mediated toxicity in Alzheimer's disease. *Frontiers in molecular neuroscience*, 15, 937056.

Runfola, M., Perni, M., Yang, X., Marchese, M., Bacci, A., Mero, S., Santorelli, F. M., Polini, B., Chiellini, G., Giuliani, D., Vilella, A., Bodria, M., Daini, E., Vandini, E., Rudge, S., Gul, S., Wakelam, M. O. J., Vendruscolo, M., & Rapposelli, S. (2021). Identification of a Thyroid Hormone Derivative as a Pleiotropic Agent for the Treatment of Alzheimer's Disease. *Pharmaceuticals (Basel, Switzerland)*, 14(12), 1330.

Sabatine, M. S., Giugliano, R. P., Keech, A. C., Honarpour, N., Wiviott, S. D., Murphy, S. A., Kuder, J. F., Wang, H., Liu, T., Wasserman, S. M., Sever, P. S., Pedersen, T. R., & FOURIER Steering Committee and Investigators (2017). Evolocumab and Clinical Outcomes in Patients with Cardiovascular Disease. *The New England journal of medicine*, *376*(18), 1713–1722.

Sabatine, M. S., Giugliano, R. P., Wiviott, S. D., Raal, F. J., Blom, D. J., Robinson, J., Ballantyne, C. M., Somaratne, R., Legg, J., Wasserman, S. M., Scott, R., Koren, M. J., Stein, E. A., & Open-Label Study of Long-Term Evaluation against LDL Cholesterol (OSLER) Investigators (2015). Efficacy and safety of evolocumab in reducing lipids and cardiovascular events. *The New England journal of medicine*, *372*(16), 1500–1509.

Sadleir, K. R., Eimer, W. A., Cole, S. L., & Vassar, R. (2015). Aβ reduction in BACE1 heterozygous null 5XFAD mice is associated with transgenic APP level. *Molecular neurodegeneration*, 10, 1.

Sagare, A. P., Deane, R., & Zlokovic, B. V. (2012). Low-density lipoprotein receptor-related protein 1: a physiological Aβ homeostatic mechanism with multiple therapeutic opportunities. *Pharmacology & therapeutics*, *136*(1), 94–105.

Sampaio, I., Quatroni, F. D., Pincela Lins, P. M., Nascimento, A. S., & Zucolotto, V. (2022). Modulation of beta-amyloid aggregation using ascorbic acid. *Biochimie*, 200, 36–43.

Sanguanini, M., Baumann, K. N., Preet, S., Chia, S., Habchi, J., Knowles, T. P. J., & Vendruscolo, M. (2020). Complexity in Lipid Membrane Composition Induces Resilience to Aβ42 Aggregation. *ACS chemical neuroscience*, 11(9), 1347–1352.

Schlunk, F., Fischer, P., Princen, H. M. G., Rex, A., Prinz, V., Foddis, M., Lütjohann, D., Laufs, U., & Endres, M. (2021). No effects of PCSK9-inhibitor treatment on spatial learning, locomotor activity, and novel object recognition in mice. *Behavioural brain research*, *396*, 112875.

Schulze, H., & Sandhoff, K. (2011). Lysosomal lipid storage diseases. *Cold Spring Harbor perspectives in biology*, 3(6), a004804.

Seidah, N. G., Benjannet, S., Wickham, L., Marcinkiewicz, J., Jasmin, S. B., Stifani, S., Basak, A., Prat, A., & Chretien, M. (2003). The secretory proprotein convertase neural apoptosis-regulated convertase 1 (NARC-1): liver regeneration and neuronal differentiation. *Proceedings of the National Academy of Sciences of the United States of America*, *100*(3), 928–933.

Sheedy, F. J., Grebe, A., Rayner, K. J., Kalantari, P., Ramkhelawon, B., Carpenter, S. B., Becker, C. E., Ediriweera, H. N., Mullick, A. E., Golenbock, D. T., Stuart, L. M., Latz, E., Fitzgerald, K. A., & Moore, K. J. (2013). CD36 coordinates NLRP3 inflammasome activation by facilitating intracellular nucleation of soluble ligands into particulate ligands in sterile inflammation. *Nature immunology*, 14(8), 812–820.

Shmuel-Galia, L., Klug, Y., Porat, Z., Charni, M., Zarmi, B., & Shai, Y. (2017). Intramembrane attenuation of the TLR4-TLR6 dimer impairs receptor assembly and reduces microglia-mediated neurodegeneration. *The Journal of biological chemistry*, 292(32), 13415–13427.

Shnerb Ganor, R., Harats, D., Schiby, G., Rosenblatt, K., Lubitz, I., Shaish, A., & Salomon, O. (2018). Elderly apolipoprotein E-/- mice with advanced atherosclerotic lesions in the aorta do not develop Alzheimer's disease-like pathologies. *Molecular medicine reports*, *17*(2), 2488–2492.

Silverberg, G. D., Messier, A. A., Miller, M. C., Machan, J. T., Majmudar, S. S., Stopa, E. G., Donahue, J. E., & Johanson, C. E. (2010). Amyloid efflux transporter expression at the blood-brain barrier

declines in normal aging. *Journal of neuropathology and experimental neurology*, *69*(10), 1034–1043.

Smits, H. A., Rijsmus, A., van Loon, J. H., Wat, J. W., Verhoef, J., Boven, L. A., & Nottet, H. S. (2002). Amyloid-beta-induced chemokine production in primary human macrophages and astrocytes. *Journal of neuroimmunology*, 127(1-2), 160–168.

Sousa, J. A., Bernardes, C., Bernardo-Castro, S., Lino, M., Albino, I., Ferreira, L., Brás, J., Guerreiro, R., Tábuas-Pereira, M., Baldeiras, I., Santana, I., & Sargento-Freitas, J. (2023). Reconsidering the role of blood-brain barrier in Alzheimer's disease: From delivery to target. *Frontiers in aging neuroscience*, *15*, 1102809.

Sparks, D. L., Hunsaker, J. C., 3rd, Scheff, S. W., Kryscio, R. J., Henson, J. L., & Markesbery, W. R. (1990). Cortical senile plaques in coronary artery disease, aging and Alzheimer's disease. *Neurobiology of aging*, *11*(6), 601–607.

Sparks, D. L., Kuo, Y. M., Roher, A., Martin, T., & Lukas, R. J. (2000). Alterations of Alzheimer's disease in the cholesterol-fed rabbit, including vascular inflammation. Preliminary observations. *Annals of the New York Academy of Sciences*, *903*, 335–344.

Sparks, D. L., Scheff, S. W., Hunsaker, J. C., 3rd, Liu, H., Landers, T., & Gross, D. R. (1994). Induction of Alzheimer-like beta-amyloid immunoreactivity in the brains of rabbits with dietary cholesterol. *Experimental neurology*, *126*(1), 88–94.

Spires-Jones, T. L., & Hyman, B. T. (2014). The intersection of amyloid beta and tau at synapses in Alzheimer's disease. *Neuron*, *82*(4), 756–771.

Staurenghi, E., Cerrato, V., Gamba, P., Testa, G., Giannelli, S., Leoni, V., Caccia, C., Buffo, A., Noble, W., Perez-Nievas, B. G., & Leonarduzzi, G. (2021). Oxysterols present in Alzheimer's disease brain induce synaptotoxicity by activating astrocytes: A major role for lipocalin-2. *Redox biology*, 39, 101837.

Stewart, C. R., Stuart, L. M., Wilkinson, K., van Gils, J. M., Deng, J., Halle, A., Rayner, K. J., Boyer, L., Zhong, R., Frazier, W. A., Lacy-Hulbert, A., El Khoury, J., Golenbock, D. T., & Moore, K. J. (2010). CD36 ligands promote sterile inflammation through assembly of a Toll-like receptor 4 and 6 heterodimer. *Nature immunology*, *11*(2), 155–161.

Stonebraker, A. R., Beasley, M., Massinople, S., Wunder, M., Li, P., Valentine, S. J., & Legleiter, J. (2023). Cholesterol impacts the formation of huntingtin/lipid complexes and subsequent aggregation. *Protein science: a publication of the Protein Society*, 32(5), e4642.

Storck, S. E., Meister, S., Nahrath, J., Meißner, J. N., Schubert, N., Di Spiezio, A., Baches, S., Vandenbroucke, R. E., Bouter, Y., Prikulis, I., Korth, C., Weggen, S., Heimann, A.,

Schwaninger, M., Bayer, T. A., & Pietrzik, C. U. (2016). Endothelial LRP1 transports amyloid-β(1-42) across the blood-brain barrier. *The Journal of clinical investigation*, *126*(1), 123–136.

Tabrizi, M., Bornstein, G. G., & Suria, H. (2010). Biodistribution mechanisms of therapeutic monoclonal antibodies in health and disease. *The AAPS journal*, *12*(1), 33–43.

Tamboli, I. Y., Tien, N. T., & Walter, J. (2011). Sphingolipid storage impairs autophagic clearance of Alzheimer-associated proteins. *Autophagy*, *7*(6), 645–646.

Tang, Z. H., Peng, J., Ren, Z., Yang, J., Li, T. T., Li, T. H., Wang, Z., Wei, D. H., Liu, L. S., Zheng, X. L., & Jiang, Z. S. (2017). New role of PCSK9 in atherosclerotic inflammation promotion involving the TLR4/NF-κB pathway. *Atherosclerosis*, *262*, 113–122.

Tang, Z., Jiang, L., Peng, J., Ren, Z., Wei, D., Wu, C., Pan, L., Jiang, Z., & Liu, L. (2012). PCSK9 siRNA suppresses the inflammatory response induced by oxLDL through inhibition of NF-κB activation in THP-1-derived macrophages. *International journal of molecular medicine*, *30*(4), 931–938.

Testa, G., Staurenghi, E., Giannelli, S., Gargiulo, S., Guglielmotto, M., Tabaton, M., Tamagno, E., Gamba, P., & Leonarduzzi, G. (2018). A silver lining for 24-hydroxycholesterol in Alzheimer's disease: The involvement of the neuroprotective enzyme sirtuin 1. *Redox biology*, 17, 423–431.

Therriault, J., Zimmer, E. R., Benedet, A. L., Pascoal, T. A., Gauthier, S., & Rosa-Neto, P. (2022). Staging of Alzheimer's disease: past, present, and future perspectives. *Trends in molecular medicine*, *28*(9), 726–741.

Toledo, J. B., Habes, M., Sotiras, A., Bjerke, M., Fan, Y., Weiner, M. W., Shaw, L. M., Davatzikos, C., Trojanowski, J. Q., & Alzheimer's Disease Neuroimaging Initiative (2019). APOE Effect on Amyloid-β PET Spatial Distribution, Deposition Rate, and Cut-Points. *Journal of Alzheimer's disease : JAD*, *69*(3), 783–793.

Tracey, T. J., Steyn, F. J., Wolvetang, E. J., & Ngo, S. T. (2018). Neuronal Lipid Metabolism: Multiple Pathways Driving Functional Outcomes in Health and Disease. *Frontiers in molecular neuroscience*, 11, 10.

Turri, M., Marchi, C., Adorni, M. P., Calabresi, L., & Zimetti, F. (2022). Emerging role of HDL in brain cholesterol metabolism and neurodegenerative disorders. *Biochimica et biophysica acta. Molecular and cell biology of lipids*, *1867*(5), 159123.

Tveten, K., Holla, Ø. L., Cameron, J., Strøm, T. B., Berge, K. E., Laerdahl, J. K., & Leren, T. P. (2012). Interaction between the ligand-binding domain of the LDL receptor and the C-terminal domain of PCSK9 is required for PCSK9 to remain bound to the LDL receptor during endosomal acidification. *Human molecular genetics*, *21*(6), 1402–1409.

Valenza, M., & Cattaneo, E. (2006). Cholesterol dysfunction in neurodegenerative diseases: is Huntington's disease in the list?. *Progress in neurobiology*, 80(4), 165–176.

van der Kant, R., & Goldstein, L. S. (2015). Cellular functions of the amyloid precursor protein from development to dementia. *Developmental cell*, 32(4), 502–515.

Vance, J. E., & Hayashi, H. (2010). Formation and function of apolipoprotein E-containing lipoproteins in the nervous system. *Biochimica et biophysica acta*, *1801*(8), 806–818.

Varma, V. R., Büşra Lüleci, H., Oommen, A. M., Varma, S., Blackshear, C. T., Griswold, M. E., An, Y., Roberts, J. A., O'Brien, R., Pletnikova, O., Troncoso, J. C., Bennett, D. A., Çakır, T., Legido-Quigley, C., & Thambisetty, M. (2021). Abnormal brain cholesterol homeostasis in Alzheimer's disease-a targeted metabolomic and transcriptomic study. *NPJ aging and mechanisms of disease*, *7*(1), 11.

Verghese, P. B., Castellano, J. M., Garai, K., Wang, Y., Jiang, H., Shah, A., Bu, G., Frieden, C., & Holtzman, D. M. (2013). ApoE influences amyloid-β (Aβ) clearance despite minimal apoE/Aβ association in physiological conditions. *Proceedings of the National Academy of Sciences of the United States of America*, *110*(19), E1807–E1816.

Villacampa, N., Almolda, B., Vilella, A., Campbell, I. L., González, B., & Castellano, B. (2015). Astrocyte-targeted production of IL-10 induces changes in microglial reactivity and reduces motor neuron death after facial nerve axotomy. *Glia*, 63(7), 1166–1184.

Villain, N., Planche, V., & Levy, R. (2022). High-clearance anti-amyloid immunotherapies in Alzheimer's disease. Part 1: Meta-analysis and review of efficacy and safety data, and medico-economical aspects. *Revue neurologique*, *178*(10), 1011–1030.

Villain, N., Planche, V., & Levy, R. (2022). High-clearance anti-amyloid immunotherapies in Alzheimer's disease. Part 2: putative scenarios and timeline in case of approval, recommendations for use, implementation, and ethical considerations in France. *Revue neurologique*, *178*(10), 999–1010.

Vorhees, C. V., & Williams, M. T. (2006). Morris water maze: procedures for assessing spatial and related forms of learning and memory. *Nature protocols*, 1(2), 848–858.

Walf, A. A., & Frye, C. A. (2007). The use of the elevated plus maze as an assay of anxiety-related behavior in rodents. *Nature protocols*, 2(2), 322–328.

Walter, S., Letiembre, M., Liu, Y., Heine, H., Penke, B., Hao, W., Bode, B., Manietta, N., Walter, J., Schulz-Schuffer, W., & Fassbender, K. (2007). Role of the toll-like receptor 4 in neuroinflammation in Alzheimer's disease. *Cellular physiology and biochemistry : international journal of experimental cellular physiology, biochemistry, and pharmacology*, *20*(6), 947–956.

Wang, G., Silva, J., Dasgupta, S., & Bieberich, E. (2008). Long-chain ceramide is elevated in presenilin 1 (PS1M146V) mouse brain and induces apoptosis in PS1 astrocytes. *Glia*, 56(4), 449–456.

Wang, L., Hou, H., Zi, D., Habib, A., Tan, J., & Sawmiller, D. (2019). Novel apoE receptor mimetics reduce LPS-induced microglial inflammation. *American journal of translational research*, 11(8), 5076–5085.

Wang, L., Wang, Z., Shi, J., Jiang, Q., Wang, H., Li, X., & Hao, D. (2018). Inhibition of proprotein convertase subtilisin/kexin type 9 attenuates neuronal apoptosis following focal cerebral ischemia via apolipoprotein E receptor 2 downregulation in hyperlipidemic mice. *International journal of molecular medicine*, *42*(4), 2098–2106.

Wang, P., Zhang, H., Wang, Y., Zhang, M., & Zhou, Y. (2020). Plasma cholesterol in Alzheimer's disease and frontotemporal dementia. *Translational neuroscience*, 11(1), 116–123.

Wang, Y., An, Y., Ma, W., Yu, H., Lu, Y., Zhang, X., Wang, Y., Liu, W., Wang, T., & Xiao, R. (2020). 27-Hydroxycholesterol contributes to cognitive deficits in APP/PS1 transgenic mice through microbiota dysbiosis and intestinal barrier dysfunction. *Journal of neuroinflammation*, 17(1), 199.

Welikovitch, L. A., Do Carmo, S., Maglóczky, Z., Malcolm, J. C., Lőke, J., Klein, W. L., Freund, T., & Cuello, A. C. (2020). Early intraneuronal amyloid triggers neuron-derived inflammatory signaling in APP transgenic rats and human brain. *Proceedings of the National Academy of Sciences of the United States of America*, *117*(12), 6844–6854.

Wu, C., Xi, C., Tong, J., Zhao, J., Jiang, H., Wang, J., Wang, Y., & Liu, H. (2019). Design, synthesis, and biological evaluation of novel tetrahydroprotoberberine derivatives (THPBs) as proprotein convertase subtilisin/kexin type 9 (PCSK9) modulators for the treatment of hyperlipidemia. *Acta pharmaceutica Sinica. B*, *9*(6), 1216–1230.

Wu, G., Lu, Z. H., Kulkarni, N., & Ledeen, R. W. (2012). Deficiency of ganglioside GM1 correlates with Parkinson's disease in mice and humans. *Journal of neuroscience research*, 90(10), 1997–2008.

Wu, H., Liu, Q., Kalavagunta, P. K., Huang, Q., Lv, W., An, X., Chen, H., Wang, T., Heriniaina, R. M., Qiao, T., & Shang, J. (2018). Normal diet Vs High fat diet - A comparative study: Behavioral and neuroimmunological changes in adolescent male mice. *Metabolic brain disease*, *33*(1), 177–190.

Wu, M., Zhang, M., Yin, X., Chen, K., Hu, Z., Zhou, Q., Cao, X., Chen, Z., & Liu, D. (2021). The role of pathological tau in synaptic dysfunction in Alzheimer's diseases. *Translational neurodegeneration*, 10(1), 45.

Wu, Q., Tang, Z. H., Peng, J., Liao, L., Pan, L. H., Wu, C. Y., Jiang, Z. S., Wang, G. X., & Liu, L. S. (2014). The dual behavior of PCSK9 in the regulation of apoptosis is crucial in Alzheimer's disease progression (Review). *Biomedical reports*, *2*(2), 167–171.

Xin, Y., Zhang, L., Hu, J., Gao, H., & Zhang, B. (2021). Correlation of early cognitive dysfunction with inflammatory factors and metabolic indicators in patients with Alzheimer's disease. *American journal of translational research*, *13*(8), 9208–9215.

Xu, S., Luo, S., Zhu, Z., & Xu, J. (2019). Small molecules as inhibitors of PCSK9: Current status and future challenges. *European journal of medicinal chemistry*, 162, 212–233.

Yamazaki, Y., Zhao, N., Caulfield, T. R., Liu, C. C., & Bu, G. (2019). Apolipoprotein E and Alzheimer disease: pathobiology and targeting strategies. *Nature reviews. Neurology*, *15*(9), 501–518.

Yang, X., Sheng, W., Sun, G. Y., & Lee, J. C. (2011). Effects of fatty acid unsaturation numbers on membrane fluidity and α-secretase-dependent amyloid precursor protein processing. *Neurochemistry international*, *58*(3), 321–329.

Ye, S., Huang, Y., Müllendorff, K., Dong, L., Giedt, G., Meng, E. C., Cohen, F. E., Kuntz, I. D., Weisgraber, K. H., & Mahley, R. W. (2005). Apolipoprotein (apo) E4 enhances amyloid beta peptide production in cultured neuronal cells: apoE structure as a potential therapeutic target. *Proceedings of the National Academy of Sciences of the United States of America*, *102*(51), 18700–18705.

Yin F. (2023). Lipid metabolism and Alzheimer's disease: clinical evidence, mechanistic link and therapeutic promise. *The FEBS journal*, *290*(6), 1420–1453.

Yoo, C. H., Kim, J., Baek, H. M., Chang, K. A., & Choe, B. Y. (2023). Neurodegenerative Changes in the Brains of the 5xFAD Alzheimer's Disease Model Mice Investigated by High-Field and High-Resolution Magnetic Resonance Imaging and Multi-Nuclei Magnetic Resonance Spectroscopy. *International journal of molecular sciences*, 24(6), 5073.

Yuan, X. Z., Sun, S., Tan, C. C., Yu, J. T., & Tan, L. (2017). The Role of ADAM10 in Alzheimer's Disease. *Journal of Alzheimer's disease : JAD*, 58(2), 303–322.

Zambón, D., Quintana, M., Mata, P., Alonso, R., Benavent, J., Cruz-Sánchez, F., Gich, J., Pocoví, M., Civeira, F., Capurro, S., Bachman, D., Sambamurti, K., Nicholas, J., & Pappolla, M. A. (2010). Higher incidence of mild cognitive impairment in familial hypercholesterolemia. *The American journal of medicine*, *123*(3), 267–274.

Zampagni, M., Cascella, R., Casamenti, F., Grossi, C., Evangelisti, E., Wright, D., Becatti, M., Liguri, G., Mannini, B., Campioni, S., Chiti, F., & Cecchi, C. (2011). A comparison of the biochemical modifications caused by toxic and non-toxic protein oligomers in cells. *Journal of cellular and molecular medicine*, 15(10), 2106–2116.

Zhang, D. W., Lagace, T. A., Garuti, R., Zhao, Z., McDonald, M., Horton, J. D., Cohen, J. C., & Hobbs, H. H. (2007). Binding of proprotein convertase subtilisin/kexin type 9 to epidermal growth factor-like repeat A of low density lipoprotein receptor decreases receptor recycling and increases degradation. *The Journal of biological chemistry*, *282*(25), 18602–18612.

Zhang, J., & Liu, Q. (2015). Cholesterol metabolism and homeostasis in the brain. *Protein & cell*, 6(4), 254–264.

Zhang, T., Chen, D., & Lee, T. H. (2019). Phosphorylation Signaling in APP Processing in Alzheimer's Disease. *International journal of molecular sciences*, *21*(1), 209.

Zhang, X., Xi, Y., Yu, H., An, Y., Wang, Y., Tao, L., Wang, Y., Liu, W., Wang, T., & Xiao, R. (2019). 27-hydroxycholesterol promotes Aβ accumulation via altering Aβ metabolism in mild cognitive impairment patients and APP/PS1 mice. *Brain pathology (Zurich, Switzerland)*, 29(4), 558–573

Zhang, Y. W., Thompson, R., Zhang, H., & Xu, H. (2011). APP processing in Alzheimer's disease. *Molecular brain*, *4*, 3.

Zhao, J., Fu, Y., Yasvoina, M., Shao, P., Hitt, B., O'Connor, T., Logan, S., Maus, E., Citron, M., Berry, R., Binder, L., & Vassar, R. (2007). Beta-site amyloid precursor protein cleaving enzyme 1 levels become elevated in neurons around amyloid plaques: implications for Alzheimer's disease pathogenesis. *The Journal of neuroscience : the official journal of the Society for Neuroscience*, 27(14), 3639–3649.

Zhao, N., Liu, C.-C., Van Ingelgom, A. J., Martens, Y. A., Linares, C., Knight, J. A., et al. (2017). Apolipoprotein E4 impairs neuronal insulin signaling by trapping insulin receptor in the endosomes. *Neuron* 96, 115–129.

Zhao, X. S., Wu, Q., Peng, J., Pan, L. H., Ren, Z., Liu, H. T., Jiang, Z. S., Wang, G. X., Tang, Z. H., & Liu, L. S. (2017). Hyperlipidemia-induced apoptosis of hippocampal neurons in apoE(-/-) mice may be associated with increased PCSK9 expression. *Molecular medicine reports*, *15*(2), 712–718.

Zimetti, F., Caffarra, P., Ronda, N., Favari, E., Adorni, M. P., Zanotti, I., Bernini, F., Barocco, F., Spallazzi, M., Galimberti, D., Ricci, C., Ruscica, M., Corsini, A., & Ferri, N. (2017). Increased PCSK9 Cerebrospinal Fluid Concentrations in Alzheimer's Disease. *Journal of Alzheimer's disease : JAD*, *55*(1), 315–320.

Zoli, M., Benfenati, F., Pich, E. M., Toffano, G., Fuxe, K., & Agnati, L. F. (1990). Aspects of neural plasticity in the central nervous system-IV. Chemical anatomical studies on the aging brain. *Neurochemistry international*, 16(4), 437–449.

Zoli, M., Guidolin, D., & Agnati, L. F. (1992). Morphometric evaluation of populations of neuronal profiles (cell bodies, dendrites, and nerve terminals) in the central nervous system. *Microscopy research and technique*, 21(4), 315–337.

Zoli, M., Zini, I., Agnati, L. F., Guidolin, D., Ferraguti, F., & Fuxe, K. (1990). Aspects of neural plasticity in the central nervous system-I. Computer-assisted image analysis methods. *Neurochemistry international*, 16(4), 383–418.

Zuin, M., Cervellati, C., Trentini, A., Passaro, A., Rosta, V., Zimetti, F., & Zuliani, G. (2021). Association between Serum Concentrations of Apolipoprotein A-I (ApoA-I) and Alzheimer's Disease: Systematic Review and Meta-Analysis. *Diagnostics (Basel, Switzerland), 11*(6), 984.